Pyry Peitso

Space weather instruments and measurement platforms

School of Electrical Engineering

Thesis submitted for examination for the degree of Master of Science in Technology.

Espoo 25.06.2013

Thesis supervisor:

Prof. Martti Hallikainen

Thesis instructor:

Prof. Eija Tanskanen

Aalto University
School of Electrical
Engineering

AALTO UNIVERSITY
SCHOOL OF ELECTRICAL ENGINEERING

ABSTRACT OF THE
MASTER'S THESIS

Author: Pyry Peitso

Title: Space weather instruments and measurement platforms

Date: 25.06.2013 Language: English Number of pages:11+82

Department of Radio Science and Technology

Professorship: Space Technology Code: S-92

Supervisor: Prof. Martti Hallikainen

Instructor: Prof. Eija Tanskanen

Space weather is a phenomenon affecting near-Earth space. It manifests itself in numerous different ways, the best known being the Aurora. Space weather causes numerous problems to several critical infrastructures, such as power grids and satellites. This master's thesis investigates current space weather instrumentation and systems to analyze their capabilities and possibly existing gaps in measurements.

Analysis of magnetospheric, ionospheric, solar and solar wind instruments and instrument platforms is conducted. Our results show that currently existing instrumentation is able to measure essentially all space weather phenomena. Magnetometer coverage in auroral regions is not sufficient for detailed space weather analysis e.g. due to the lack of capability for measuring magnetic field at the sea. Ionospheric measurements have similar problems with coverage, but they also have rather short time series. Solar and solar wind observations are concentrated on a small number of orbital observatories that are difficult to replace and expensive.

In conclusion, testing of CubeSat mounted fluxgate magnetometers, adoption of underwater magnetometers and improvements in coverage of ionospheric and magnetospheric measurements are suggested. Maintenance of the ability to conduct *in situ* measurements of solar wind and and solar observations are recommended.

Keywords: space weather, magnetometer, space physics

AALTO-YLIOPISTO
SÄHKÖTEKNIIKAN KORKEAKOULU

DIPLOMITYÖN
TIIVISTELMÄ

Tekijä: Pyry Peitso

Työn nimi:

Päivämäärä: 25.06.2013 Kieli: Englanti Sivumäärä:11+82

Radiotieteen ja -tekniikan laitos

Professuuri: Avaruustekniikka Koodi: S-92

Valvoja: Prof. Martti Hallikainen

Ohjaaja: Prof. Eija Tanskanen

Avaruussää on Maapallon lähiavaruuden ilmiö. Sillä on useita ilmenemismuotoja, joista tunnetuin on revontulet. Avaruussää aiheuttaa haittaa kriittisille infrastruktuureille, kuten satelliiteille ja sähköverkoille. Tämän diplomityön tarkoituksena on tutkia nykyisiä avaruussääinstrumenttejä sekä mittausjärjestelmiä ja kartoittaa niiden toimintakyky sekä heikkouksia.
Magnetometri-, ionosfääri, aurinkotuuli- ja Aurinkoinstrumentaatiolle ja järjestelmille suoritetaan kattava analyysi. Lopputulokset osoittavat että nykyiset instrumentit kykenevät mittaamaan kaikkia avaruussäähän liittyviä ilmiöitä. Magnetometrimittausten peitto revontuliovaalilla ei ole riittävä tarkkaan avaruussäätutkimukseen, sillä magneettikenttää ei kyetä mittaamaan merellä. Ionosfäärimittauksilla on samanlaisia ongelmia maantieteellisen peiton kanssa ja niistä on saatavilla lyhyempiä aikasarjoja. Aurinko- ja aurinkotuulimittaukset ovat keskittyneet pienelle määrälle satelliitteja jotka ovat kalliita ja hankalia korvata.
Lopputuloksina suositellaan CubeSat-satelliittien kyytiin asennettavien magnetometrien testausta, vedenalaisten magnetometrien käyttöönottoa sekä parannuksia ionosfäärin ja magnetosfäärin mittauspeitossa. Kykyä suorittaa jatkuvia Aurinko- ja aurinkotuulimittauksia avaruuteen sijoitetuilla järjestelmillä pitäisi myös ylläpitää.

Avainsanat: space weather, magnetometer, space physics

Preface

This thesis was done in the Finnish Meteorological Institute, Earth Observations unit. I would like to thank the following people for their help in its completion:

Eija Tanskanen and Martti Hallikainen for their instructions and supervision, Riitta and Matti Peitso for support, Maria Komu, Timo Nikkanen, Stig-Arne Grönroos for help, Minna Palmroth, Tero Raita, Johannes Norberg, Risto Pirjola, Emilia Kilpua, Ari Viljanen, Noora Partamies, Kirsti Kauristie, David Perez Suarez, Jeffrey J Love, Eftyhia Zesta, Claudia Stolle, Dan Baker, Alexander Janzhura, Truls Lynne Hansen, George Maeda, Esa Turunen, Tim White, Esa Kallio, Olaf Amm, Daniel Whiter, Tero Siili, Aapo Poutanen, Tapani Pihlajamäki, Nuno Silvia, all my co-workers at Dynamicum (especially the coffee break group), the Aalto-1 team, and anyone who offered assistance or help with this and I forgot to mention.

Espoo, 25.06.2013

Pyry Peitso

Contents

Symbols and abbreviations

Symbols

γ	photon
Δ&*phi*	difference in phase between two signals in radians
μ_0	vacuum permeability 4πx10^{-7} Vs/Am
τ_e	electron gyromagnetic ratio
τ_p	proton gyromagnetic ratio
A	ampere, unit of electric current
arcsec	second of arc, 1/60 of arcminute, unit of angular measurement
AU	astronomical unit, average distance of the Earth from the Sun, $\approx 150x10^9$m.
B	magnetic flux [T]
c	speed of light in a vacuum 299,792,458 m/s
C	Celsius, unit of measurement for temperature
dt	sample time in TEC calculations
e^+	positron
e^-	electron
eV	electron volt, unit of energy, 1.6x10^{-19} J
f	signal frequency
Fe	iron
g	gram, unit of mass
G	number of observed sunspot groups
H	hydrogen
Hα	red hydrogen spectral line, 656.28 nm
He	helium
I_T	Total current to spacecraft surface
I_E	Incident negative electron current
I_I	Incident positive ion current
I_{SE}	Secondary emitted electron current due to I_E
I_{SI}	Secondary emitted electron current due to I_I
I_{BSE}	Back scattered electron current due to I_E
I_{PH}	Photoelectron current
k	Boltzmann constant, 8.6173324x10^{-5} eV/K
K	kelvin, base unit of temperature in International system of units
K	station dependent scaling factor for sunspot numbers (Chapter 4.3.)
m	meter, unit of measurement
n	refractive index
n_e	electron density of a medium, electron/m^3
Ni	nickel
pfu	proton flux units = particles/steradian x cm^{2}s
R_E	radius of the Earth 6471 km
R_i	International Sunspot Number
r_e	radius of an electron, 2.81794x10^{-15}m
S	number of observed sunspots
sr	steradian, SI unit of solid angle
Sv	sievert, unit of equivalent radiation dose in SI units, Sv = J/kg.
t	time
T	tesla, unit of magnetic flux, T = Wb/m^2

V	surface potential [V]
V	volt, unit of electric potential, $\mathrm{kgm^2/As^3}$
v_e	electron neutrino
W	unit of power, $\mathrm{kgm^2/s^3}$
Wb	weber, unit of magnetic flux in SI units, 1 Wb = 1 Vs.
$\underline{x}$	3D location in TEC calculations
Å	Ångström, unit of length, 1 Å = 0.1 nm.

Abbreviations

3DP	3D Plasma Analyzer
AARDDVARK	Antarctic-Arctic Radiation-belt (Dynamic) Deposition-VLF Atmospheric Research Konsortium
AARI	Arctic and Antarctic Research Institute
AC	Alternating Current
AD	Analog-to-digital
ACE	Advanced Composition Explorer
AIA	Atmospheric Imaging Assembly
ASPOC	Active Spacecraft Potential Control
ATA	Applications Technology Satellite
CANOPUS	Canadian Auroral Network for the OPEN Program Unified Study
CANMOS	CANadian Magnetic Observatory System
CARISMA	Canadian Array for Realtime InvestigationS of Magnetic Activity
CCD	Charge-coupled Device
CELIAS	Charge, Element, and Isotope Analysis System
CGSM	Canadian Geospace Monitoring
CHIME	The CubeSat Heliospheric Imaging Experiment
CIR	Corotating Interaction Region
CIS	Cluster Ion Spectrometry
CMD	Continous Magnetospheric Dissipation
CME	Coronal Mass Ejection
COSMOS	Cabled Observatories for Monitoring of the Ocean System
COTS	Commercial off-the-shelf
CPMN	Circum-pan Pacific Magnetometer Network
CRIS	Cosmic Ray Isotope Spectrometer
CSA	Canadian Space Agency
CTOF	Charge Time of Flight
DNP	Dynamic Nuclear Polarization
DSCOVR	Deep Space Climate Observatory
DSP	Digital Signal Processor
EDI	Electron Drift Instrument
EFI	Electric Field Instrument
EFW	Electric Field and Wave
EISCAT	European Incoherent Scatter Scientific Association
EPAM	Electron, Proton and Alpha Monitor
EPD	Energetic Particle Detector
EPS	Energetic Particle Sensor
ERNE	Energetic and Relativistic Nuclei and Electron
ESA	European Space Agency
ESA	Electrostatic Analyzer
ESP	EUV SpectroPhotometer
EESA	Electron Electrostatic Analyzers
ESD	Electrostatic Discharge
ESONET	European Seas Observatory NETwork
EU	European Union
EUI	Extreme Ultraviolet Imager
EUV	Extreme Ultraviolet
EVE	Extreme Ultraviolet Variability Experiment
FGM	FluxGate Magnetometer

FMI	Finnish Meteorological Institute
FPC	Fast Particle Correlator
FPGA	Field-programmable gate array
GIC	Geomagnetically Induced Current
GIN	Geomagnetic Information Node
GNSS	Global Navigation Satellite System
GOES	Geostationary Operational Environmental Satellite
GPS	Global Positioning System
HEPAD	High Energy Proton and Alpha Detector
HMI	Helioseismic and Magnetic Imager
HSS	High Speed Stream
ICME	Interplanetary Coronal Mass Ejection
ICI-2	Investigation of Cusp Irregularities
IMF	Interplanetary Magnetic Field
ISES	International Space Weather Services
MAG	Magnetic Field Experiment
MAG	Magnetometer
MAGDAS	MAGnetic Data Acquisition System
MEGS	Multiple EUV Grating Spectrographs
METIS	Multi Element Telescope for Imaging and Spectroscopy
MFI	Magnetic Field Investigation
MDI	Michelson Doppler Imager
MIRACLE	Magnetometers Ionospheric Radars Allsky Cameras Large Experiment
m-NLP	multi-Needle Langmuir Probe
MSK	Minimum Shift Keying
MTOF	Mass Time of Flight
NASA	National Aeronautics and Space Administration
NEPTUNE	Northeast Pacific Undersea Networked Experiments
NGL	Narod Geophysics Ltd
NOAA	National Oceanic and Atmospheric Administration
HMI	Helioseismic and Magnetic Imager
IAGA	International Association of Geomagnetism and Aeronomy
ICME	Interplanetary Coronal Mass Ejection
IMF	Interplanetary Magnetic Field
IMAGE	International Monitor for Auroral Geomagnetic Effects
ISS	International Space Station
LEO	Low Earth Orbit
PEACE	Plasma Electron and Current Experiment
PM	Proton Monitor
P-POD	Poly Picosatellite Orbital Deployer
RAPID	Research with Adaptative Particle Imaging Detectors
RF	Radio Frequency
RPW	Radio and Plasma Wave analyser
RSTN	Radio Solar Telescope Network
RTSW	Real Time Solar Wind
RWC	Regional Warning Center
SCM	Search Coil Magnetometer
SCATHA	Spacecraft Charging AT High Altitude
SDO	Solar Dynamics Observatory

SDR	Software Defined Radio
SEE	Single Event Effect
SEM	Space Environment Monitor
SEP	Solar Energetic Particle
SEPICA	Solar Energetic Particle Ionic Charge Analyzer
SEU	Single Event Upset
SIDC	Solar Influences Data Centre
SIS	Solar Isotope Spectrometer
SLAM	Spacecraft Loads and Acoustics Measurements
SMC	Steady Magnetospheric Convection
SMS	Synchronous Meteorological Satellite
SOHO	Solar and Heliospheric Observatory
SoloHI	Solar Orbiter Heliospheric Imager
SOON	Solar Optical Observing Network
SPICE	Spectral Imaging of the Coronal Environment
SST	Semi-conductor detector telescopes
SST	Solid State Telescope
STAFF	Spatio-Temporal Analysis of Field Fluctuations
STIX	Spectrometer/Telescope for Imaging X-rays
SWA	Solar Wind Analyzer
SWE	Solar Wind Experiment
SWEPAM	Solar Wind Electron, Proton and Alpha Monitor
SWIMS	Solar Wind Ion Mass Spectrometer
SWICS	Solar Wind Ion Composition Spectrometer
SWOT	Strength, Weakness, Opportunity, Threat
SWPC	Space Weather Prediction Center
SWRC	Space Weather Research Center
SXI	Solar X-ray Imager
TEC	Total Electron Content
THEMIS	The Time History of Events and Macroscale Interactions during Substorms
UHF	Ultra High Frequency
ULEIS	Ultra Low Energy Isotope Spectrometer
USA	United States of America
USAF	United States Air Force
USGS	United States Geological Survey
UT	Universal Time
UV	Ultraviolet
VHF	Very High Frequency
VLF	Very Low Frequency
WDB	Wide Band Data
WEC	Wave Experiment Consortium
WHISPER	Waves of High Frequency and Sounder for Probing of Elecron density by Relaxation
XRS	Solar X-Ray Sensor

1 Introduction

This M.Sc. thesis investigates current space weather instruments and systems in order to analyze our current capability to measure and study space weather and space climate.

Space weather affects the near-Earth space in numerous ways. Almost all phenomena are somewhat harmful to several important infrastructures, except the aurora. Satellites, power grids, oil and gas pipelines and similar long structured infrastructures are all at risk to a multitude of phenomena. The best documented space weather event of the space age has been the Halloween Storm of 2003. Numerous problems were reported with power grids and a total of 28 different failures took place on different satellites, including the total loss of one spacecraft. More powerful Solar events have happened in history, but they have caused less problems for several reasons, e.g. Carrington event in 1859 due to the lack of current technology.

Space weather is measured using several different methods. Magnetometers deployed both on the Earth and on several satellite systems are the most numerous instruments. Solar wind is monitored with plasma instrumentation and spectrometers. The Sun is surveyed with different kinds of telescopes and coronagraphs. Ionospheric conditions are measured with for example incoherent scatter radars, riometers, balloon experiments and satellites.

This thesis consists of seven chapters. The **second chapter** covers background on the Sun. The Near-Earth space and certain important layers of the Earth atmosphere are described as well. Several different solar phenomena related to space weather are listed and their characteristics described. Geomagnetic indices that are used to measure geomagnetic activity are examined. Space weather effects in interplanetary space, magnetosphere, ionosphere, neutral atmosphere and the Earth surface are described. Parameters for the extreme space weather conditions are also provided.

In **chapter three** a multitude of different instruments are investigated, the most important being different kinds of magnetometers. Both the Earth based observatory equipment as well as space-borne instruments are examined. Results show that all phenomena can be measured with the current instrumentation.

Notable magnetometer networks on the Earth as well as space weather focused satellite missions are examined in **chapter four**. Details on instrumentation is provided and examples of data are displayed. Space weather services making use of the data and information on new types of ionospheric measurements are provided and gap analysis is conducted for instrument platforms.

Future space weather systems are covered in **chapter five**, including CubeSats, underwater magnetometers and E-sail.

In **chapter six** space weather capabilities are assessed by a SWOT analysis of magnetometer, ionospheric, solar and solar wind measurements.

Finally the **seventh chapter** provides discussion and conclusions to this master's thesis.

2 Background

2.1 The Sun

The Sun is the source of almost all space weather phenomena except disturbances from interstellar space. From an astronomical point of view, the Sun is a fairly typical type G2 star with a visual magnitude of 4.8. It is a massive ball of gas that consists mostly of hydrogen and helium. These are mostly ionized due to the very high temperatures.Facts about the Sun are provided in Table 1.

Table 1: Facts about the Sun.[104]

Age	4.5x10^9 yr
Mass	1.99x10^{30} kg
Radius	696 000 km
Mean density	$1.4x10^3 kgm^{-3}$
Mean distance from Earth (1 AU)	150x$10^6 km$
Surface gravity	274 ms^{-2}
Radiation emitted (luminosity)	3.86x10^{26} W
Equatorial rotation period	26 days
Mass loss rate	$10^9 kgs^{-1}$
Effective blackbody temperature	5785 K

The Sun is 330 000 times heavier than the Earth and its radius is about 109 times larger. The Sun produces its energy by nuclear fusion, with a power of roughly 4x10^{26} Watts. During one second, 600 million tonnes of hydrogen are fused into 596 million tonnes of helium and the remaining 4 million tonnes are turned into energy. During the Sun's lifetime so far it has spent around 5% of its fuel. Most of the hydrogen used is from the core and the most important fusion chain is the proton-proton-chain. Chemical reactions illustrated by Equations 1,2 and 3 happen inside Sun-sized and larger stars.

$$^1H +^1 H \rightarrow^2 H + e^+ + v_e \quad (1)$$

$$^1H +^1 H + e^- \rightarrow^2 H + v_e$$

$$^2H +^1 H \rightarrow^3 He + \gamma \quad (2)$$

$$^3He +^3 He \rightarrow^4 He + 2^1He \quad (3)$$

In the first part two hydrogen nuclei undergo fusion into deuterium and release a positron and an electron neutrino. Both halves of the first part are extremely rare so the process is very slow. The second part where deuterium and protons fuse together to form ^{3}He (and one photon) happens relatively quickly, and thus there is very little deuterium inside a star. The last part can happen in three different ways. The version above is the most likely scenario and it is called the pp I branch. A ^{4}He is created from the fusion of two ^{3}He, additionally 2 ^1He are created. In the Sun 91% of ^{3}He follows this path. Other possible branches are pp II and pp III.[104][95]

Figure 1 illustrates the different layers of the Sun. The very heart of the Sun is the core. The fusion reactions take place in the core. The temperature in the core is around 15 000 000 K and its radius is one quarter of the Sun's radius (174 000 km).

From the core of the Sun the fusion-produced energy flows to the radiative zone. There the photons are constantly absorbed and emitted by the surrounding material. This considerably slows down the movement of the protons and their journey through this layer can take up to 10 million years. The radiative zone extends up to 522 000 km from the center of the Sun. The temperature here is approximately $8x10^6$ K.

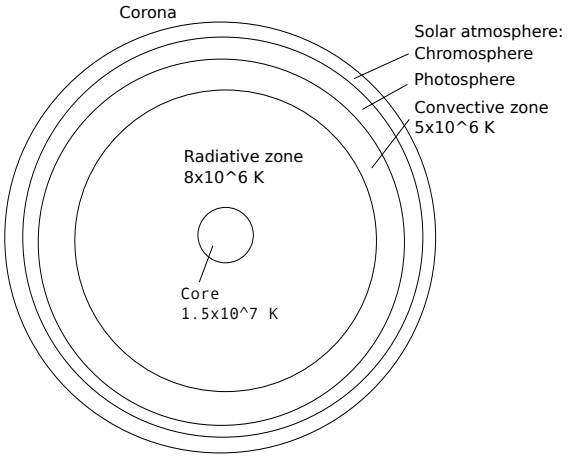

Figure 1: Structure of the Sun.[104]

The next layer from the radiative zone is the convective zone. This layer functions like a liquid warmed from the bottom. This means that heating from the inner Sun leads to convective instability. In this case warm matter rises up, cools down and sinks down again. This up-down movement in combination with the Sun's rotation causes an electric current, that in turn creates the Sun's magnetic field. Thus, the Sun's dynamo is not situated at its core. The temperature is around $5x10^6$ K. After the convective zone is the atmosphere. The Sun's atmosphere has three distinct parts. Most of the sunlight comes from the photosphere, which is the lowest of the layers. The temperature of the photosphere is around 6600 K at its inner boundary and around 4300 K at its outer boundary. The next layer outward is the chromosphere. Its density is so low that light from the photosphere goes through it. After the chromosphere comes the outermost layer of the Sun, the corona. The solar wind originates from here. Temperature counterintuitively rises in the upper regions of the corona. The reasons for this are unclear. Many solar observations make use of the coronagraph. It works by having a disk in front of the Sun itself thus allowing measurements to concentrate on imaging the corona. Coronagraphs were invented in the 1930s and they have been widely adopted.[126]

Solar activity manifests itself through different phenomena of which easiest to spot are sunspots. These can be seen even with the naked eye, which explains the sunspot observations from as early as the 17th century. The dark center of the

sunspot is called the *umbra* and the lighter outer part is called the *penumbra*. The dark color is the result of a 1500 K lower temperature than the surrounding area. The sunspot is cooler than the surrounding environment because its magnetic field prohibits convection. Sunspot numbers vary in cycles of roughly 11 years.

Prominences are seen as thin, dark filaments in Hα pictures of the Sun's surface. Hα is a hydrogen spectral line used extensively in stellar astronomy. Prominences are huge vertical sheets of plasma that are much colder and denser than the surrounding environment. They are essentially huge flux-tubes, turning very slowly possibly due to Coriolis force. The temperature in prominences is as high as 10000 to 20000 K.

Flares are eruptions that develop from prominences. A prominence and the overlaying magnetic area (called *arcade*) rise slowly due to instabilities. The magnetic field lines below slowly stretch and start to reconnect. Reconnection releases energy explosively and causes the flare phenomenon. Flares release large amounts of energy stored in the magnetic field in a very short time.

A *Coronal mass ejection(CME)* is a massive solar eruption. These are related to flares, though flares can also occur on their own. In a CME a cloud of magnetic particles is ejected from the Sun. Shock waves travel with the cloud, accelerating the particles. CMEs cause various disturbances on the Earth, such as geomagnetic storms.[95][104][102]

Coronal holes are regions of extremely low density in the solar corona. They appear within 60 degrees of latitude from the solar equator. They are characterized by weak and diverging magnetic field lines and the chromosphere beneath is extremely quiet. Coronal holes are a source of fast solar wind and possibly also slow solar wind.[7]

Coronal dimmings are usually observed as decreases in soft X-rays and Extreme Ultraviolet (EUV) data. The underlying cause of these dimmings is currently unclear. The two most accepted causes are a density depletion caused by an evacuation of plasma or a change in the bulk plasma temperature. These events could possible be used to predict CMEs.[85][173][143]

Active regions are regions on the Solar surface which have a potential to produce space weather disturbances. By the National Oceanic and Atmospheric Administration (NOAA) definition active regions and sunspots are synonymous, but by other definitions active regions are candidates for producing sunspots. Active regions are caused by enhanced magnetic fields and they are bipolar. NOAA maintains a sequential numbering system for active regions.[143]

2.2 Solar wind

The solar wind is a constant stream of ionized particles that flows out from the solar coronal holes to the rest of the heliosphere. Coronal holes are magnetically open regions. Active processes, such as flares, allow plasma to escape from the surface of the Sun. The solar wind is caused by the large difference in gas pressure between the corona and interstellar space. The solar wind itself is made up of mostly electrons and protons, but some Helium atom nuclei are also present. The solar wind velocity is around 800 km/h in the Sun's polar region, 300 km/h in the equator and 500 km/h

near the Earth. Solar wind magnetic field is called the Interplanetary Magnetic Field (IMF). Most of the space weather phenomena are related to IMF orientation and strength and there are several instruments dedicated to measuring it.[95][104]

Interplanetary Coronal Mass Ejections (ICME) are the interplanetary counterparts to Coronal Mass Ejections (CME). Common plasma signatures of ICMEs are counterstreaming electrons, low proton and electron temperature, strong magnetic fields, low plasma beta and smooth field rotation. Plasma beta is the ratio of the thermal pressure (NkT, N is the number of particles, k the Boltzmann constant, T the absolute temperature) to the magnetic pressure($B^2/2\ \mu_o$, B is the magnetic flux, μ_o the vacuum permeability). Thermal pressure shows the correlation between pressure and temperature. Magnetic pressure is the energy density of the associated magnetic field. ICME occurrence is highest at the solar maximum.[187][101][102]

Shocks are formed when plasma flow and magnetic field interact. Within the solar system there are shocks in front of all the planets as well as their magnetotails. Shocks are also present in the solar corona and solar wind. Inside shocks plasma and field go through dramatic changes in density, temperature, field strength and flow speed.[104][102]

High-Speed Stream (HSS) or High-Speed Plasma Stream is defined as a large increase in the solar wind velocity lasting from several days to weeks. Exact definitions vary, but generally a velocity of 450-500 km/s or an increase of 150 km/s lasting for several days is required. Other signs of HSS are increased ion density and/or rapidly varying magnetic field.[116][171][17]

Alfven waves are low-frequency traveling oscillations of ions and magnetic field in a plasma. They transport energy rapidly through the corona to the lower atmosphere of the Sun and originate from reconfiguration of magnetic fields. They are present in the solar wind and are related to other solar phenomena, such as solar active regions.[6][84]

Corotating Interaction Regions (CIR) are co-rotating structures of solar wind flow. They are produced when high-speed solar wind runs into slower plasma ahead. When the flow pattern of solar wind originating from the Sun is roughly time-stationary, these two compressed regions form a spiral in the solar equatorial plane. This flow pattern corotates with the Sun, giving the phenomenon its name. The structures form in the inner heliosphere and they are well formed at the Earth's orbit. [76]

Steady Magnetospheric Convection (SMC) is a phenomenon in the magnetosphere; a mode of response to solar wind coupling. It is characterized as convection lasting for longer than a typical substorm recovery phase. Three conditions are needed for classification as steady magnetospheric convection. The AE index must be more than 200 nT; a geomagnetically disturbed time. The rate of change of AL must be more than -25 nT/m, indicating no substorm expansion. Geomagnetic indices are discussed later in this chapter. Finally these conditions must persist for more than 90 minutes to guarantee that substorm recovery phases have ended. As the name implies, the solar wind and the magnetotail plasma flow is unusually steady during this phenomenon.[122]

Continous Magnetospheric Dissipation (CMD) is a magnetospheric mode where

the solar wind plasma continously flows via the magnetotail towards ionospheric altitudes without storage to the magnetotail lobes. For CMD the plasma sheet convection is not expected to be steady, but turbulent intervals are allowed.[172][94]

Sawtooth events are a magnetospheric phenomenon that are identified as large-amplitude, quasiperiodic oscillations of the energetic particle flux. These oscillations are strongest in the proton channels, they occur typically during storm intervals and periods of enhanced ring current, have a quasiperiodicity of 2-4 hours and are usually driven by moderate to strong ($B_z \approx$ -10 nT) and continuously southward Interplanetary Magnetic Field conditions. The term "sawtooth" comes from the fact that the flux versus time profile plot resembles the teeth on a saw blade.[82]

2.3 Magnetosphere

The magnetosphere is defined as a region where the Earth's magnetic field dominates the flow of charged particles instead of the Sun's magnetic field. Different regions around the magnetosphere are illustrated in Figure 2. The magnetosphere's distinct shape is created by the interaction of solar wind and the Earth's magnetosphere. Even though the name would suggest a spherical structure, the magnetosphere actually has a tail-like composition. The magnetosphere is divided into day- and nightside, with the spherical dayside facing the Sun. The nightside has a distinct tail-like shape due to the interaction of the magnetopause and the solar wind.

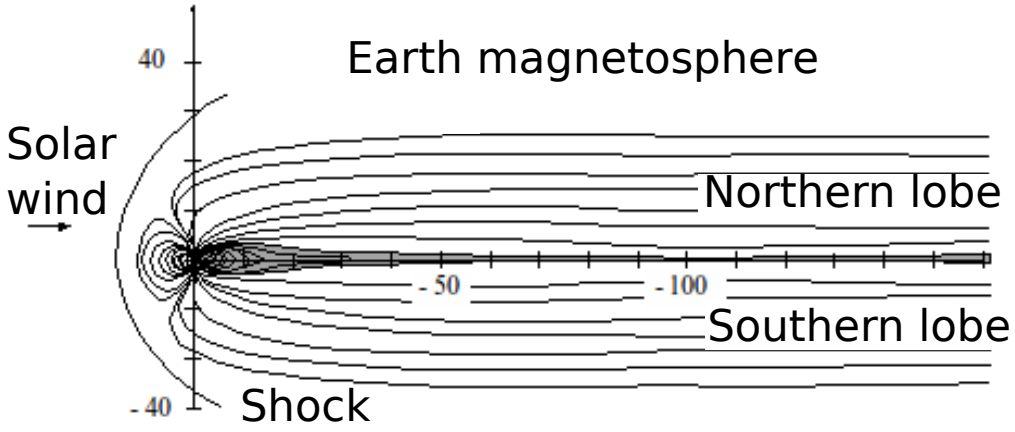

Figure 2: Structure of the magnetosphere [52].

The first line of contact between the solar wind and the Earth's magnetic field is called the bow shock. Here the solar wind plasma encounters the Earth's magnetic field, resulting in a collisionless shock. This slows down the solar wind to subsonic speeds and creates the distinct shape. The bow shock nose is about 14 R_E from the Earth. Between the bowshock and magnetopause lies the magnetosheath. It is a turbulent region about 3 R_E wide that features high particle flux.

The final boundary between the solar wind and the Earth's magnetosphere is the magnetopause. It separates the geomagnetic field and plasma of primarily terrestrial origin from solar wind plasma. These areas do not remain at a fixed distance from

the Earth because their exact positions vary with solar activity. All planets that have a magnetic field around them also have a magnetosphere.

Magnetic reconnection is an important concept in the magnetosphere. Magnetic reconnection is a process in which the magnetic topology of two different plasmas are rearranged as they collide with each other. Magnetic energy is converted to kinetic energy, thermal energy and particle acceleration. Magnetic reconnection plays a large part in magnetosphere energy transport. There are numerous electric currents in the magnetosphere. *Chapman-Ferrano currents* flow in the magnetopause. *Tail currents* flow in the magnetosphere tail section. The inner magnetosphere features *ring currents* that flow westward in circles approximately centered around the Earth. *Birkeland currents* connect to the tail and magnetopause boundary layer. Radiation belts circle the Earth in orbits from 1000 km to geocentric orbits of around 6 R_E. These boundaries are not constant and vary with the Sun's activity. The Earth's dipole field acts as a magnetic bottle, trapping the particles. There are essentially three radiation belts: one proton belt with energies above 10 MeV and two electron belts with energies in the range of keV and MeV.[104][102]

The strengths of geomagnetic disturbances caused by solar originated structures are measured with different **geomagnetic indices**. Indices are calculated from constant measurements of numerous magnetic observatories. There are several indices currently in use around the world, many of them having been calculated since the 19th century. In addition to geomagnetic indices, sunspot and substorm numbers are also calculated and catalogued.

The *Dst index* monitors the magnetic storm level at the equator. Dst is the averaged horizontal component of the geomagnetic field from mid-latitude and equatorial magnetograms from all over the world. Negative Dst index values indicate a magnetic storm is in progress and more negative values mean more intensive storms. Dst has a resolution of 1 hour. Figure 3 is an example plot of the Dst index.

The *Kp index* is derived from several ground-based magnetometers. Kp index values range between 0 and 9 and they are used by NOAA to issue geomagnetic storm warnings. The index represents a 3-hour averaged value of planetary geomagnetic activity and it has been calculated since 1932. Local Kp indices are developed by several space weather centers and observatories around the world.

The longest existing geomagnetic index, the *aa index* was measured originally from Greenwich and Melbourne. From 1926 to 1959 the British part was Abinger and currently it is Hartland. Australian measurements were taken in Toolangi from 1920 to 1979 and currently they are conducted in Canberra. The aa index is derived from eight 3-hourly readings and the data are available from 1.1.1868. It describes the overall geomagnetic conditions at 3 h resolution.[20]

The *AE index* measures the intensity of the auroral electrojet current system. It is available in one-minute resolution and has been calculated since 1978. The AL and AU indices are meant to measure westward and eastward electrojet activity respectively.

Geomagnetic data collections are combined by several iniatives to better consolidate the information. One of the earliest is INTERMAGNET. Approximately half of the world's geomagnetic observatories belong to INTERMAGNET. INTERMAG-

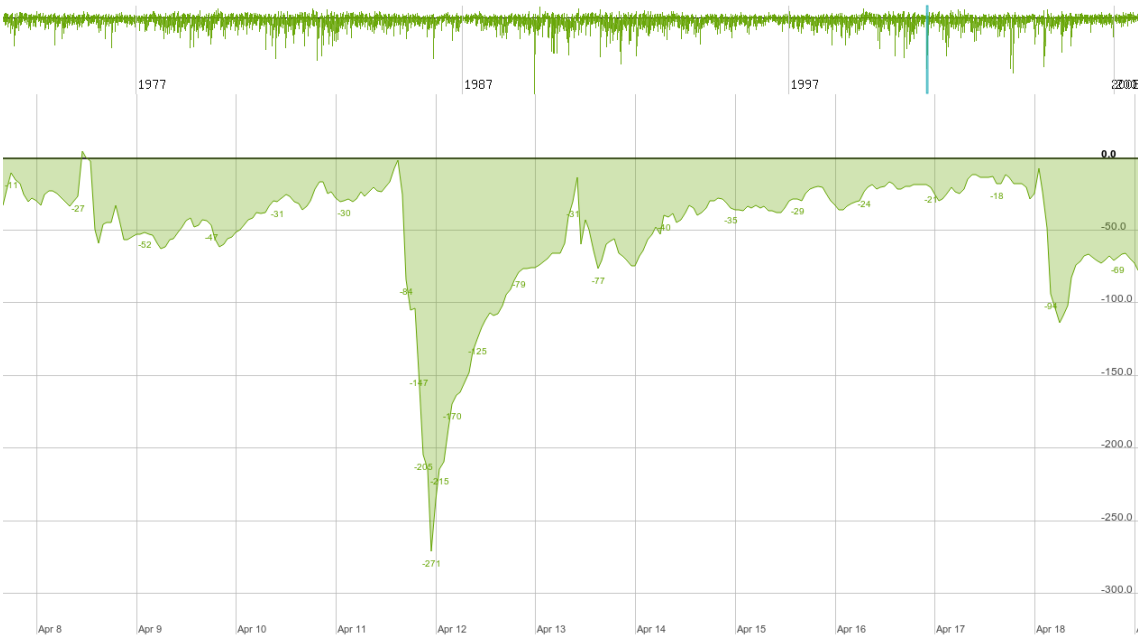

Figure 3: Dst index example plot from Substorm Zoo.[168]

NETs mission is to have geomagnetic observatories adopt standardized practices and equipment for production of geomagnetic data. Data handling is coordinated through data collection centers known as Geomagnetic Information Nodes (GINs). There are six of these located around the world: Edinburgh, United Kingdom, Golden, USA, Kyoto, Japan, Ottawa, Canada and Paris, France. Another traditional iniative is the World Data Archive for Geomagnetism. Based in Japan, this observatory is responsible for calculating the Dst and AE indices. [98][168][178]

2.4 Ionosphere

The ionosphere is part of the upper atmosphere around the altitude of 100 km. The ionosphere is situated below the magnetosphere and above the neutral atmosphere. An ionosphere is produced around each celestial object with an atmosphere. As the name suggests, ionization happens in the ionosphere. Ionization means a situation where an atom or molecule is converted to an ion, by addition or removal of charged particles. The ionizing particles originate from the Sun, magnetosphere, the ionosphere itself or the rest of the galaxy as cosmic rays. The flow of particles into the ionosphere is called precipitation. Radio waves propagate in the ionosphere, thus space weather affecting the ionosphere influences radio communication. The conditions of the ionosphere can be measured using, for example, magnetometers, auroral cameras and incoherent scatter radars. [102][104]

2.5 Space weather and space climate

Space weather is a phenomenon affecting the near-Earth space. Its area of effect ranges from the edges of the heliosphere all the way down to the Earth. Space

weather manifests itself in numerous different ways, the best known and only visual sign being the Aurora. Almost all space weather phenomena have their basis in solar-terrestrial interactions. Space weather is driven by Ultraviolet (UV), Extreme Ultraviolet (EUV), X-rays emitted from the Sun, fast particles emitted from solar flares, galactic cosmic rays and the solar wind and its magnetic field. These phenomena interact with the terrestrial magnetosphere and atmosphere in multiple ways, creating a highly dynamic system.[140]

Space weather effects can be classified e.g. by separating the effects according to the domain. This is called domain-oriented classification, and it was used in the report "Space weather effects catalogue"[106]. Domain-oriented classification has the following areas of effect: interplanetary space, magnetosphere, ionosphere, neutral atmosphere and the Earth's surface.

Effects in *interplanetary space* are: solar radiation storms, radio blackouts, cosmic rays, spacecraft charging and micrometeoroids. Systems operating at this area are spacecraft and their possible human occupants.

1. Solar radiation storm

   Solar radiation storm refers to a situation where the Sun emits a stream of high energy particles. Acceleration of these particles is mainly caused by flares and shock waves in the corona and interplanetary space. Solar radiation storms consist mostly of accelerated protons but electrons and neutrons are also present. Solar Energetic Particle (SEP) events refer to a similar situation of a high energy particle stream. The terms are sometimes used interchangeably. NOAA operated space weather services use the term Solar Radiation Storm to describe high particle flux. NOAA space weather scales determine the solar radiation storm level according to the flux of 10 MeV particles. The exact definition is particles in second through steradian of cm^2. The most dramatic SEPs occur only once every 10-20 years, making them rather difficult to study. Low level SEPs occur several times per year on average.[155]

   One of the effects on spacecraft systems caused by these particles is Single Event Upsets (SEU), sometimes called Single Event Effects. These are errors induced in electronics by charged particles. These effects can be either permanent or temporary. Effects include noise in measurement devices, changes in memory slots, unexpected behavior in software and other unwanted activity. Error correcting algorithms can be implemented to mitigate the problem. Within the Earth's magnetic field SEUs are mostly caused by trapped protons. Outside the Earth's magnetic field the main cause is cosmic rays. SEUs are a very common, daily occurrence on satellite missions.[63][25]

2. Radio blackouts

   Solar radio bursts originate from solar flares. A large number of electrons are accelerated from the flare which interact with the surrounding plasma and magnetic field. Energy is converted into ordinary-mode electromagnetic radiation at a frequency equal to the local plasma frequency. This electromagnetic radiation is the solar radio burst. Typically the bursts last from tens of seconds

to a few hours. In the worst case scenario all radio communication on the Sun facing side of the Earth is blocked for a number of hours. Solar radio bursts cause increases in the spectral noise density, lowering the carrier-to-noise ratio of the signal. NOAA space weather scales determine radio blackout severity by measuring the solar flare class and particle flux.[30][51]

3. Cosmic rays

   Cosmic rays are high energy particles that originate from outside the Solar System. They consist mostly of protons (90 %) and fully ionized nuclei of helium (10 %) but heavier nuclei are also present. Their energies vary between 10^8 - 10^20 eV. The particles originate from supernovas of massive stars. Cosmic rays produce secondary particles when they collide with the atmosphere. These can be used to detect them. Cosmic rays can also cause Single Event Upsets (SEU) and spacecraft charging.[95]

4. Spacecraft charging

   Surface charging is one of the major effects of space weather on spacecraft. Since a spacecraft in space is constantly bombarded by charged particles, there are numerous positive and negative currents running through its hull at all times. Electrostatic discharges are also part of surface charging effects. Surface charging can be defined by the current balance equation (see Equation 4 and Table 2).

$$I_T(V) = -I_E(V) + (I_I(V) + I_{SE}(V) + I_{SI}(V) + I_{BSE}(V) + I_{PH}(V)) \quad (4)$$

Table 2: Surface charging parameters.[65]

Parameter	Description
V	Surface potential relative to space
I_T	Total current to spacecraft surface at V. This is 0 at equilibrium when all the current sources balance
I_E	Incident negative electron current
I_I	Incident positive ion current
I_{SE}	Secondary emitted electron current due to I_E
I_{SI}	Secondary emitted electron current due to I_I
I_{BSE}	Back scattered electron current due to I_E
I_{PH}	Photoelectron current

Surface charging can cause several forms of anomalous behavior. Charging can degrade thermal properties of materials and cause failures in solar arrays. Charges can also build up unevenly on the spacecraft surface, and when these charges discharge the resulting transients can cause numerous errors in the spacecrafts electronics. Surface charging can be mitigated through proper spacecraft design.[65][9]

Another spacecraft charging effect is internal charging. This refers to a situation where electrical charge accumulates on the interior of ungrounded metals, or inside dielectric components within the spacecraft. Electrons with an energy of of 500 keV are considered the primary cause of internal charging. Electrostatic Discharges (ESD) caused by these electrons are very close to spacecraft electronics. The problem of spacecraft charging will most likely get worse in the future. Economic factors are leading to less and less shielding, lighter structures and smaller electronics on spacecraft which make matters worse.

The Spacecraft Charging AT High Altitude (SCATHA) program was essential in understanding the spacecraft charging phenomenon. Satellite P78-2 (SCATHA) launched in 1979 was used to study the charging phenomenon, the environment where it occurs and for finding possible ways of mitigating the problem. The satellite's instruments measured, for example, the surface potential of various materials, electric and magnetic fields, electron and ions counts and solar absorptance.[60]

5. Meteoroids and micrometeoroids

   Meteoroids and micrometeoroids are small celestial objects, originating from the asteroid belt, asteroid collisions and comets. Micrometeoroids are smaller than asteroids, but the line between these two is not clearly defined. 10^5 meteoroids impact the Earth each day. Larger meteoroid impacts can cause catastrophic failures in space based systems. Smaller meteoroids and micrometeoroids generally degrade the optical and thermal properties of affected materials. [95][106]

The *Magnetosphere* contains spacecraft and possible human occupants, but the space weather phenomena there are somewhat different than in interplanetary space. The magnetosphere itself provides safety against several interplanetary disturbances.

1. Magnetic storm

   A magnetic storm is a period of magnetic disturbance in the Earth's magnetosphere where a ring current is forming at the equator. A magnetic storm is best characterized by the weakening of the Earth's magnetic field horizontal component (H). The storms consist of three distinct phases: initial phase, main phase and recovery phase. Typically a sudden commencement starts the initial phase. Interplanetary Coronal Mass Ejections (ICME) and zones of fast solar wind hitting the Earth are the usual causes of magnetic storms. Magnetic storms are usually called geomagnetic storms when their effect reaches the Earth. Magnetic storms' severity can be measured by many different activity indices, for example Dst and Kp.[104][102]

2. Space debris

   Space debris covers a wide variety of man-made objects and pieces of those objects. These range from aluminium oxide dust particles, instrument covers, nuts and bolts to rocket upper stages. "Zombie" satellites, which have

stopped working due to system failures or lack of fuel, are also effectively space debris. Space debris sizes vary from 0.001 mm to 10 m in diameter. Smaller debris poses a threat to solar arrays, optical surfaces and detectors. Larger debris threatens even large scale constructs such as the International Space Station (ISS). Space debris can be mitigated by planning end-of-mission disposal of the spacecraft, such as moving it to a lower orbit where it will disintegrate in the atmosphere. Collisional cascading of space debris objects can further compound the issue. This type of situation is known as the Kessler Syndrome.[63][99]

Ionospheric space weather effects include e.g. scintillation, ionospheric absorption and substorms.

1. Scintillation, Ionospheric absorption

   The ionosphere can become turbulent and develop irregularities of electron density. These irregularities and turbulences can scatter radio waves in the frequency range of 1000 MHz - 4 GHz. The relative motion between a satellite, the ionosphere and the receiver causes the signal to exhibit temporal fluctuations of phase and intensity. These are called scintillations. Ionospheric storms also cause situations where radio waves are absorbed in the ionosphere instead of propagating normally. Blackouts are also possible where degraded signal quality can last for several hours.[117][23][16]

2. Magnetospheric substorms

   Substorms are a transient phenomenon where a large amount of solar originated energy is carried into the magnetosphere and further down to the ionospheric altitude of 100 km where the westward and eastward currents are intensified. Despite the name "substorm" they should be thought of as a completely separate phenomenon from magnetic storms. Most of the time substorms occur independently of magnetic storms, but very few magnetic storms are found without substorms. The most obvious manifestation of a substorm is the aurora, though the phenomenon manifests itself in different ways. Substorms have three phases: growth phase, onset of expansive phase and recovery phase. During the growth phase the magnetosphere prepares for the substorm and its end is characterized by the auroral breakup. The largest and brightest auroras are displayed at this time. The next phase is called the expansive phase which typically lasts for about half an hour. The substorm concludes in the recovery phase where geomagnetic disturbances subside. During a geomagnetic storm a new growth phase may begin before the previous storm has subsided, and it is normal for storms to have several sub-onsets before or after the main auroral breakup.[102][104]

3. Aurora

   The aurora (northern lights, polar lights) is the only space weather phenomenon that is harmless to critical infrastructures. Aurora is the optical

manifestation of auroral-particle precipitation and its interaction with the atmosphere. The primary auroral particles are electrons and ions with energies from less than 100 eV up to 100 keV. These particles collide with the atoms and molecules of the Earth's upper atmosphere. Part of the auroral particle kinetic energy is converted into energy stored in the chemically excited states of atmospheric particles. Thus photons of varying wavelengths are released, causing different spectacles of light. They appear at around 80-300 km height, mainly above 55 ° of magnetic latitude. The term auroral oval denotes the roughly oval-shaped bands centered about the north and south magnetic poles where bright aurora and strong magnetic disturbances are observed. There are numerous mentions of aurora in historical records, since the strange looking lights in the sky have always been found fascinating.[102][95]

The *Neutral atmosphere* features mainly commercial aircraft as targets of space weather phenomena.

Space weather affects many areas of airline operations, such as avionic systems, communication, Global Positioning System (GPS) navigation and crew safety through radiation exposure. Principal hazards to humans are from galactic cosmic rays. These particles start interacting with the atmosphere at around 39 km. The radiation dose from these and the secondary particles reach maximum intensity at around 20 km, after which they slowly decrease with altitude. Dosage increases with latitude until reaching a constant level at around 50 ° of latitude. At an altitude of 8 km in temperate latitudes the dosage is typically up to 3 microSieverts (μSv) per hour, but near the equator this is only 1-1.5 μSv. A London to Los Angeles flight typically accumulates approximately 6 μSv per/hour. Solar cycle fluctuations affect this by 20 %. The recommended European Union (EU) dose limit is a 5-year average dose of 20 μSv per year. For pregnant crew members the limit is 1 mSV. Solar Energetic Particle (SEP) events temporarily increase the dosage, for example in September and October 1989 SEPs caused a 2 mSv dosage instead of the average of 3 μSv. Previously described Single Event Upsets (SEU) and communication and GPS outages also affect airline operations.[92]

The *Earth's surface* features mainly effects caused by induced currents.

Geomagnetically Induced Currents (GIC) are the most significant space weather effect at the Earth's surface. GIC are generated when space weather disturbances cause rapid variations in the Earth's geomagnetic field. These variations induce electric currents into power transmission lines and other similar long structures, such as oil and gas pipelines and railways. GICs can cause transformer heating, increased power consumption and Alternating Current (AC) harmonics.[22][181]

2.6 Extreme space weather conditions

To put the space weather parameters discussed here into perspective, description of extreme space weather conditions is given. "Quiet" values are also provided as reference. Table 3 gives examples of these values. Two major space weather

events from the past provide most of the extreme values listed below. First is the Great Magnetic Storm of August-September 1859, also known as the Carrington Event, and the second is the Halloween storm series. Space weather effects during the Carrington storm were limited to spectacular auroral displays, problems in the telegraph network and off-the-scale measurements at geomagnetic observatories. If the Carrington event had taken place during the current digital age, damage on satellite and power systems would have been significant. It is thus quite vital to understand the limits of extreme space weather.[12]

A major space weather event experienced during the space age was the Halloween storm of 2003. It began on 19.10.2003 as three large and intensive sunspots emerged on the Sun's surface and continued with CMEs and flares until around 7.11. Power grid transformer problems and power outages were reported, astronauts on ISS were ordered to emergency shelters because of the rise in particle flux and a total of 28 different failures were reported on numerous spacecraft, among them the complete loss of the ADEOS-2 satellite.[179]

Table 3: Extreme space weather values.

Variable	largest measured value	theoretical limit	quiet time value
Solar wind velocity	900 km/s	2800 km/s	400 km/s[104]
Flare scale	X30 4.11.2003[36]	X40[36]	-
10 MeV particle flux	4 10^4 pfu[36]	1-3 10^5 pfu[36]	0.3 pfu (proton flux) [88]
30 MeV particle flux	18.8 10^9 pr cm^{-2} August-September 1859 [35]	2-6 $10^{10} pfu$[36]	-
Dst index value	-1160 nT 2.9.1859 [36]	-2500 nT [36]	-32 nT [88]

Data from pre-satellite era space weather events can be obtained from geomagnetic observations that have been made regularly from the 19th century onwards.[35] The largest values from Carrington Event have several estimates, since measurements from the 18th century are not uniform. Estimates vary between 625 and 1760 nT.[35][36] The largest GIC current measured is from Sweden on 6.4.2000 with a value of 300 A. The largest time derivative values of ground magnetic fields have been measured as 2500 nT/min during July 1982. Theoretical limits for these values are difficult to estimate.[182]

3 Space weather instruments

3.1 Ground-based instruments

3.1.1 Fluxgate magnetometer

Magnetometers are the most widely used space weather instruments both on the ground and in space. They can be broadly divided to scalar and vector magnetometers. Scalar magnetometers measure only the strength of the magnetic field, while vector magnetometers also measure the direction of the field.

Majority of the systems covered in this thesis use fluxgate type magnetometers. Their use is widespread in both ground and space based applications. Fluxgate magnetometers were developed during the 1930s. Initial applications were in the field of airborne magnetic surveys and submarine detection during World War II. Later on they were applied to airborne, seaborne and underwater geomagnetic studies, mineral prospecting and magnetic measurements in outer space. Despite being rather old, fluxgate magnetometers are still widely used due to their relative simplicity, economy, reliability and ruggedness.[75]

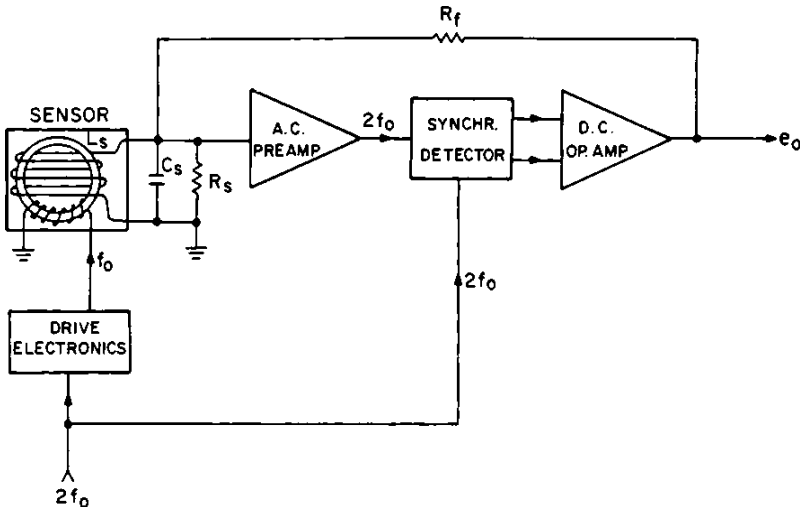

Figure 4: Circuit diagram of a very simple fluxgate type magnetometer[4]

There are numerous different configurations available for fluxgates, but the basic principle is that the ferromagnetic core (or cores) is driven to saturation by a periodic current. This creates a magnetic field, that induces a current into the coil. The asymmetry between the original current and the induced current can be measured and thus the magnetic field determined. Figure 4 is a circuit diagram of a very simple fluxgate type magnetometer. Figure 5 shows a Danish observatory magnetometer.[145]

Fluxgates can be divided into parallel-gated and orthogonal-gated types. Parallel types have the magnetizing field parallel to the external magnetic field, orthogonal sensors have their field orthogonal to the external field. Other types include single-core, two-core and ring-core configurations. Because of the relation to the magnetic field direction fluxgates are vector magnetometers.

Figure 5: Danish FGM-FGE fluxgate magnetometer, one of the most widely used observatory magnetometers in the world.[49]

3.1.2 Pulsation magnetometers

Pulsation magnetometers are used mainly by Sodankylä Geophysical Observatory. They are used to detect pulsations and other rapid changes in the magnetic field. Pulsation magnetometers are significantly cheaper than fluxgate magnetometers, but they are not suited to measure longer periodicities. Pulsation magnetometers consists of three induction coils. These are pointed to magnetic north, 90 ° East from North and the third is used to measure vertical directions.[149] The induction coils are built from two 9750 turn solenoids. The core is Fe-Ni bar 1000 mm long and in 20 mm diameter. LEMI-magnetometer manufacturer Lviv Center of Institute of Space Research has provided the metal bars. Signals from all three coils are amplified and filtered by individual preamplifier boxes for all coils. 5-pole Chebysev and 10-pole Bessel filters are used in series. Pulsation signal is digitized by 16-bit analog-to-digital (AD) converter and sampled with 40 Hz. AD-unit internal clock is synchronized with GPS pulse-per-second signal. Data from AD-converters are stored in hourly files in MATLAB compatible format. Sodankylä Geophysical Observatory maintains a network of six pulsation magnetometer stations in Sodankylä, Kilpisjärvi, Ivalo, Rovaniemi, Oulu and Nurmijärvi.[157][141]

3.1.3 Proton, Overhauser and other magnetometers

The most common scalar magnetometer is the proton magnetometer, or proton precession magnetometer. It is based on the phenomenon of magnetic resonance. A sample of liquid rich in protons surrounded by a coil is magnetically polarized

to align its magnetic moment in a given direction. This sample is then allowed to "relax" in the presence of an external magnetic field. The protons that have been aligned parallel to the polarizing field will precess around the ambient magnetic field and induce an alternating current (AC) signal in the polarizing coil. The signals frequency is called the Larmor frequency (Equation 5).

$$f(Hz) = \tau_p B/(2\pi) \tag{5}$$

B is the magnitude of the external field, τ_p is the gyromagnetic ratio of the proton, defined as the ratio of the proton's magnetic moment to its spin angular momentum. The value of $(2\pi/\tau p)$ is known from quantum mechanical principles, and thus the external field can be measured. Structurally proton magnetometers consist of a tank for the liquid sample, polarizing/sensing coil surrounding the sample, an AC amplifier and a duty cycled current source. Proton magnetometers are very accurate but the liquid tank required is relative large and heavy. They are used mainly in observatories to calibrate other magnetometers.[4]

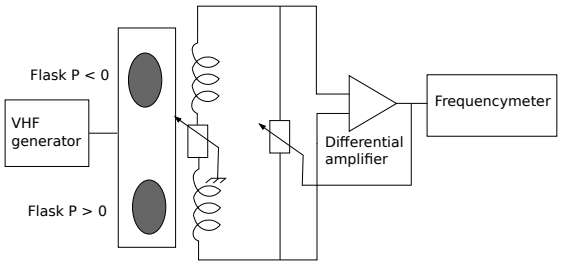

Figure 6: Overhauser type magnetometer circuit diagram.

Overhauser magnetometers use the same magnetic resonance phenomenon as proton magnetometers. Overhauser magnetometers use the dynamic nuclear polarization (DNP), where the moments of protons and electrons are linked together. In this way the spin magnetic polarization requires much less energy than in proton magnetometers. DNP requires a liquid that has lots of protons and free radicals. Figure 6 shows the circuit diagram of an Overhauser magnetometer. Overhauser magnetometers require much smaller tanks than proton magnetometers, making them more feasible to space based solutions. Their main purpose is to provide calibration references for other magnetometers.[50][5]

Induction coil magnetometers (also known as search coil magnetometers) are used to measure magnetic field pulsations. The sensor is a coil where voltage is induced. This voltage correlates to the number of coil windings and strength of the magnetic flux inside the coil. Both air coils and ferromagnetic core coils are in use. The induction is dependent upon the direction of the magnetic flux and thus induction coil magnetometers are vector instruments.[176][5]

3.1.4 Riometers

Riometers, also called relative ionospheric opacity meters, are very sensitive radio receivers continuously measuring the cosmic noise level incident at the Earth's surface. This received noise level is affected by the level of absorption in the ionosphere, thus allowing measurements of ionospheric conditions. Most riometers in use have an antenna with a wide beam. This results in the absorption measurements being averaged over a large area. The first riometers were developed during the late 1950s.[23][117] There is a riometer chain in Finland, the Finnish Riometer Chain, maintained by Sodankylä Geophysical Observatory, where measurements started in 1965.[157]

3.1.5 All-sky cameras

All-sky cameras are specialized devices for photographing auroras which have been used since the 1950s. All-sky cameras have spherical mirrors, allowing the cameras lens to cover nearly the whole night sky with 180 ° arc. The camera is placed under a heated dome, so that the dome does not freeze. All-sky cameras photograph the night sky automatically, thus producing massive amounts of data. Finnish Meteorological Institute has conducted regular auroral photography using all-sky cameras since the Geophysical year of 1957. Figure 7 shows a Finnish Meteorological Institute all-sky camera.[130][165]

Figure 7: Finnish Meteorological Institute all-sky camera at Sodankylä in the 1980s.[130]

3.1.6 Incoherent scatter radars

Incoherent scatter radars are important tools for studying the ionosphere. Incoherent scatter radars work by beaming a radar signal to the ionosphere. There the signal is scattered, and the resulting signal is measured. The scattering happens

of 'ion-acoustic' waves, created by the thermal motion of ionospheric electrons. If the complete scattered signal is measured with adequate signal-to-noise ratio up to eight parameters of the ionosphere can be measured. These are electron density, electron temperature, ion temperature, ion mass, plasma drift velocity, ion-neutral collision frequency, electric current and part of the spectrum of suprathermal electrons. Suprathermal refers to particles that are very energetic, or generated by very energetic particles. The height where a particular scattering comes has to determined. This can be done by sending a short pulse and measuring the time delay between transmission and reception. The pulse has to be much higher than the plasma frequencies encountered in the atmosphere. Another way is to transmit a signal vertically upwards by one antenna, and then receive the scattered signal by a second antenna. The former method is more common because it requires only one antenna. Incoherent scatter facilities require a powerful radar transmitter, at least one large antenna, low-noise receivers and powerful data-processing equipment. European Incoherent Scatter Scientific Association (EISCAT) is an example of an incoherent scattering radars and will be discussed in Section 4.1.4.[19]

3.1.7 Neutron monitors

Neutron monitors provide continuous ground-based recordings of the hadronic component in atmospheric secondary radiation. This is primary related to cosmic rays. Primary particles not rejected by the geomagnetic field enter the atmosphere and undergo multiple interactions that result in showers of secondary particles. These secondary particles can reach ground level and they can be detected by neutron monitors (NM). These secondary particles include neutrons, protons, muons and pions.

A neutron monitors consist of a neutron sensitive proportional tube surrounded by moderator material, a lead producer and an outer moderator. These are used to detect near-thermal neutrons produced locally from interacting incident particles. Proportional tubes are filled with either $^{10}BF_3$ or ^{3}B gas that respond to neutrons by exothermic reactions. Surrounding these proportional tubes is a moderator which serves to reduce the energy of neutrons, increasing the probability of an absorption inside the counter while reflecting low energy neutrons. The moderator is surrounded by a lead producer that provides a thick large-nucleus target for inelastic interactions where secondary neutrons are produced. This lead is surrounded by an outer moderator, which serves to contain low energy neutrons produced in interactions within the lead as well as to keep unwanted low-energy neutrons away from the detector. The Earth's atmosphere must be closely monitored at each station to ensure accurate measurements, since meteorological changes can affect the counting rate. For example, pressure and temperature changes and high winds can affect the passage of particles through the atmosphere.[33]

3.2 Spaceborne instruments

3.2.1 Magnetometers

Magnetometers in space are used to measure magnetic fields of planetary bodies, Interplanetary Magnetic Field and for navigational purposes. Space-based magnetometers present unique challenges to the measurements. Temperature varies greatly from near absolute zero to hundreds of degrees Celsius depending on the satellites position and orientation in relation to the Sun. Space-based magnetometers are also one of the few tool available for remote sensing of the deep interiors of planets. Space-based magnetometers also have to cope with a large dynamic ranges of measurements. For example, the Interplanetary Magnetic Field (IMF) may be as low as 0.05 nT at around Uranus or Neptune, while Jupiter's north magnetic pole field is more than 1 400 000 nT. Scalar magnetometers are often used as absolute calibration tools in space applications. They are larger and heavier than vector magnetometers and typically consume much more power. Fluxgate magnetometers are the most common scientific instrument on board space platforms. Figure 8 gives an example of a spaceborne fluxgate magnetometer.

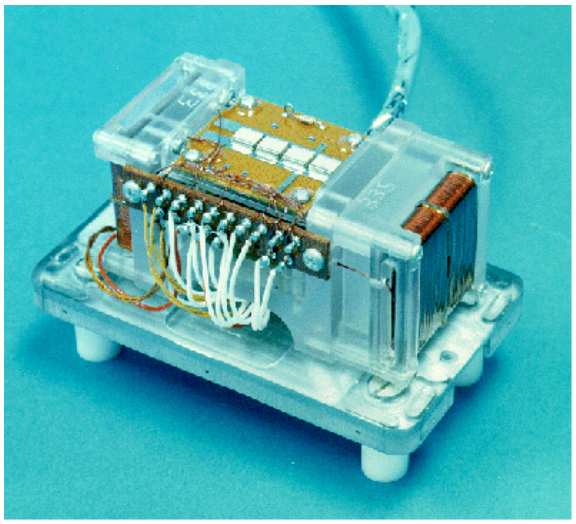

Figure 8: MFI fluxgate magnetometer from WIND satellite.[123]

In addition to scientific measurements, space-based magnetometers serve an important function in navigation. They allow a reliable, simple and cost-effective solution for spacecraft orbit and attitude determination. The Earth's magnetic field provides a convenient "natural" frame of reference for the measurements. Magnetic sensors are not as accurate as inertial sensor-based systems, but they are significantly more reliable, simpler and cheaper.

The spacecraft itself distorts magnetometer measurements with its own magnetic field. These fields have to be minimized and taken into account during spacecraft design to ensure successful measurements. One solutions is to place magnetometers at the end of a long boom stretching out from the satellites main body. Even more sophisticated solution is to use two different booms. This allows calculations to rule

out the satellites own magnetic field. Large solar arrays have doubled as booms for magnetometers in some cases, such as the Mars Global Surveyor. This however requires that the currents in the array and solar cells are taken into account when conducting the measurements. Twin boom setup also provides redundancy in case one of the instruments fail.

Magnetometer types mentioned in the ground segment of this thesis (fluxgate magnetometer, proton magnetometer, Overhauser magnetometer) are also in use in space, with the exception of pulsation magnetometers. In addition optically pumped magnetometers have found a use in space based applications. They consist of a discharge lamp, gas cell and a solid state photodetector. The discharge lamp irradiates one end of the gas cell through a system of filters and polarizers. At the opposite side of the gas cell, the photodetector measures the intensity of the incident light. The electrons in the gas cell will precess about the axis of the external magnetic field at the Larmor frequency of the element chosen for the magnetometers gas. The output from the photodetector is an AC signal at the Larmor frequency (Equation 6), τ_e is the electron gyromagnetic ratio for the chosen gas element.

$$f = \tau_e B/(2\pi) \tag{6}$$

Optically pumped magnetometers allow higher time resolution measurements than proton precession instruments. They also have a very high resolution because of the small frequencies involved. Vector helium magnetometers are a variant of the optically pumped magnetometers. They feature a Helmholtz coil around the gas cell, which causes sweep field to be generated to the photodetector output. These can be used to derive vector information about the external magnetic field, thus turning the instrument from a scalar instrument to a vector instrument. [4][63]

3.2.2 X-ray instruments

In space weather applications Röntgen radiation (X-ray) telescopes are mainly used to study the Sun and its active phenomena. X-ray astronomy covers wavelengths from 10-0.01 nm. Famous X-ray telescopes include American Chandra and European XMM-Newton. X-ray telescopes designed exclusively for solar observations include Japanese Yohkoh and Hinode and the European Solar and Heliospheric Observatory (SOHO). Unlike normal telescopes, X-ray radiation does not reflect from normal mirrors. Thus X-ray telescopes have to use grazing reflection for measurements. This means that the X-ray radiation hits a paraboloid mirror in a very gentle curve, reflects further to a hyperboloid mirror and then to the focal plane. X-ray telescope mirrors are insides of slowly narrowing cylinders. Paraboloid and hyperboloid are located at the front and end of the cylinder respectively. This is usually achieved by a series of tubes. Solar X-rays enter the telescope through filters that block most visible and IR radiation. Figure 9 illustrates the basic structure of a X-ray telescope.[109][95]

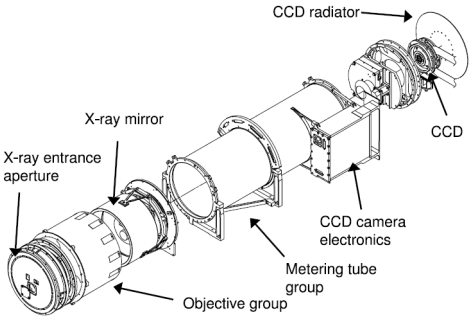

Figure 9: Exploded view of the GOES N Solar X-ray imager[109]

3.2.3 Plasma instruments

Plasma instruments are used to measure different properties of space-born plasma. These include electron and ion density, temperature and velocities. One example of a plasma instrument is the Langmuir probe. Langmuir probes are essentially conductors immersed in plasma with a bias voltage. This bias voltage is varied and the current collected is measured as a function of the voltage. This relationship provides information on the plasma density and temperature. Langmuir probes have been used extensively in space plasma measurements for decades. Figure 10 is a picture of a Langmuir probe. [108]

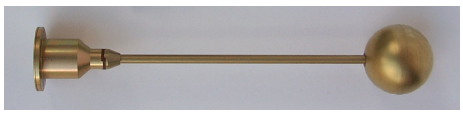

Figure 10: Langmuir probe from Rosetta spacecraft[151]

Specific instruments on board different missions are discussed in Section 4.2.

3.2.4 Electric field measurement devices

Electric field measurement devices can be used to study the plasma environment. This was done on the Cluster mission with the Cluster Electric Field and Wave (EFW) instrument. The instrument consists of 4 spherical probes at the end of long wire booms. Each sphere can measure the average electric field and density between the probes. The Cluster mission is discussed in more detail in the Section 4.2.4. Figure 11 shows space born electric field measurement devices.[79]

3.2.5 Mass Spectrometers

Mass spectrometers determine the mass of atoms or molecules in a given sample. Modern mass spectrometers typically include at least an ion source, a mass analyzer and a detector. The ion source is used to produce ions in the gas phase, the mass analyzer will separate the ions and the detector will count the ions. Additionally a

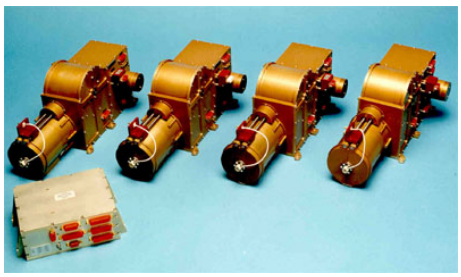

Figure 11: Electric field measurement instrument EFW onboard Cluster satellite. 4 boom units and electronics box are depicted [39]

device is required to introduce the sample to the analyzer. The result of the analysis is the spectrum of the masses of the particles of the sample. Figure 12 shows an example of solar wind observation spectrometer. Mass spectrometers should not be confused with imaging spectrometers, which are also used on space-born platform but for remote sensing purposes. Several mass spectrometers are discussed in Chapter 4.2.[43]

Figure 12: Solar Isotope Spectrometer instrument on board Advanced Composition Explorer satellite.[159]

3.2.6 Electrostatic analyzers

Electrostatic analyzers are instruments that measure charged particle, such as electron or ion, energy distributions. This is achieved by use of electric field that allows passage of particles of a given energy. There are many different configurations available for the plates, such as toroidal and cylindrical setups. Electrostatic analyzers have a long history of usage in space missions. The instrument originates from the beginning of the 20th century, and their basic design has not changed significantly since the 1920s. [8][86][137][121]

3.3 Results and gap analysis

Currently available space weather instruments are capable of adequate measurements of essentially all currently known space weather phenomena. These instruments include numerous types of magnetometers, riometers, all-sky cameras, incoherent scatter radars, neutron monitors, electrostatic analyzers, electric field measurement devices, mass spectrometers, x-ray instruments and plasma instruments. The resolution, coverage and length of the data series is far from sufficient for good space weather prediction, but they are good enough for space weather monitoring. Telescopes are problematic because they are very large, and are thus difficult and expensive to deploy in space based platforms. Current limitations are mainly in the deployment of instruments, not the instruments themselves. Table 4 lists different instruments and the phenomena they can be used to measure.

Specifications for several observatory instruments were difficult to find. Many observatories also had purpose build custom instrumentation, with very little documentation available. Space based systems were generally well documented. Not all magnetometer types were listed in this thesis.

Table 4: Space weather instruments

Phenomenon	Instrument
Geomagnetic disturbance, Interplanetary Magnetic Field, magnetosphere	Fluxgate magnetometer, proton magnetometer, Overhauser magnetometer
Solar wind	Mass spectrometer, plasma instrument, electrostatic analyzer, electric field measurement device
Solar activity	X-ray telescopes
Ionospheric conditions	Incoherent scatter radar, riometer
Cosmic rays	Neutron monitor
Auroral activity	All-sky cameras, magnetometers

4 Space weather measurement systems and services

4.1 Ground-based systems

Ground-based space weather measurement networks will now be described. Figure 13 illustrates their approximate location and area of operation on the Earth.

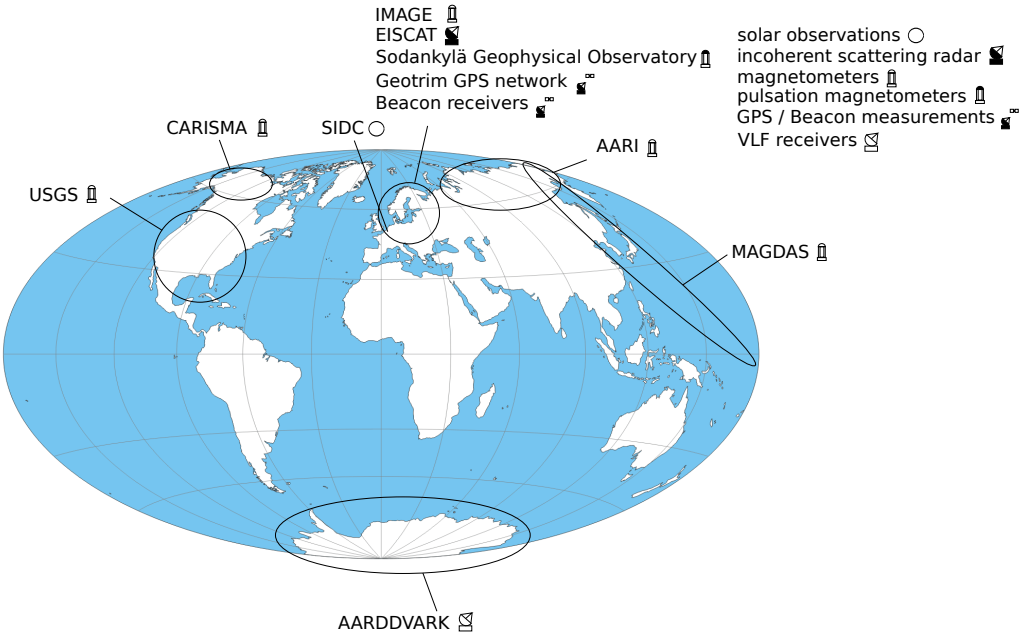

Figure 13: Ground-based space weather measurement systems from this thesis and their approximate areas of operation.

4.1.1 IMAGE magnetometer network

International Monitor for Auroral Geomagnetic Effects (IMAGE) is a magnetometer network of 31 stations maintained by 10 different institutions from Estonia, Finland, Germany, Norway, Poland, Russia and Sweden. Primary objective is the study of auroral electrojets and moving two-dimensional current systems. Substorm research is also heavily featured, along with comparing measurements with EISCAT, all-sky cameras, riometers and satellite observations. In Finland the IMAGE magnetometers are operated and maintained by Finnish Meteorological Institute and Sodankylä Geophysical Observatory. Figure 14 shows an example plot from IMAGE.[87]

The most widely used observatory magnetometer in the world is the 3-axis Fluxgate Magnetometer Model FGM-FGE. More than 200 such magnetometers are deployed across the world[166]. There are both normal and suspended versions available. The suspended version has bronze bands to stabilize the magnetometer and

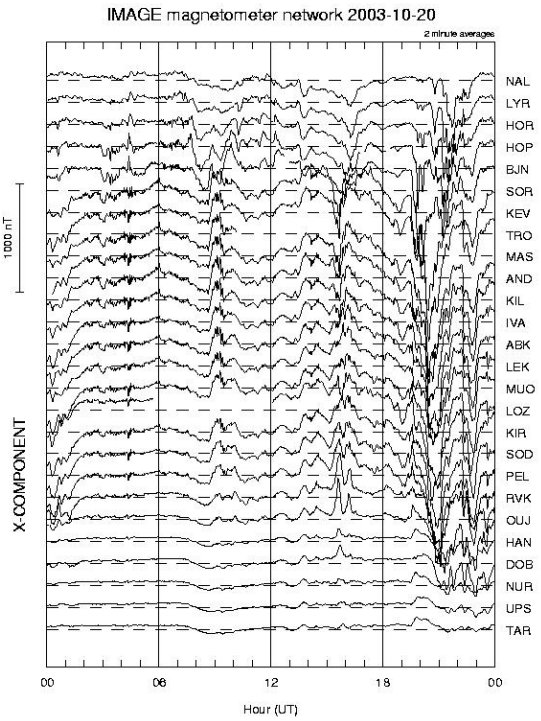

Figure 14: Example of plotted IMAGE magnetometer data. The image presents data from the 2003 Halloween storm. "Gramplot" type positioning of measurements below each other allows the user to grasp the scale of the event in progress. Notice that only data from the "evening" (18-00 Universal Time (UT)) can be utilized. This is because the particles get to the Earth through nightside reconnection, thus only weak activity is measured on the dayside.[87]

reduce measurement errors due to drift. It has a resolution of 0.1 nT, dynamic range of +/- 64000 nT and drift of 3 nT/year. The suspended system weighs 20 kg, non-suspended 9.5 kg. Operating temperature is from 0 to 60°C. Power requirements are 3 W 230 VAC. Reliability and stability have been the main design objectives. [49]

IMAGE stations use FGM-FGE, LEMI-004 and LEMI-025 magnetometers [141]. Their specifications are listed in Table 5. LEMI-025 is a fluxgate magnetometer with a resolution of 0.01 nT and a dynamic range of +/- 70000 nT. It has a power supply of 10-15 V and a power consumption of less than 4 W. The sensor, cable and electronic unit weigh a total of 9.1 kg and the GPS antenna an extra 3.4 kg. Design emphasizes low noise level. Operating temperature is -10 to +50°C.[111]

LEMI-004 is also a fluxgate magnetometer. It features a measuring range of +/- 120000 nT, resolution of 0.1 nT, temporal drift of $<$ +/- 5 nT/year and has an operating temperature range of -20 to 50°C. It has a power supply of 12 V, 0.25 A and it weighs 5.2 kg. [103]

Table 5: Ground-based magnetometers from IMAGE.[111][103][49]

Instrument	FGM-FGE	LEMI-025	LEMI-004
Type	3-axis fluxgate	fluxgate	fluxgate
Resolution	0.1 nT	0.01 nT	0.1 nT
Dynamic range	+/- 64000 nT	+/- 70000 nT	+/- 120000 nT
Drift	3 nT/year	-	< +/- 5 nT
Mass	9.5/20 kg	9.1 kg	5.2 kg
Operating temperature	0 to 60°C	-10 to +50°C	20 to 50°C
Power requirements	3 W 230 VAC	< 4 W	12 V, 0.25 W
Size	300x270/550x270mm	-	-

4.1.2 Other ground-based magnetometer networks

Russian *Arctic and Antarctic Research Institute (AARI)* Department of Geophysics maintains networks of magnetometers both at Arctic and Antarctic. The stations have both Danish FGM-FGE and LEMI-022 fluxgate magnetometers.[91] Most stations also have riometers and ionospheric instruments.

LEMI-022 is a 3-axis fluxgate magnetometer. It has a resolution of 0.01 nT, yearly drift of < 5 nT. Operating temperature is 10 to 50°C. Power consumption is 0.5 W 5 V. The sensor and test cable weigh 0.18 kg, the electric unit 0.12 kg. [146][152]

MAGnetic Data Acquisition System (MAGDAS) is a real-time space weather monitoring system. It consists of two operations: MAGDAS-A is a new magnetometer system installed at old Circum-pan Pacific Magnetometer Network (CPMN) and MAGDAS-B is a data acquisition and monitoring system installed at Space Environment Research Center (SERC), Kyushu University. The MAGDAS system allows real-time monitoring and modeling of global current systems, plasma density and electric fields. The stations are mostly concentrated along a vertical line stretching from New Zealand to Siberia. As of 2012 MAGDAS has 64 real time stations around the world. Magnetometers from Tierra Tecnica and Meisei Electrics are in use.[119] Table 6 shows the specifications of the instruments used at AARI and MAGDAS.

One of the instruments in use at MAGDAS is the FRG-604RC magnetometer. It is a 3 component fluxgate magnetometer, with resolution of 0.01 nT and dynamic range of +/- 70000 nT. Power requirements are 5 W, 12 V 400 mA. It weighs 22.95 kg and has a size of 449x351x229 mm.[186][119]

United States Geological Survey (USGS) operates a network of 14 magnetometer stations from Guam to San Juan. USGS itself was established in 1878. Permanent network of magnetometer stations was built at the start of the 20th century and K-index calculations began in 1930s. Even then there was some connection to space weather, as these calculations were intended to record "the terrestrial effects of solar corpuscular radiation by measuring the intensity of the geomagnetic activity caused by the electric currents produced round the Earth by that radiation". The concept

Table 6: Ground-based magnetometers from AARI and MAGDAS.[146][119]

Instrument	LEMI-022	FRG-604RC
Type	3-axis fluxgate	3-axis fluxgate
Resolution	0.01 nT	0.01 nT
Dynamic range	+/- 68000 nT	+/- 70000 nT
Drift	< 5nT	-
Mass	0.3 kg	22.95 kg
Operating temperature	10 to 50°C	-60 to 60°C
Power requirements	0.5 W 5 V	90-240 VAC or 12 V DC
Size	-	449x351x229 mm

of magnetosphere had not been developed at that time. Dst calculations started with International Geophysical Year 1957-1958, AE index calculations shortly after this. The current USGS Geomagnetism Program is funded under natural hazards mission. The survey is part of U.S. government's National Space Weather Program (NSWP), which includes NOAA, National Aeronautics and Space Administration (NASA), the Department of Defence and the National Science Foundation.

USGS stations are equipped with both fluxgate and Overhauser magnetometers. Table 7 gives specifications of USGS instruments. Most important data product from the stations are the 1-minute-average data. This data was crucial in investigating both the March 1989 magnetic storm and the Halloween storm of 2003. 1-second-average data is also available, and it is used in conjunction with satellite observations for further space weather research.[118] USGS observatories use Gem Systems GSM-19 Overhauser magnetometers, Narod Geophysics Ltd. Narod Tri-axial Fluxgate Magnetometers and D&I Magnetometer Model G fluxgate magnetometers.[180]

GSM-19 is a Overhauser effect magnetometer. The device is designed for portable use in addition to observatory measurements. It features an integrated GPS receiver and an antenna. It has a resolution of 0.01 nT, accuracy of +/- 0.1 nT and power requirements of 12 V 200-300mA. Operating temperature range is -40°C to +50°C. Console weighs 2.1 kg, staff 0.9 kg and sensors 1.1. kg each.[71]

Narod Tri-Axial Fluxgate Magnetometers acquire measurements from all three components of the magnetic field. They have temperature stability of < 0.1 nT/deg and long term drift of < 10 pT/day. Accuracy is not absolute and frequent calibrations are required.[180]

D&I Fluxgate Magnetometer Model G has a resolution of 0.1 nT, power requirements of 11-15 V and 2 W and an operating temperature of -10°C to 40°C. The instrument is used at USGS to calibrate the Narod magnetometer. Figure 15 shows the D&I magnetometer.[44]

Canadian Array for Realtime InvestigationS of Magnetic Activity (CARISMA) is a magnetometer array with stations across a wide area of the North American continent. CARISMA started conduction measurements in the year 2005. It is

Table 7: Ground-based magnetometers from USGS.[111][44][71]

Instrument	GSM-19	D&I Model G
Type	Overhauser	3-axis fluxgate
Resolution	0.01 nT	0.1 nT
Dynamic range	15000 to 120000 nT	-
Drift	-	-
Mass	4.1 kg	0.8 kg
Operating temperature	-40 to 50°C	-10 to 40°C
Power requirements	12 V 200-300 mA	11-15 V and 2 W
Size	-	100x70x160 mm

Figure 15: D&I Fluxgate magnetometer Model G.[44]

Figure 16: LEMI-30 induction coil magnetometer.[110]

the successor to the Canadian Auroral Network for the OPEN Program Unified Study (CANOPUS) magnetometer array. There are currently 27 stations with one more under construction. CARISMA is part of the Canadian Geospace Monitoring (CGSM) program, a multi-instrument program funded by the Canadian Space Agency (CSA). Scientific goals include study of magnetospheric convection, magnetotail instabilities, auroral particles and energetic particles in the magnetosphere. CARISMA contributes directly to the Time HIstory of Events and Macroscale Interactions during Substorms (THEMIS) program with study of substorms, storm-time electrons and solar wind-magnetosphere coupling. THEMIS is described in section 4.2.4.

Stations are equipped with fluxgate magnetometers, riometers, and all-sky cameras. Some stations also have induction coil magnetometers. Stations cover a wide part of the North American continent, roughly half of Canada.

Fluxgate magnetometers are manufactured by Narod Geophysics Ltd (NGL). Narod specifications are given in Table 8. Induction coil magnetometers are type LEMI-30 from Ukraine. Figure 16 is a picture of the instrument. NGL magnetometers have resolution of 0.025 nT, dynamic range of +/- 70000 nT and drift of $<$ 0.01 nT/day. Power consumption is $<$ 1.3 W. The induction coil magnetometers are based on LEMI-30. LEMI-30 is intended for study of magnetic field fluctuations in the range of 0.001-30 Hz. Power supply voltage is +/- 6-12 V and power consumption $<$ 3 W. Operating temperature range is -10 to 50°C. Sensor dimensions are 870 mm x 85 mm and weight is 5.6 kg.[110]

Table 8: Narod Geophysics Ltd magnetometer from CARISMA.[120]

Instrument	NGL magnetometer
Type	fluxgate
Resolution	0.025 nT
Dynamic range	+/- 70000 nT
Drift	$<$ 0.01 nT/day
Mass	-
Operating temperature	-
Power requirements	$<$ 1.3 W average
Size	-

CARISMA station have good data logging capabilities, with satellite Internet link available for direct data transfer as well as redundant disk drives at all stations. CARISMA is considered one of the foremost magnetometer arrays in the world. Numerous different data products are available on the web. In addition to CARISMA Canada also operates CANadian Magnetic Observatory System (CANMOS). It is an automated data-acquisition system serving the Canadian Magnetic Observatories.[120][27]

4.1.3 MIRACLE instrument network

Magnetometers - Ionospheric Radars - Allsky Cameras Large Experiment (MIRACLE) is an instrument network designed for mesoscale studies of auroral electrodynamics. It covers a large area in Scandinavia from roughly Estonia to Svalbard and Western Norway to Eastern Finland. It has its origins in the International Magnetospheric Study project of 1976-1979. Several auroral phenomena are the main research targets. Pattern recognition methods have also been developed for detecting auroras from all-sky camera footage. Time resolution of observations is 10 s for magnetometers and 20 s for radar and all-sky cameras. Previously described IMAGE network is part of MIRACLE, with IMAGE being its most widely used part.

MIRACLE has cooperation with several satellite missions that will be discussed in Chapter 4.2. Cluster, Swarm and THEMIS data have been or will be used together with MIRACLE observations. MIRACLE network data is also utilized in the Auroras Now! and GIC Now! forecast services discussed in Chapter 4.3.[124]

4.1.4 EISCAT

European Incoherent Scatter Scientific Association (EISCAT) is considered to be the world leader in incoherent scatter radar measurements. Ultra High Frequency (UHF) radar transmitter and one receiver is located at Tromsø, Norway, other receivers are in Kiruna, Sweden and Sodankylä, Finland. It operates in the 931 MHz band with 2.0 MW peak transmitter power and 32 m parabolic dish antenna. VHF radar is located at Tromsø, featuring 224 MHz band with peak power of 2 x 1.5 MW and 120 m x 40 m parabolic cylinder antenna. The EISCAT radar at Svalbard is 500 MHz, with peak power of 1.0 MW with 32 m and 42 m antennas. Main objective is to study the lower, middle and upper atmosphere and ionosphere using the incoherent scatter radar technique. Basic data gained from EISCAT measurements are profiles of electron density, electron and ion temperature and ion velocity. EISCAT facilities are located at good positions for both space and atmospheric studies. The mainland stations are within the Auroral oval, while the Svalbard facility is within the polar region. Figure 17 is an example of EISCAT data.

Measurements from MIRACLE magnetometers and Cluster and THEMIS satellites have been used together with EISCAT measurements. The coming Swarm mission will also combine measurements with EISCAT. Mesospheric heating is another major field of research. This is done to better understand the relationship between the Sun's activity and terrestrial weather. EISCAT has also been used to measure space debris in the Earth's orbit.

EISCAT will be upgraded with the EISCAT-3D system. It will be a multistatic radar, with one of the transmitters and receivers located in the current EISCAT facilities. Additional stations will be located at Lapland, Northern Sweden and Norway. The new system features increased measurement accuracy, faster antenna targeting, better time and location resolution and allows new applications for measurements.[136][53]

4.1.5 Geotrim GPS network

Ionospheric electron density can be estimated using Total Electron Content (TEC) measurements with multiple satellites and receivers. This is done using an inversion procedure. When a radio signal is transmitted between two antennas, the velocity of the signal depends on the refractive index n of the medium it is traversing. If the medium is ionized, as it is in the case of ionosphere, n depends on the level of ionization. Refractive index can be calculated using Equation 7.

$$n \approx 1 - \frac{N_e r_e c^2}{2\pi f^2} \tag{7}$$

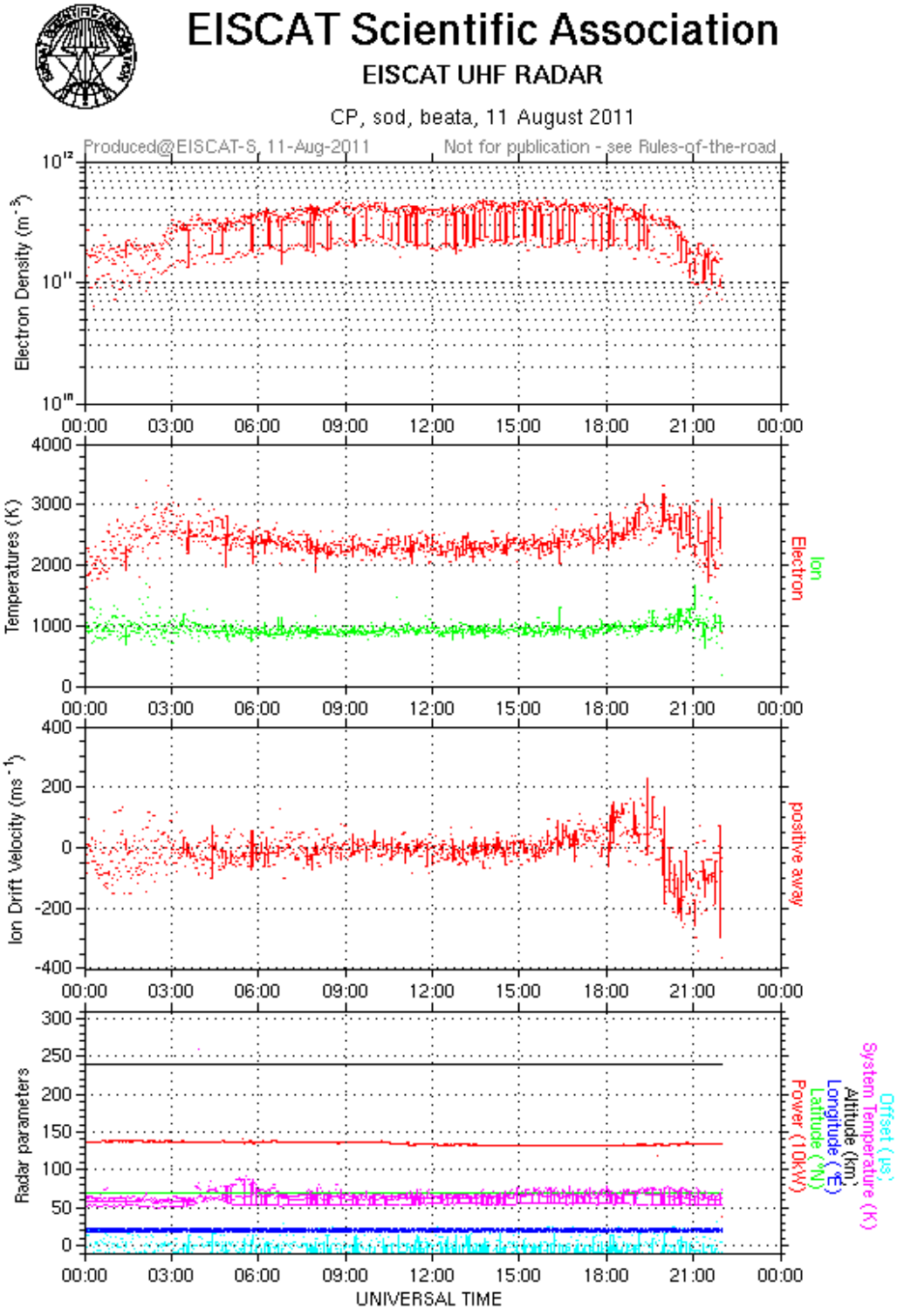

Figure 17: Plotted example of EISCAT measurement data.[53]

N_e is the electron density of the medium (electron/m^3, r_e is the radius of an electron (2.81794x10^{-15}m),c is the speed of light in vacuum (299792458 m/s), f is the frequency of the signal (Hz).

The needed for the signal to cover the distance from transmitter to receiver is found by integrating the velocity along the signal path, and thus it depends on the refractive index n. The integrated electron density along the path is referred to as the Total Electron Content (TEC), expressed as electron/m^2.

However it is not possible to measure the exact time a signal took to reach the receiver this way. This is where the dual-frequency beacons of the GPS satellites are useful. Since the refractive index n also depends on the frequency f of the signal the total travel time will be different for the two frequencies. By measuring the phase difference between the signals at different frequencies which travel through the same medium, their difference in travel time can be determined and that is directly related to TEC. The relation between phase difference and TEC is illustrated in Equation 8.

$$TEC = \frac{f_1}{r_e c(f_1^2/f_2^2 - 1)} \Delta\&phi \tag{8}$$

f_1 and f_2 are the two frequencies of the signal, $\Delta\&phi$ is the difference in phase between the two signals (in radians)

From this is calculated the differential TEC, since larger than 2π phase differences become ambiguous as phase of 2π is equal to a phase of zero. Differential TEC is change in time of the phase difference. These GPS measurements only give the TEC for every measured path between the satellite and receiver, not the 3-dimensional electron density N_e. This can however be determined by using the inversion procedure.

The procedure looks for the electron density distribution as a function of 3D location and time, so that the integrated electron density along the path is equal to the measured TEC for each path between any satellite and any receiver. This is illustrated in Equation 9.

$$\int N_e(\underline{x}, t)dl - \int N_e(\underline{x}, t - dt)dl = dTEC_l(t) \tag{9}$$

Where $\underline{x}$ is 3D location, dt is sample time

The solution area is divided into 4D voxels, resulting in a single equation for each voxel, expressing relation of the electron density of the voxel with that of all other voxels and measured values. Next the inversion procedure tries to find a solution of 4D electron density which matches this system of equations. This is done iteratively and more measurements mean better results. Thus as many satellites and receivers as possible are preferred. Geotrim measurements are illustrated in Figure 18.

Finnish Meteorological Institute uses Geotrim GPS network to conduct ionospheric electron density measurements in Finland. There are 86 receiver stations in

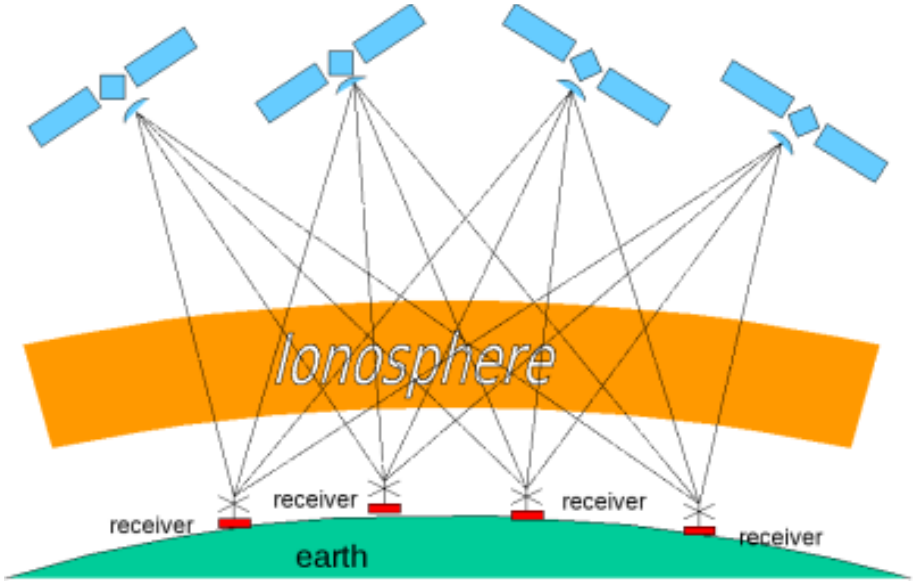

Figure 18: Illustration on Geotrim GPS ionospheric measurements.[66]

Finland, stationed mostly less than 100 km apart. Similar networks also operate in Sweden and Norway.[97][66]

4.1.6 Beacon network

Another new method for ionospheric studies is the TomoScand project beacon network. Quite similar to the Geotrim GPS network, beacon network allows ionospheric studies from satellite beacons with rather simple equipment.[135] Measurements of the ionospheric delay of electromagnetic waves from satellite to receiver are used to estimate ionospheric electron density. This is called ground-based ionospheric tomography. Unlike the Geotrim network described previously, this method allows ionospheric studies from Low Earth Orbit (LEO) with VHF/UHF dual frequency beacon satellites. This allows larger areas of the Earth surface to be covered faster than with navigational satellites traveling at higher orbits.

Ground segment of beacon receiver station is quite simple. Software defined radio is used, so normal computers can be used for signal processing instead of custom built devices. Beacon satellite receiver stations consists essentially of a radio frequency (RF) front end (antenna, amplifier, filter), computer with a digital receiver connected to the front end, software to provide satellite positioning information, recording software for the satellite signal and phase curve calculation software, which allows the calculation of the relative phase curves from two beacon frequencies. This kind of measurement setup is considerably cheaper than traditional ionospheric measurements. Results obtained from TomoScand have been compared to incoherent scatter radar measurements and found to be quite useful. Satellites COSMOS 2407, COSMOS 2414, COSMOS 2429, COSMOS 2463, COSMOS 2454, RADCAl, DMSP F15 have been successfully used in beacon network tests. Five 150/400 MHz beacon satellite receivers have been deployed as part of Finnish Meteorological Institute

TomoScand project. More receivers are under construction.

4.1.7 AARDDVARK VLF receivers

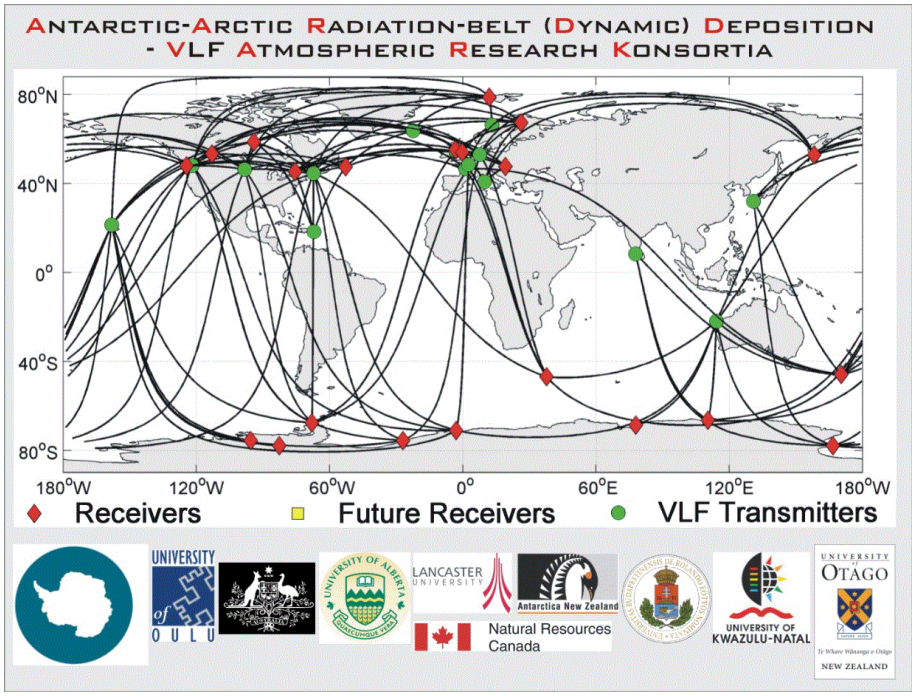

Figure 19: Location of AARDDVARK facilities and list of participating organizations.[1]

Antarctic-Arctic Radiation-belt (Dynamic) Deposition-VLF Atmospheric Research Konsortium (AARDDVARK) is a measurement network designed to make continuous long-range observations of lower ionosphere at mid to high-latitude regions. Mid and high-latitude regions are defined as 50° and 60° degrees of magnetic latitude. As of 2009, one of the ten AARDDVARK stations is located in Sodankylä Geophysical Observatory. AARDDVARK site locations are given in Figure 19.

The Earth ground and ionosphere create a waveguide for radio signals traveling on the Earth. The Earth part is essentially stable, but space weather phenomena disrupts the ionospheric part. These disruptions can be investigated with Very Low Frequency (VLF) receivers. Measurements are done using cheap, easy to install and maintain sensors. The VLF measurements can be combined with satellite measurements to create even more comprehensive data.

Several different receivers are used at AARDDVARK. All of them record the amplitude and phase of Minimum Shift Keying (MSK) modulated VLF radio transmissions. OmniPAL narrowband VLF receiver is a software defined radio (SDR) system. It consists of a custom built Analog Device's ADSP-21xx Digital Signal Processor (DSP) board with a standard desktop computer. It is able to receive up to 6 VLF transmissions simultaneously. UltraMSK narrowband VLF receiver is also a software defined radio, unlike OmniPAL it uses GPS instead of DSP to synthesize

required reference frequencies. VELOX AARDVARK is a PC-based system using LabVIEW graphical programming for data acquisition. It is capable of digitizing VLF signals up to 95 kHz using a DSP card. AARDDVARK has contributed to a wide variety of space weather research topics. These include SEPs, substorms and CME impact on radiation belts.[34]

4.2 Spaceborne systems

4.2.1 SOHO, Solar Dynamics Observatory, Solar Orbiter

Several prominent space weather measurement systems in space will now be described. Figure 20 illustrates their approximate locations in the near Earth space.

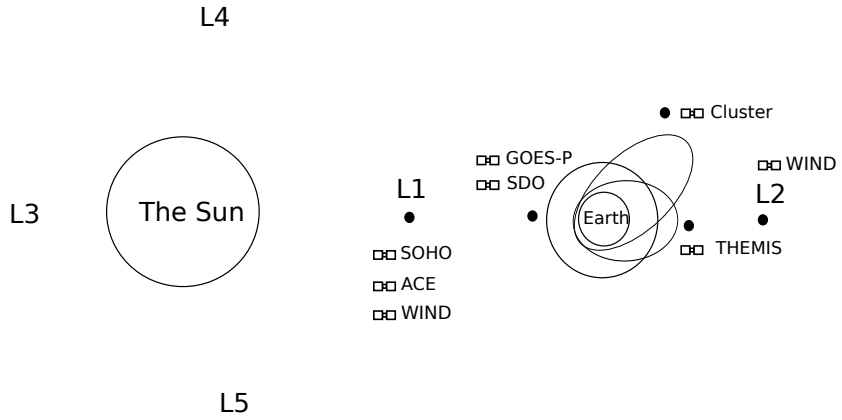

Figure 20: Satellites from this thesis and their approximate locations. Picture not to scale. L1, L2, L3, L4 and L5 are Lagrangian points[63]. Lagrangian points are positions in an orbital configuration where small objects affected by gravity can stay at the same relative locations in relation to two larger objects, in this case the Sun and the Earth. WIND has taken observations on numerous locations.

Solar and Heliospheric Observatory (SOHO) is a solar observatory with a multitude of scientific objectives. These include the study of the structure, chemical composition and dynamics of the solar interior, the structure, dynamics and composition of the outer solar atmosphere and the solar wind. The NASA led SOHO mission was launched in December 1995 into a halo orbit around the Lagrangian point L1. This gives it excellent point of view for studying the Sun and solar wind. The satellite is permanently outside of the Earth's magnetosphere, allowing more accurate results of solar wind measurements.

One of the SOHO instruments is the Michelson Doppler Imager (MDI). MDI uses a refracting telescope to feed sunlight through filters onto a Charge Coupled Device (CCD) camera. CCD cameras are very common in astronomical instruments. They are constructed from light sensitive silicon diodes arranged into a rectangular grid. A photon impacting the detector releases electrons, which are trapped in the grid. This allows for detection of incoming light. Even some commercial-of-the-shelf CCD cameras can be used for astronomical applications. Two interferometers

define a 94 mÅ bandpass that can be tuned across the Ni I 6768 Å solar absorption line. Å or Ångström is an old measurement of wavelength. 1 Å is 0.1 nm. MDI consists of optics and electronics packages. Optics part is the telescope itself, image stabilization system, spectral and polarization filters, beam distribution system, shutter and the CCD camera. It is designed to study the internal structure and dynamics of the Sun using helioseismological methods.[153][95]

The MDI instrument was terminated on 12.4.2011, and has been superseded by the Solar Dynamic Observatory (SDO) Helioseismic and Magnetic Imager (HMI) instrument which will be discussed in the SDO section.[163]

Table 9: SOHO instruments

Acronym	Instrument full name	Operative
GOLF	Global Oscillations at Low Frequencies	Solar observations
VIRGO	Variability of solar IRradiance and Gravity Oscillations	Solar observations
SOI/MDI	Solar Oscillations Investigation/Michelson Doppler Imager	Solar observations
SUMER	Solar Ultraviolet Measurement of Emitted Radiation	Solar observations, plasma measurements
CDS	Coronal Diagnostic Spectrometer	Solar observations
EIT	Extreme ultraviolet Imaging Telescope	Solar observations
UVCS	UltraViolet Coronagraph Spectrometer	Solar observations
LASCO	Large Angle and Spectrometric Coronagraph	Solar observations
SWAN	Solar Wind Anisotropies	Solar wind measurements
CELIAS	Charge ELement and Isotope Analysis System	Solar wind measurements
COSTEP	Comprehensive SupraThermal and Energetic Particle analyser collaboration	Solar wind measurements
ERNE	Energetic and Relativistic Nuclei and Electron experiment	Solar wind Measurements

The three instrument groups, helioseismology, solar wind and outer layer of the Sun, carry out different kinds of research e.g. helioseismology is the study of propagation of acoustic pressure wave oscillation in the Sun. These waves are created by gas movement in the Sun's convective zone. Very low and high modes of oscillation can be observed using these instruments, because unlike terrestrial observations, the Earth's atmosphere and diurnal rotation have no effect in measurements conducted at L1.[95]

Solar atmospheric remote sensing is done using telescopes and spectrometers. Temperature, density and velocity of material on the outer solar atmosphere can be derived from these operations. "In situ" part measures real time composition of solar wind and energetic particles originating from the Sun. SOHO instruments are listed in Table 9 and their details are provided next.

Charge, Element, and Isotope Analysis System(CELIAS) is an electrostatic analyzer and it measures solar particles. It includes two sensors for solar wind composition measurements: Charge Time Of Flight (CTOF) and Mass Time Of Flight (MTOF). Proton Monitor (PM) provides solar wind proton measurements. CTOF covers the energy per charge range of 0.1 to 55 keV/charge. MTOF determines high-resolution mass spectra of heavy solar wind ions. The CELIAS/MTOF package is used for SOHOs space weather monitoring and it measures numerous solar wind parameters. [93][29][28]

Energetic and Relativistic Nuclei and Electron (ERNE) is a high-energy particle instrument, consisting of two sensors: the low-energy detector and high-energy detector. Low-energy detector operates at energies from 2.5 MeV up to 30 MeV, high-energy detector works in energies one order of magnitude upwards. Both detectors are particle telescopes, where particle identification and total energy calculation are based on sampling the ionization losses along the track of the particle and absorbing the residual energy of the stopping particle in one detector layer. From a space weather perspective, ERNE is used to measure high energy proton flux. [175][54]

SOHO has been hugely successful, having generated thousands of scientific articles and vast photographic material of the Sun. Location of SOHO also allows for space weather monitoring and forecasting. By observing the sources of CMEs and flares up to three days of warning can be provided for these events.[48][62]

Solar Dynamics Observatory (SDO) is a currently operating NASA solar observation mission. The satellite is illustrated in Figure 21. SDO is the first satellite in the Living With a Star program and it is considered a flagship mission. First scientific data was received on 1 May 2010. Science targets include determining how the Sun's magnetic field is generated and structured, how the stored magnetic energy is released into the heliosphere and geospace as the solar wind, energetic particles, and variations in the solar irradiance. Geospace is defined as a near Earth area consisting of the magnetosphere, or more broadly as the entire heliosphere.

Operative space weather measurement focus on several data products necessitates continuous downlink of measurement data. It has very accurate pointing and positional stability capabilities to allow registration of successive images. Fairly large amounts of data are produced to achieve this. Approximately 150 000 high-resolutions full-Sun images and 9000 EUV spectra, totaling 1.5 terabytes, are generated daily.[144]

SDO has three experiments on board, Atmospheric Imaging Assembly (AIA), Extreme Ultraviolet Variability Experiment (EVE), Helioseismic and Magnetic Imager (HMI).

AIA is a combination of four Cassegrain telescopes. They are optimized to observe narrow band passes in the EUV to observe solar emissions from the transition region and corona. They provide view of the entire corona and coverage of the full thermal range at very high resolution. Uninterrupted measurements for months at a time with very good temporal resolution are provided. Science objectives include the study of coronal heating and irradiance, coronal energy input, storage and release

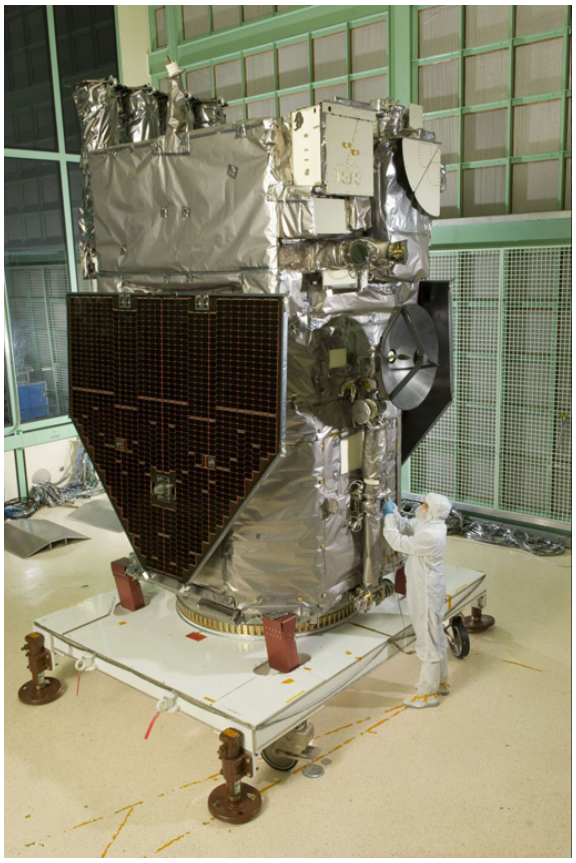

Figure 21: SDO satellite on ground.[156]

and coronal seismology.[113]

EVE on board SDO measures extreme solar ultraviolet radiation and it consists of several instruments. The Multiple EUV Grating Spectrographs (MEGS)-A measures solar EUV irradiance in the 5 to 37 nm range, MEGS-B in the 35 to 105 nm range. MEGS instruments are calibrated with the EUV SpectroPhotometer (ESP) which conducts solar EUV irradiance measurements in the broadband between 0.1 to 39 nm. Finally MEGS-Photometer measures the Sun's hydrogen emission at 121.6 nm. This is used to track potential changes in MEGS sensitivity. MEGS instruments are spectrographs, which separate incoming waves into a frequency spectrum. They function much in the same way as spectrometers. Science objectives are mainly concerned with study of solar EUV radiation. EVE produces valuable space weather information with its level 0C and level 0CS data. These are the solar EUV irradiance measurements delivered as soon as possible. This data can be used to predict numerous solar phenomena related to space weather, such as flares and SEP events.[185]

HMI on board SDO is a telescope designed to study the Doppler shift, line-of-sight magnetic field, intensity and vector magnetic field at the solar photosphere. HMI design is based on the Michelson Doppler Imager (MDI) on board SOHO, with a few improvements. HMI has aperture of 14.0 cm, optical resolution of 0.91 arcsec and a pixel size of 0.505 arcsec. Arcsec is 1/60 of an arcminute, which in turn is

1/60 of one degree. It observes the full solar disk in the Fe I absorption line at 6173 Å with a resolution of 1 arcsec. HMI consists of the telescope, polarization selector, image stabilization system, a narrow band tunable filter and two CCD cameras with mechanical shutters.

The front window of the HMI is a 50 Å bandpass filter that reflects most of the incident sunlight. It is followed by the telescopes primary and secondary lens. This is followed by the polarization selector, then a narrow band tunable filter and two CCD cameras with mechanical shutters.[154]

Solar Orbiter is a planned European Space Agency (ESA) and NASA collaboration mission to study the heliosphere. Solar Orbiter includes instruments measuring the changes in the Sun and solar wind (see list of instruments in Table 10). It is part of ESA's Cosmic Vision 2015-2025 programme. The mission has several major scientific goals. These include: (1) What drives the solar wind and where does the coronal magnetic field originate from? (2) How solar eruptions produce energetic particles? (3) How does the solar dynamo work and drive connections between the Sun and the heliosphere?. Solar Orbiter will approach the Sun as close as 0.28 AU. This means combined *in situ* measurements of solar wind, high-resolution imaging and spectroscopic observations along with a new inner-heliospheric position. This distinguishes Solar Orbiter from previous solar missions.

Table 10: Solar Orbiter instrumentation

Acronym	Instrument full name	Operative
EPD	Energetic Particle Detector	Solar wind measurements
MAG	Magnetometer	Magnetic field measurements
RPW	Radio and Plasma Wave analyser (RPW)	Magnetic and electric field measurements
SWA	Solar Wind Analyser	Solar wind measurements
EUI	Extreme Ultraviolet Imager	Solar observations
METIS	Multi Element Telescope for Imaging and Spectroscopy	Solar observations
SoloHI	Solar Orbiter Heliospheric Imager	Solar observations
SPICE	Spectral Imaging of the Coronal Environment	Solar observations
STIX	Spectrometer/Telescope for Imaging X-rays	Solar observations

In-situ instruments are Energetic Particle Detector (EPD), Magnetometer (MAG), Radio and Plasma Wave analyzer (RPW) and Solar Wind Analyser (SWA). EPD measures properties of suprathermal ions and energetic particles, MAG is a magnetometer, RPW determines characteristics of electromagnetic and electrostatic waves in the solar wind SWA is used for detailed analysis of solar wind composition. Solar remote sensing consists of Extreme Ultraviolet Imager (EUI), Multi Element Telescope for Imaging and Spectroscopy (METIS), Solar Orbiter Heliospheric Imager

(SoloHI), Spectral Imaging of the Coronal Environment (SPICE) and Spectrometer/Telescope for Imaging X-rays (STIX). EUI images solar atmosphere from the photosphere to the corona, METIS will produce a coronagraph in the visible, Ultraviolet (UV) and Extreme Ultraviolet (EUV) band, SoloHI will measure disturbances in the solar wind by observing visible sunlight scattered by solar wind electrons, SPICE will characterize plasma properties of different regions in and around the Sun and finally STIX provides imaging spectroscopy of solar X-ray emissions. Current estimate for launch of the mission is January 2017. [127]

4.2.2 ACE, WIND

Advanced Composition Explorer (ACE) is a NASA Explorer program mission. The primary object is the studying of the elemental, isotopic, and ionic charge state composition of nuclei from H to Ni from solar wind energies to galactic cosmic ray energies. ACE is located at the Lagrange point L1, 240 R_E sunward of the Earth. There it can take numerous measurements of the solar wind, solar energetic particles, particles energized by interplanetary shocks, partially ionized particles from the local interstellar medium and galactic cosmic rays.

ACE needs to be situated well outside of the Earth's magnetosphere in order to measure solar wind, which is why a location around Lagrangian point L1 was chosen. The site gives excellent position for the measurements, as interplanetary magnetic field and solar wind can be measured before they interact with the Earth's magnetosphere. ACE has enough propellant as of 2013 to maintain its orbit around L1 until about 2024.

Table 11: ACE instruments.

Acronym	Instrument full name	Operative
SEPICA	Solar Energetic Particle Ionic Charge Analyzer	Solar wind measurements
ULEIS	Ultra Low Energy Isotope Spectrometer	Solar wind measurements
SWIMS	Solar Wind Ion Mass Spectrometer	Solar wind measurements
SWICS	Solar Wind Ion Composition Spectrometer	Solar wind measurements
SWEPAM	Solar Wind Electron, Proton, and Alpha Monitor	Solar wind measurements
EPAM	Electron, Proton and Alpha Monitor	Solar wind measurements
MAG	Magnetic Field Experiment	Magnetic field measurements
SIS	Solar Isotope Spectrometer	Solar wind measurements
CRIS	Cosmic Ray Isotope Spectrometer	Cosmic ray measurements
SLAM	Spacecraft Loads and Acoustics Measurements	Spacecraft launch environment measurements

Special design features were included to allow continuous operation through solar

flares. This is achieved through use of triple voting cells in the Field-programmable gate arrays (FPGS) to mitigate Single Event Upset (SEU) damage. The memory is also fitted with error detection and correction.

The secondary mission goal for ACE is space weather monitoring. This is accomplished through the Real Time Solar Wind (RTSW) experiment. The instruments participating in this are the Magnetic Field Experiment (MAG), Electron, Proton and Alpha Monitor (EPAM), Solar Wind Electron, Proton and Alpha Monitor (SWEPAM) and Solar Isotope Experiment (SIS). This part of the mission is managed by National Oceanic and Atmospheric Administration (NOAA). List of ACE instruments is provided in Table 11 and their details are provided below. Solar Energetic Particle Ionic Charge Analyzer (SEPICA) instrument terminated operations on 20.4.2011 due to failure in gas valves.[2]

MAG on board ACE is a fluxgate magnetometer that is used to study the solar wind and the interplanetary magnetic field (IMF). It will allow interpretation of particle distribution function, determination of the source for the solar wind thermal and solar energetic particles and characterization of IMF fluctuations over a wide range of frequencies. Galactic Cosmic Ray interference can also be detected on MAG. The instrument provides continuous measurements from Lagrange point L1, which makes it very useful for space weather monitoring. Measurement accuracy is 0.1 nT, sensitivity is high (0.008-0.0005 nT/step) and noise is low ($<$ 0.006 nT rms). Measurement range is wide, +/-4 nT to +/-65536 nT. It consists of two boom-mounted triaxial fluxgate sensors that are located 4.19 m from the center of the spacecraft. MAG is based on the WIND satellites MFI instruments flight spare. Full redundancy and conservatism of design are emphasized to provide high reliability. The sensor is also quite light and has a low power consumption, heaters and electronics consume a total of 3.4 W, while the sensors and electronics weigh a total of 2.55 kg. Example of MAG instrument data is provided in Figure 22.[160]

EPAM instrument on board ACE is a monitor to characterize the dynamic behavior of electron and ions accelerated by solar flares, Coronal Mass Ejections (CME) and Co-rotating Interaction Regions (CIR). The energy range for these electrons and ions is 0.03 to 5 MeV. Solar Wind Electron, Proton, and Alpha Monitor (SWEPAM) is used to measure three-dimensional characteristics of solar wind and suprathermal electrons in ranges of 1-900 eV and ions from 0.26 to 35 keV. Solar isotope Spectrometer (SIS) is a spectrometer that measures elemental and isotopic composition of energetic nuclei in the energy range of 10-100 MeV. These include nuclei from large solar particle events and different galactic cosmic rays. This allows real time *in situ* monitoring of the solar wind, giving NOAA the ability to make forecasts of space weather events.[132]

Ultra Low Energy Isotope Spectrometer (ULEIS) measures mass and kinetic energy of nuclei from He to Ni. The energy range covered includes solar energetic particles, particles accelerated by interplanetary shocks and low-energy anomalous cosmic rays. SEPICA measured charge state, kinetic energy and the nuclear charge of energetic ions in energy range of 0.2 to 3 MeV/nucleon. Solar Wind Ion Mass Spectrometer (SWIMS) measures solar wind isotopic composition. Similar instrumentation is present on board Wind and SOHO spacecraft. Solar Wind Ion Compo-

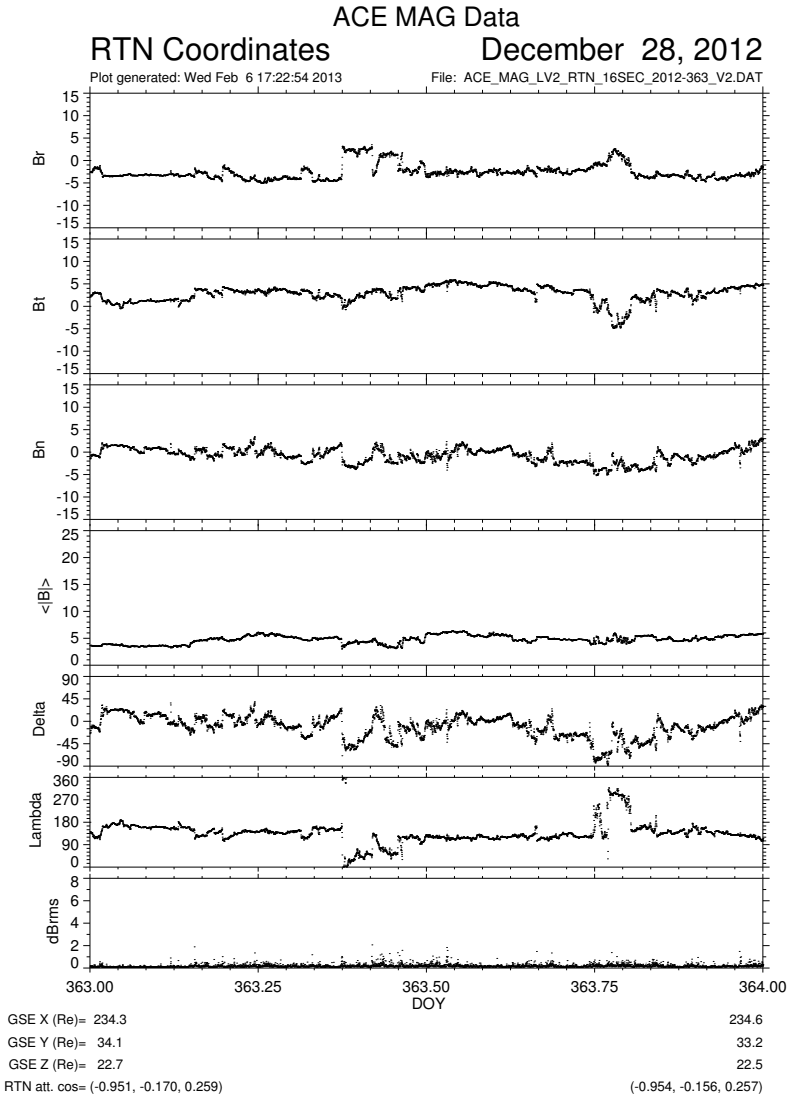

Figure 22: ACE MAG magnetometer data plotted from 28.12.2012. Different components of the magnetic field are shown during a rather quiet time.[3]

sition Spectrometer (SWICS) is used to study the elemental and ionic charge state composition of all major solar wind ions from H to Fe. Cosmic Ray Isotope Spectrometer (CRIS) studies galactic cosmic ray elemental and isotopic composition. It works in the energy range of 100 to 600 MeV/nucleon.[167][31][2]

WIND spacecraft was launched in 1994 to L1 Lagrange point. It is part of Global Geospace Science Program, which is part of International Solar Terrestrial Physics program. WIND was designed to study solar wind acceleration processes, energetic particle acceleration and Interplanetary Coronal Mass Ejections (ICME) internal structure. Despite being launched in 1994, WIND is still active and contin-

ues to provide data. Of the original eight instruments only the gamma-ray detector has been turned of (after exceeding its planned design life). It is used as a reference for 1 AU measurements in several other missions. WIND is the third vantage point for the STEREO mission and along with SOHO the backup to STEREO. Since WIND has been around during three solar cycles, it has very valuable time series of data available. During WINDs lifetime it has taken measurements at L1, L2 and 350 R_E from Sun-Earth line. Unique fieature of WIND is that it is the only radio wave instrument equipped near-Earth satellite. WINDs instruments are listed in Table 12.

Table 12: List of WIND instruments.

Acronym	Instrument full name	Operative
MFI	Magnetic Field Investigation	Magnetic field measurements
SWE	Solar Wind Experiment	Solar wind measurements
3DP	3D Plasma Analyzer	Interplanetary medium measurements
SWICS	Solar Wind Ion Composition Spectrometer	Solar wind measurements
MASS	High Mass Resolution Spectrometer	Solar wind measurements
STICS	Suprathermal Ion Composition Spectrometer	Solar wind measurements
EPACT	Energetic Particle Acceleration Composition, and Transport	Solar flare measurements
WAWES	Radio and Plasma Wave experiment	Radio wave measurements
TGRS	Transient Gamma-Ray Spectrometer	Gamma-ray measurements
KONUS	Gamma-ray instrument	Gamma-ray measurements

Magnetic Field Investigation (MFI) on board WIND is a boom-mounted dual triaxial fluxgate magnetometer. Dual configuration was chosen because of redundancy and it allows the removal of the dipolar portion of the spacecraft magnetic field. The instrument has a very wide dynamic range of measurement capabilities. Design goal of high reliability has been reached with the long life of the instrument. Figure 23 provides examples of MFI data.[112]

Solar Wind Experiment (SWE) on board WIND is a set of sensors designed to investigate solar wind physics. It features two Faraday cup sensors, a vector electron and ion spectrometer and a strahl sensor. Faraday cup is an instrument designed to catch charged particles. The resulting current can be measured and thus the number of electrons and ions can be measured. The strahl sensor is designed to detect a very specific feature of the solar wind electron velocity distribution. Electrons with energies above approximately 40 eV moving along magnetic field can travel to 1 AU with very little scattering. This is due to rapid fall-off in density and the number of collisions when the particles move out of the corona. This results in observations close to the field direction sometimes detecting the presence of a beam ('Strahl' in German) of higher energy electrons. The strahl sensor is designed to study this

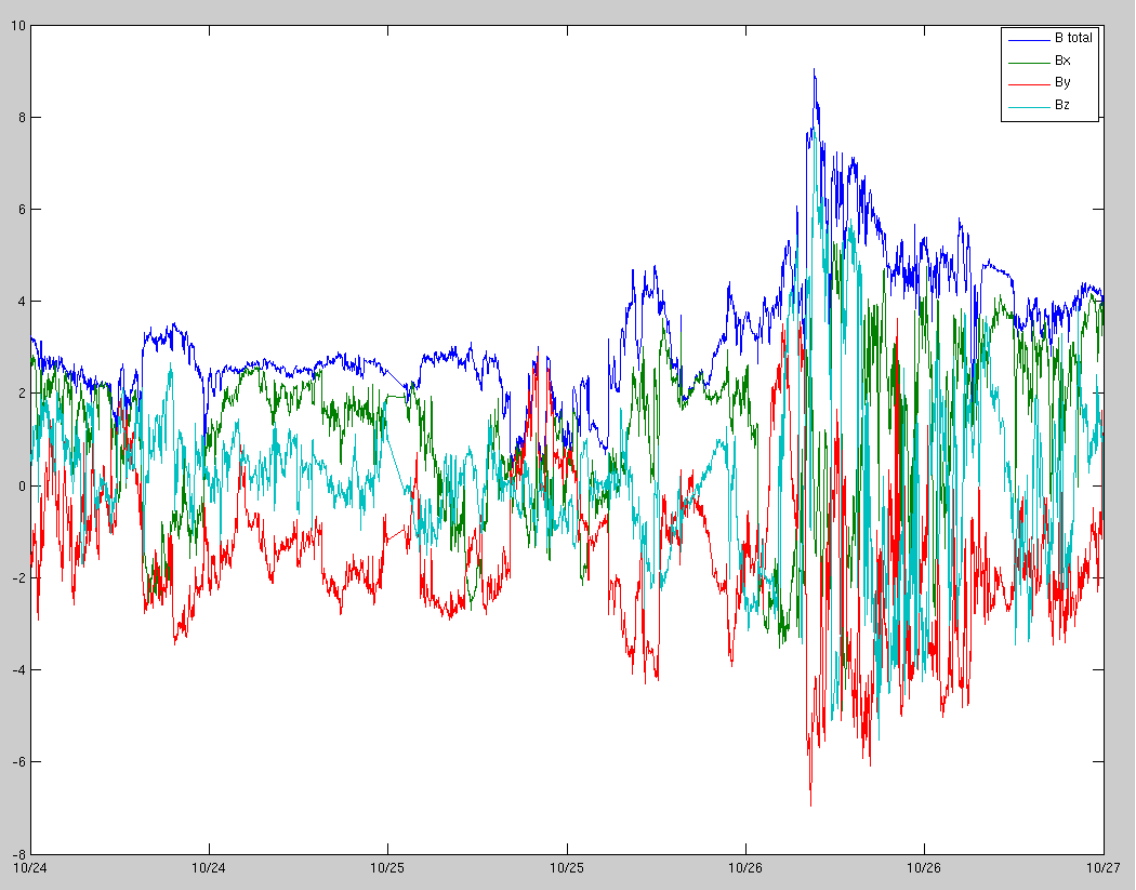

Figure 23: WIND MFI instrument data from 24-26.10.2008, plotted in Matlab. Measured values are in nanoteslas.

phenomenon. The instrument itself is a truncated, toroidal electrostatic analyzer. [137]

3D Plasma Analyzer (3DP) instrument consists of three separate detectors and a particle correlator: The semi-conductor detector telescopes (SST), the electron electrostatic analyzers (EESA), the ion electrostatic analyzers (PESA) and the Fast Particle Correlator (FPC). PESA and EESA are electrostatic analyzers, designed to measure interplanetary ion and electron populations in the 3 eV to 30 keV range. SST is made up of three arrays of pairs of double-ended semi-conductor detector telescopes. These provide high sensitivity, high energy resolution 3D measurements of $>$ 20 keV electron and ions.[115][170][183]

4.2.3 GOES

Geostationary Operational Environmental Satellite (GOES) is a groundbreaking NASA weather satellite program which started in 1975 with the launch of GOES-1. It has its origins in Synchronous Meteorological Satellite (SMS) and Applications Technology Satellite (ATS) demonstrations. There have been in total 16 GOES satellites (GOES 1-15), with one launch failure (GOES-G). Further satellites are

planned for the program. Though primary a weather satellite, GOES program has conducted plenty of space weather measurements. The most important instruments on board for space weather applications are the Space Environment Monitor and the Solar X-ray Imager.[45]

On board all GOES satellites is a Space Environment Monitor (SEM) package. This includes a three-axis fluxgate magnetometer, allowing for space weather measurements. The unusually long time series generated by the GOES program are an important part of its contribution to space weather research. GOES 8-12 carried fluxgate magnetometers manufactured by Schonstedt Instrument Company. These sensors were mounted on three-meter booms, primary one at the end and a second redundant sensor 0.3 meters from of the first. These measurement range of these magnetometers was +/- 1000 nT, with sensitivity of 0.03 nT and accuracy of 1 nT.[161]

In addition to the magnetometer, SEM includes the Energetic Particle Sensor (EPS) and High Energy Proton and Alpha Detector (HEPAD) from GOES-8 onwards, which are often referred together as Energetic Particle Sensors. EPS detectors have both telescope and dome type configurations. The telescope is made up of two silicon surface barrier detectors. The dome types consists of three sets of two solid state silicon surface barrier detectors. HEPAD uses a telescope with two silicon surface barrier detectors and a Cerenkov radiation photomultiplier tube detector. Together these two instruments are able to cover a very wide range of energies, from 0.7 MeV to over 700 MeV. Space weather products from Energetic Particle Sensors measurements include proton fluxes at different energy levels.[138]

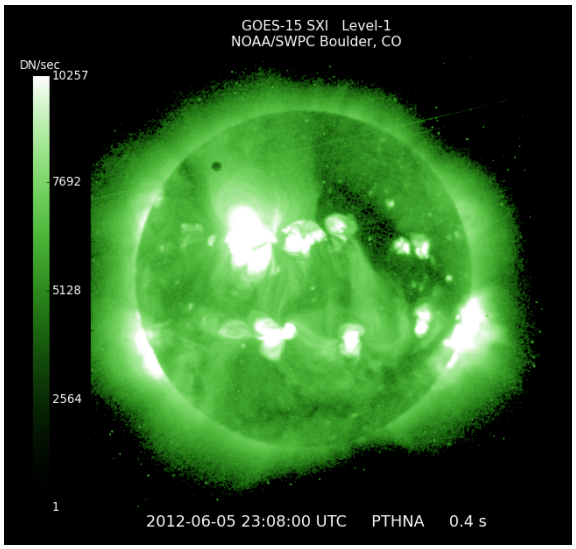

Figure 24: Transit of Venus as observed by GOES SXI instrument.[74]

Finally the SEM contains a Solar X-Ray Sensor (XRS, not to be confused with the Solar X-ray Imager). XRS is an X-ray detector, and they have been deployed on GOES spacecraft since 1974. The basic structure is a telescope with a baffle structure for electrons, permanent magnet, X-ray collimator and an ion chamber. Baffle and strong permanent magnets are used to prevent electrons of energies below

several MeV from entering and ionizing the ion chamber gas. The ion chamber is shielded by lead in all direction except the field-of-view. X-ray detection is done in the ion chamber, the ion chamber having a certain wavelength dependent response to X-rays.[80]

GOES satellites beginning with GOES-12 also have the Solar X-ray Imager (SXI) instrument, an X-ray telescope, on board. GOES-12 was the first operational mission to study the Sun's X-ray corona. Images provided by SXI form a crucial part of NOAAs space weather forecast system. The very first SXI instrument on board GOES-12 failed due to electrical error and was forced to be deactivated. SXIs flown on GOES-13 and beyond have proven to be very successful. SXI has several forecast goals. It attempts to locate coronal holes to forecast solar activity. Active regions are surveyed for flare eruptions. Flares are studied to provide forecast for Solar Energetic Particle (SEP) events. Coronal Mass Ejection occurrence is also a point of study. Fresh GOES images can be viewed from NOAA Space Weather Prediction Center: http://www.swpc.noaa.gov/. Figure 24 illustrates the Transit of Venus from the SXI perspective.[139]

4.2.4 Cluster, THEMIS

Cluster and THEMIS are both multi spacecraft missions including 4 and 5 spacecraft respectively. The **Cluster** mission is a constellation to study plasma structures in key regions around the Earth. The unique feature of the Cluster mission is the ability to take three-dimensional measurements. This is achieved with the use of multi-point measurements, high resolution and identical instrumentation on all four of the satellites. The scientific objectives are to study the small-scale structures and macroscopic turbulences in magnetospheric plasma. These studies are conducted in the solar wind and bow shock, the magnetopause, the polar cusps, the magnetotail and the auroral zones. Cluster instrumentation features a wide variety of systems to measure different particles at different energy levels, given in Table 9. Figure 25 gives an overview of different Cluster instrument plots.

Electric Field and Wave (EFW) instrument studies fast time- and space-varying vectorial electric fields. It is essentially an electric field measuring device or plasma instrument. It measures spacecraft potential, electron density and electron temperature when in Langmuir mode. Main structure is four spherical sensors deployed with 50 m cables in the spin plane of the spacecraft. Dynamic range of EFW is 0.1 mV/m to 700 mV/m.

Spatio-Temporal Analysis of Field Fluctuations (STAFF) on board Cluster measures magnetic components of electromagnetic fluctuations and cross-correlation between electric and magnetic components. These will be used to determine the shape, current density and motion of small-scale current structures. STAFF consists of a search coil magnetometer and a spectrum analyzer and it covers the frequency range up to 4 kHz.

Waves of High frequency and Sounder for Probing of Electron density by Relaxation (WHISPER) is a transmitter/receiver instrument designed to measure plasma density. The transmitter emits a short pulse to stimulate plasma resonances and

Table 13: Cluster instrument list.

Acronym	Instrument full name	Operative
FGM	FluxGate Magnetometer	Magnetic field measurements
STAFF	Spatio-temporal analysis of Field fluctuation experiment	Magnetic field measurements
EFW	Electric field and waves experiment	Electric field measurements
WHISPER	Waves of high frequency and sounder for probing of electron density by relaxation	Electric field measurements
WBD	Wide band data	Electric field measurements
DWP	Digital Wave Processing	Measurement coordination
EDI	Electron Drift Instrument	Electric field measurements
ASPOC	Active Spacecraft potential Control	Spacecraft electrostatic potential regulation
CIS	Cluster Ion Spectrometry	Solar wind measurements
PEACE	Plasma Electron and Current Experiment	Solar wind measurements
RAPID	Research with Adaptative Particle Imaging Detectors	Solar wind measurements

after emission the receiver is activated to detect plasma echoes in the frequency range of 4-80 kHz. These echoes allow the determination of plasma density.

Wide Band Data (WBD) receiver measures electric field waveforms and spectrograms of terrestrial plasma waves and radio emissions. Digital Wave Processing (DWP) instrument coordinates Wave Experiment Consortium (WEC) measurements and performs particle correlation. WEC consists of EFW, STAFF, WHISPER, WDB and DWP instruments.

Fluxgate Magnetometer (FGM) is a magnetometer, designed to provide intercalibrated measurements of the magnetic-field vector. The formation of four Cluster satellites allow the FMGs on board to calculate current density vector, wave vectors and the geometry and structure of discontinuities. FGM also provides the magnetic-field vector to other instruments.

Electron Drift Instrument (EDI) is a electric field measurement device, based on the emission and detection of tracer electrons. Two different measuring methods are employed, for strong and weak ambient magnetic fields.

Active Spacecraft potential Control (ASPOC) is an ion emitter, designed to maintain the spacecraft electrostatic potential at a very low level in relation to the ambient plasma. This is done to ensure accurate measurements. The instrument is linked with PEACE and EFW to provide current spacecraft surface potential.

Cluster Ion Spectrometry (CIS) experiment is a spectrometer designed for ion measurements. It has two sensors to allow 3D-measurements, and also precise measurements of the large flux of ion beams in the solar wind as well as low flux of ions in the magnetospheric lobes.

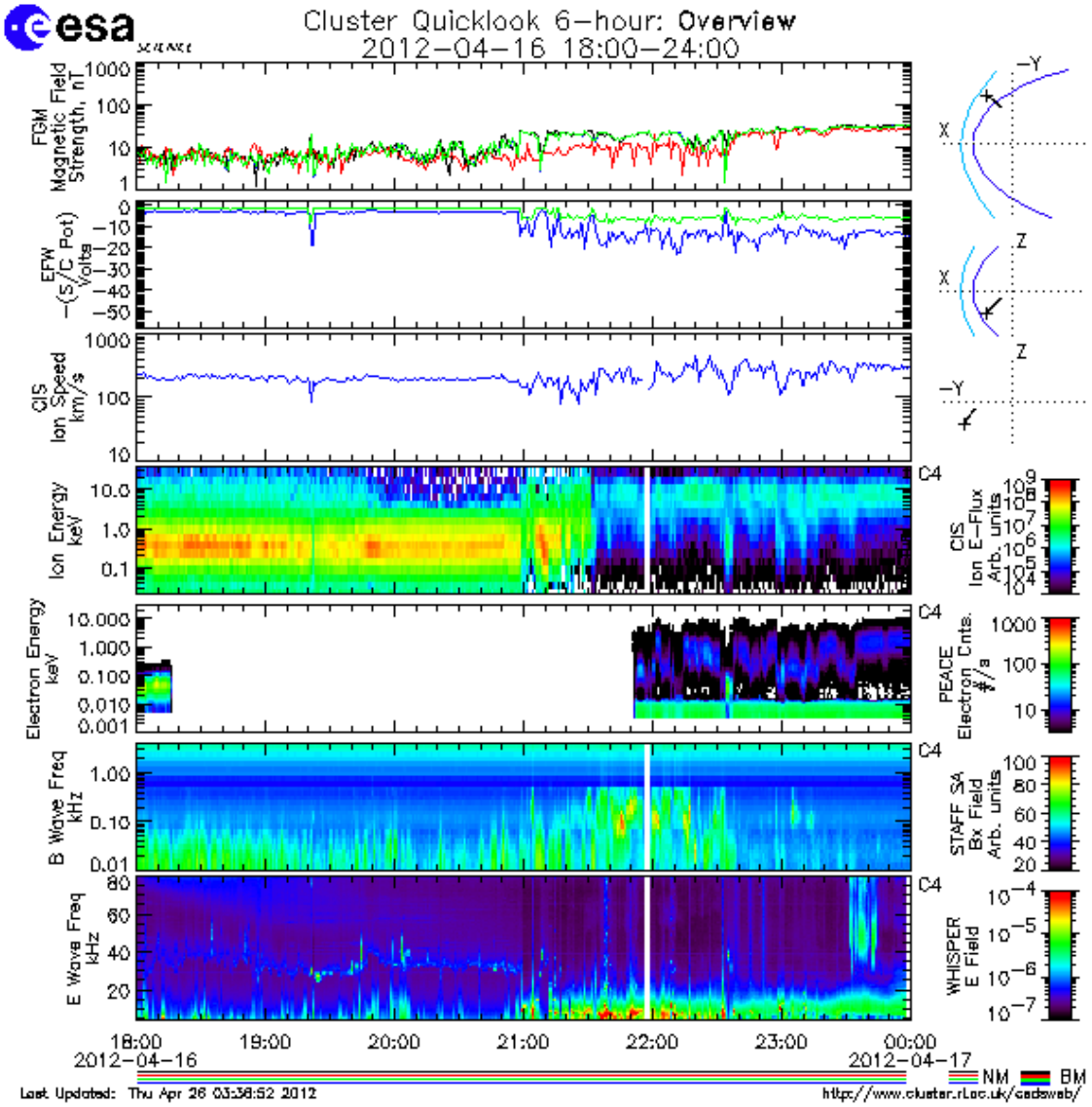

Figure 25: Data from numerous Cluster instruments obtained and plotted from Cluster Active Archive.[38]

Research with Adaptative Particle Imaging Detectors (RAPID) is a set of two spectrometers: Imaging Ion Mass Spectrometer to measure ion distribution function from 30 to 1500 keV and the Imaging Electron Spectrometer (IES) for electrons from 20 to 450 keV.

Plasma electron measurements are conducted with Plasma Electron and Current Experiment (PEACE). It is also divided into two different instruments, one for low energy electrons (0.7 to 10 eV) and one for high energy electrons (up to 30 keV). These sensors are mounted opposite to each other on the spacecraft, allowing three-dimensional distribution function to be calculated.

The Cluster satellites fly in a tetrahedron formation to allow 3d measurements of the plasma environment. The distance between different satellites varies between

200 km to 18000 km depending on mission status. The orbit is fixed around inertial system, thus the rotation of the Earth around the Sun will cause the Cluster formation to cross the various near-Earth plasma regions during its mission. The Cluster mission is actually Cluster II, since the original satellites were lost to a launch failure in 1996. Cluster II is essentially identical in design to the Cluster I. The mission has been extended until the end of 2014.[56][57][37]

The Time History of Events and Macroscale Interactions during Substorms (THEMIS) is a NASA mission to study substorms. It is a constellation of five identical probes, allowing for 3d measurements of magnetosphere structures and particle motion. The fifth probe is mainly for redundancy purposes and is not critical to the mission. First objective is to study the onset and evolution of substorm instabilities. This includes timing of different phases of substorms and interaction between different currents in the near-Earth environment. Secondary goal is to study the source and acceleration mechanisms of storm-time MeV electrons, and the third goal goal is to study the nature, extent and cause of magnetopause transient events.

Table 14: List of THEMIS instruments.

Acronym	Instrument full name	Operative
FGM	FluxGate Magnetometer	Magnetic field measurements
ESA	ElectroStatic Analyzer	Solar wind measurements
SST	Solid State Telescope	Solar wind measurements
SCM	Search Coil Magnetometer	Magnetic field measurements
EFI	Electric Field Instrument	Electric field measurements

All five THEMIS probes are equipped with five instruments (see Table 14). FluxGate Magnetometer (FGM) is designed to measure DC magnetic field up to 128 S/s in the magnetosphere. It is mounted on a 2 m deployable boom. ElectroStatic Analyzer (ESA) measures ion and electrons between 5 eV and 25 keV, Solid State Telescope (SST) measures these between 25 keV and 1 MeV range. Search Coil Magnetometer (SCM) measures magnetic fields from 1 Hz to 4 kHz and also comes with a 1 m boom. Electric Field Instrument (EFI) measures the electric field in the magnetosphere. It consists of four spherical sensors, mounted on two pairs of 20 m and 25 m long Spin-plane Booms. THEMIS mission also features extensive ground-based assets, with stations featuring all sky cameras and magnetometers.[10][121]

4.2.5 Swarm

Swarm is a planned ESA mission to study the Earth's geomagnetic field and its temporal evolution. Swarm has several objectives ranging from study of the Earth's core and geodynamic processes to investigation of electric currents flowing in the magnetosphere and ionosphere. It will be the first satellite to measure coupling currents between solar wind and upper atmosphere.

Like previously mentioned Cluster and THEMIS, it is a constellation of satellites. Swarms three satellites will allow for 3d measurements of the geomagnetic environment. It can be regarded as complement to ESA's Cluster mission. Cluster is designed to make measurements at the boundary or deep inside of the magnetosphere, whereas Swarm will concentrate on the near-Earth field aligned currents. These measurements are accomplished with the use of three instruments: A scalar magnetometer for the magnetic field strength measurements, a vector magnetometer for the direction and a stellar compass to provide a reference attitude to the vector magnetometer. Stellar compass is essentially an advanced star tracker. Star trackers are instruments that determine spacecraft attitude by taking pictures of star constellations and comparing these to known celestial references. Global Navigation Satellite System (GNSS) measurements complement the magnetic field measurements. Swarm is currently scheduled to be launched in late 2013.[64][55][63]

4.3 Space weather services

NOAA Space Weather Prediction Center (SWPC) provides a multitude of space weather products, including the NOAA Space Weather alerts as issued by the NOAA Space Weather Scales. Data for these predictions and models is provided by NOAA, NASA, United States Air Force (USAF), USGS and universities and research institutes. In total, 39 types of event-driven space weather operational products are available, 50 % of these are from GOES data, 38 % from ground-based magnetometer measurements, 7 % from USAF ground-based Solar Optical Observing Network (SOON) and Radio Solar Telescope Network (RSTN) and 2 % from NASA's ACE spacecraft. Primary data sources are required to be continuous and redundant, but this is met only with ACE.

NOAA forecasts use the NOAA Space Weather Scales to categorize different space weather phenomena in much the same way as with tornado and other extreme weather warnings. R-scale, obtained from GOES solar X-ray instrument, is given for radio blackout alerts, S-scale is used for magnitude of solar proton events and G-scale for geomagnetic storms. Space Weather Scales are widely used around to world to issue space weather related warnings. Data products available include warnings issued in accordance with the space weather scales and predictions for several indices for days ahead. NOAA Space Weather Scales are illustrated in Figure 26.[12][132]

NOAA SWPC operates a prediction model for Solar Energetic Particle (SEP) events. It is based in the connection between flares and SEPs. Input parameters are X-ray flux, peak X-ray flux, existence of solar radio bursts and flare location on the surface of the Sun. The model output is probability for a SEP event, its maximum particle flux and duration.[13]

Other largely used space weather services are provided by *NASA Goddard Space Weather Research Center (SWRC)*. SWRC addresses the space weather needs of NASA's robotic missions with real-time space weather information. Additionally SWRC has developed Mobile applications for space weather data analysis on cell phones.[128][147]

SuperMAG is a worldwide collaboration of national agencies and organizations

NOAA Space Weather Scales

Category		Effect	Physical measure	Average Frequency (1 cycle = 11 years)
Scale	Descriptor	Duration of event will influence severity of effects		
Geomagnetic Storms			Kp values* determined every 3 hours	Number of storm events when Kp level was met; (number of storm days)
G 5	Extreme	Power systems: widespread voltage control problems and protective system problems can occur, some grid systems may experience complete collapse or blackouts. Transformers may experience damage. Spacecraft operations: may experience extensive surface charging, problems with orientation, uplink/downlink and tracking satellites. Other systems: pipeline currents can reach hundreds of amps, HF (high frequency) radio propagation may be impossible in many areas for one to two days, satellite navigation may be degraded for days, low-frequency radio navigation can be out for hours, and aurora has been seen as low as Florida and southern Texas (typically 40° geomagnetic lat.).**	Kp=9	4 per cycle (4 days per cycle)
G 4	Severe	Power systems: possible widespread voltage control problems and some protective systems will mistakenly trip out key assets from the grid. Spacecraft operations: may experience surface charging and tracking problems, corrections may be needed for orientation problems. Other systems: induced pipeline currents affect preventive measures, HF radio propagation sporadic, satellite navigation degraded for hours, low-frequency radio navigation disrupted, and aurora has been seen as low as Alabama and northern California (typically 45° geomagnetic lat.).**	Kp=8	100 per cycle (60 days per cycle)
G 3	Strong	Power systems: voltage corrections may be required, false alarms triggered on some protection devices. Spacecraft operations: surface charging may occur on satellite components, drag may increase on low-Earth-orbit satellites, and corrections may be needed for orientation problems. Other systems: intermittent satellite navigation and low-frequency radio navigation problems may occur, HF radio may be intermittent, and aurora has been seen as low as Illinois and Oregon (typically 50° geomagnetic lat.).**	Kp=7	200 per cycle (130 days per cycle)
G 2	Moderate	Power systems: high-latitude power systems may experience voltage alarms, long-duration storms may cause transformer damage. Spacecraft operations: corrective actions to orientation may be required by ground control; possible changes in drag affect orbit predictions. Other systems: HF radio propagation can fade at higher latitudes, and aurora has been seen as low as New York and Idaho (typically 55° geomagnetic lat.).**	Kp=6	600 per cycle (360 days per cycle)
G 1	Minor	Power systems: weak power grid fluctuations can occur. Spacecraft operations: minor impact on satellite operations possible. Other systems: migratory animals are affected at this and higher levels; aurora is commonly visible at high latitudes (northern Michigan and Maine).**	Kp=5	1700 per cycle (900 days per cycle)

* Based on this measure, but other physical measures are also considered.
** For specific locations around the globe, use geomagnetic latitude to determine likely sightings (see www.swpc.noaa.gov/Aurora)

Solar Radiation Storms			Flux level of ≥ 10 MeV particles (ions)*	Number of events when flux level was met**
S 5	Extreme	Biological: unavoidable high radiation hazard to astronauts on EVA (extra-vehicular activity); passengers and crew in high-flying aircraft at high latitudes may be exposed to radiation risk. *** Satellite operations: satellites may be rendered useless, memory impacts can cause loss of control, may cause serious noise in image data, star-trackers may be unable to locate sources; permanent damage to solar panels possible. Other systems: complete blackout of HF (high frequency) communications possible through the polar regions, and position errors make navigation operations extremely difficult.	10^5	Fewer than 1 per cycle
S 4	Severe	Biological: unavoidable radiation hazard to astronauts on EVA; passengers and crew in high-flying aircraft at high latitudes may be exposed to radiation risk.*** Satellite operations: may experience memory device problems and noise on imaging systems; star-tracker problems may cause orientation problems, and solar panel efficiency can be degraded. Other systems: blackout of HF radio communications through the polar regions and increased navigation errors over several days are likely.	10^4	3 per cycle
S 3	Strong	Biological: radiation hazard avoidance recommended for astronauts on EVA; passengers and crew in high-flying aircraft at high latitudes may be exposed to radiation risk.*** Satellite operations: single-event upsets, noise in imaging systems, and slight reduction of efficiency in solar panel are likely. Other systems: degraded HF radio propagation through the polar regions and navigation position errors likely.	10^3	10 per cycle
S 2	Moderate	Biological: passengers and crew in high-flying aircraft at high latitudes may be exposed to elevated radiation risk.*** Satellite operations: infrequent single-event upsets possible. Other systems: effects on HF propagation through the polar regions, and navigation at polar cap locations possibly affected.	10^2	25 per cycle
S1	Minor	Biological: none. Satellite operations: none. Other systems: minor impacts on HF radio in the polar regions.	10	50 per cycle

* Flux levels are 5 minute averages. Flux in particles·s^{-1}·ster^{-1}·cm^{-2} Based on this measure, but other physical measures are also considered.
** These events can last more than one day.
*** High energy particle (>100 MeV) are a better indicator of radiation risk to passenger and crews. Pregnant women are particularly susceptible.

Radio Blackouts			GOES X-ray peak brightness by class and by flux*	Number of events when flux level was met; (number of storm days)
R 5	Extreme	HF Radio: Complete HF (high frequency**) radio blackout on the entire sunlit side of the Earth lasting for a number of hours. This results in no HF radio contact with mariners and en route aviators in this sector. Navigation: Low-frequency navigation signals used by maritime and general aviation systems experience outages on the sunlit side of the Earth for many hours, causing loss in positioning. Increased satellite navigation errors in positioning for several hours on the sunlit side of Earth, which may spread into the night side.	X20 ($2x10^{-3}$)	Fewer than 1 per cycle
R 4	Severe	HF Radio: HF radio communication blackout on most of the sunlit side of Earth for one to two hours. HF radio contact lost during this time. Navigation: Outages of low-frequency navigation signals cause increased error in positioning for one to two hours. Minor disruptions of satellite navigation possible on the sunlit side of Earth.	X10 (10^{-3})	8 per cycle (8 days per cycle)
R 3	Strong	HF Radio: Wide area blackout of HF radio communication, loss of radio contact for about an hour on sunlit side of Earth. Navigation: Low-frequency navigation signals degraded for about an hour.	X1 (10^{-4})	175 per cycle (140 days per cycle)
R 2	Moderate	HF Radio: Limited blackout of HF radio communication on sunlit side of the Earth, loss of radio contact for tens of minutes. Navigation: Degradation of low-frequency navigation signals for tens of minutes.	M5 ($5x10^{-5}$)	350 per cycle (300 days per cycle)
R 1	Minor	HF Radio: Weak or minor degradation of HF radio communication on sunlit side of the Earth, occasional loss of radio contact. Navigation: Low-frequency navigation signals degraded for brief intervals.	M1 (10^{-5})	2000 per cycle (950 days per cycle)

* Flux, measured in the 0.1-0.8 nm range, in W·m^{-2}. Based on this measure, but other physical measures are also considered.
** Other frequencies may also be affected by these conditions.

URL: *www.swpc.noaa.gov/NOAAscales* April 7, 2011

Figure 26: NOAA Space Weather Scales.[133]

that operate ground-based magnetometers. SuperMAG collects data from more than 200 magnetometers and provides electrojet indices produced from the data and related spacecraft measurements. SuperMAG resamples the raw data to 1-minute temporal resolution and converts all units into nanoteslas. Artifacts and errors are also removed and finally a common baseline is subtracted from all measurements. As global measurements are very important in illustrating geomagnetic disturbances, SuperMAG offers a unique service.[70][169]

International Space Environment Services (ISES) is an organization with a mission to encourage and facilitate near-real-time international monitoring and prediction of space environment. ISES provides a multitude of space weather data products. Geophysical Data Codes are available for geomagnetic, auroral and cosmic-ray measurements from ground-based sensors. Alerts and forecasts are provided for numerous solar events from radio bursts to optical measurements of sunspots and flares. Ionospheric conditions and data from satellite based sensors are also covered. Several geomagnetic indices are also available.

ISES works mainly through its Regional Warning Centers (RWC). Currently there exists a total of 14 Regional Warning Centers. These are located in China (Beijing), USA (Boulder), Russia (Moscow), India (New Delhi), Canada (Ottawa), Czech Republic (Prague), Japan (Tokyo), Australia (Sydney), Sweden (Lun), Belgium (Brussels), Poland (Warsaw), South Africa (Hermanus), South Korea (Jeju) and Brazil (São José dos Campos). ESA Noordwijk facility provides a venue fo data exchange in Europe and Associate Warning Center in France (Toulouse) provides specialized services to different customers. Boulder, USA acts as a "World Warning Agency" and data hub. Users of this data include HF radio communication users, mineral surveyors, power and pipeline authorities and satellite operators.[89]

Most of the European countries have their own targeted space weather services including nationally produced data, models and predictions. One of the oldest is the Royal Observatory in Belgium. It was established in 1981 as the Sunspot Index Data Center (SIDC). The main data product is the International Sunspot Number R_i. It is obtained from a fairly simple formula given by Equation 10.

$$R_i = K(10G + S) \tag{10}$$

Where S is the number of observed sunspots, G is the number of observed sunspot groups and K is a station dependent scaling factor. K is used to compare results from different observatories, with Locarno acting as a reference station. These results from individual observatories are combined to calculate the overall R_i. Example of sunspot numbers is given in Figure 27. As of 2003, 82 station from around the world (mostly from Europe) contributed to the sunspot observations. In addition to solar observations the SIDC (Solar Influences Data Center) also provides space weather predictions and alerts. Real-time alerts for flares and CMEs are provided, as well as 3 day forecasts for solar and geomagnetic activity. Other activities include operating a solar radio observatory, solar image processing and co-operation with several satellite missions, including planned operations with Solar Orbiter described previously this thesis.[177][158]

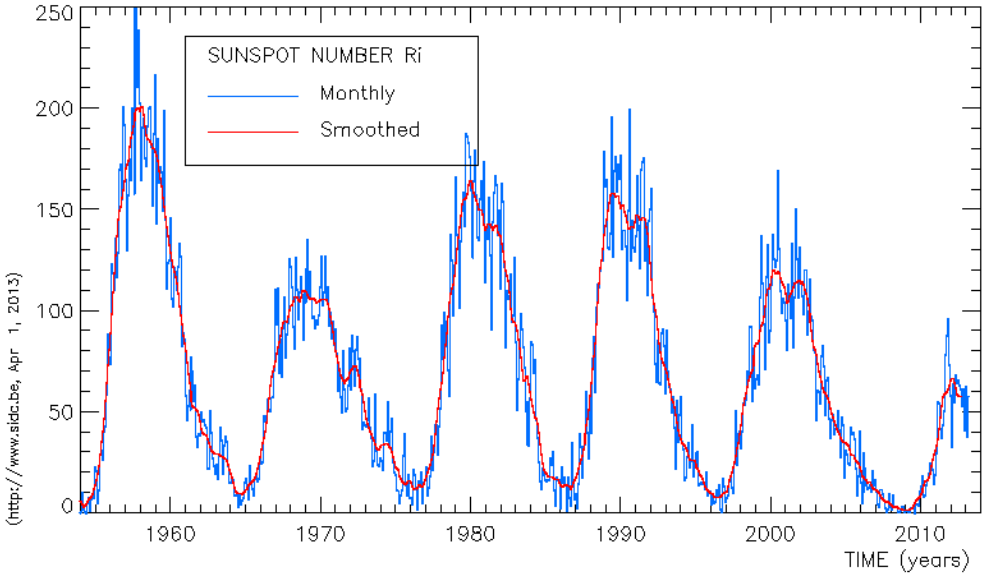

Figure 27: Monthly sunspot numbers from SIDC.[158]

In Finland the space weather services and related science is done at Finnish Meteorological Institute, Oulu university, Helsinki University and Aalto University as well as provided by few citizen science projects. Finnish Meteorological Institute (FMI) operates the *Auroras Now!* space weather service at http://aurora.fmi.fi/public_service/. It collects all-sky-camera images to allow real time monitoring of auroras and provides single aurora predictions. Archived data is provided and users can also order email alerts of auroras.[11] *GICNow!* service is a similar service related to Auroras Now! used to track Geomagnetically Induced Currents (GIC) in the Finnish natural gas pipeline. Real time data from several measurement stations is available.[68]

Other Finnish space weather services include Substorm Zoo (www.substormzoo.org), which provides browser-based tools for time-series analysis of heliospheric, magnetospheric and ionospheric data, operative real-time services and e-tools for social data analysis including discussion groups and LabNotebook for teaching. University of Oulu provides geomagnetic storm related services (dcx.oulu.fi) and CME information is provided by University of Helsinki (www.helsinki.fi/ ekilpua/avaruussaa.html). Other useful links to international space weather services include:
http://www.spaceweather.com/
http://www.solarmonitor.org/

4.4 Results and gap analysis

Currently, space weather measurement systems cover a wide range of different phenomena. However, there are several fields where improvements are needed. Currently existing instrumentation is able to provide most of the needed space weather measurements, but their coverage remains very limited in some areas. Space weather measurement coverage and quality at the auroral oval is limited due to several reasons: (1) large sea areas, where instrument installation is challenging, (2) low resolution instruments, and (3) limited resources for instruments in new inland locations. Ionospheric measurements have very short time series and geographical coverage remains limited. Especially solar wind observations are conducted on a rather small number of satellites since most of them have to be forward deployed to Lagrangian point L1, which is very far away. Solar observations are also conducted by a few expensive solar observatories, but they have more redundancy and are positioned to more easily accessible Earth orbits.

Table 15: Space based magnetometers described in this thesis.[160][161][112][72][14]

Instrument	MAG	MFI	SEM	SEM	FGM	FGM
Satellite	ACE	WIND	GOES I-M	GOES N	Cluster	THEMIS
Type	fluxgate	fluxgate	fluxgate	fluxgate	fluxgate	fluxgate
Resolution	0.1 nT	0.001 nT	1 nT	0.03 nT	$\approx$ 0.1 nT	3 pT
Dynamic range	+/-65536 nT	+/-65536 nT	+/-1000 nT	+/-512 nT	-4096 to 4094 nT	-
Mass	2.55 kg	0.255 kg	-	-	-	-
Power requirements	3.4 W	2.4 W	-	-	-	-

Table 15 lists space based magnetometers from this thesis. These instruments feature far wider spectrum of resolution and range than their ground-based counterparts. GOES-mounted SEM magnetometers have far lower performance, but they are secondary payloads when compared to missions such as ACE and WIND. Solar observation instruments are listed in Table 16 and Table 17 has plasma instrumentation. In addition to large solar observatories, GOES satellites carry Solar X-Ray Sensors to detect x-rays in 0.5 to 3 Å and 1 to 8 Å bands. These are not deployed as near to the Sun as other described instruments.

Table 16: Solar observation instrumentation described in this thesis.[139][185][154][107][46]

Instrument	SXI	MEGS-A	MEGS-B	HMI	AIA	LASCO	EIT
Satellite	GOES N	SDO	SDO	SDO	SDO	SOHO	SOHO
Wavelength	1-6 nm	5-37 nm	35-105 nm	617 nm	9.4-33.5 nm	530-656 nm	17.1-30.4 nm
Resolution	5 arcsec	0.1 nm	0.1 nm	0.91 arcsec	1.5 arc-sec	-	-
Field of view	42.7 ar-cmin	-	-	-	41x41 arcmin	-	-

Table 17: Plasma instrumentation described in this thesis.
[121][167][29][93][29][175][54][56][57]

Instrument	Satellite	Energy range	Field of view
plasma instrument	THEMIS	electrons 2 eV to 32 keV, ions 1.6 eV to 25 keV	180 ° x 6 °
SWIMS	ACE	1 keV/nuclei to 10 keV/nuclei	62 ° x 62 °
CELIAS CTOF	SOHO	0.1 to 55 keV/charge	50 °
CELIAS MTOF	SOHO	0.3 to 3 keV/charge	-
CELIAS STOF	SOHO	20 to 3000 keV/charge	-
ERNE	SOHO	2.5 MeV/nuclei to 300 MeV/nuclei	-
CIS	Cluster	ion distribution 0 to 40 keV	-
PEACE	Cluster	low energy electrons 0.7 to 10 eV or 0.7 to 30 keV	-
RAPID	Cluster	ion distribution 30 to 1500 keV, electron distribution 20 to 450 keV	-

5 Future space weather platforms and systems

5.1 CubeSats

CubeSats are a new generation of microsatellites. The CubeSat project began in 1999 as a collaboration between California Polytechnic State University and Stanford University's Space Systems Development Laboratory. CubeSat objective is to provide standard for design of picosatellites to reduce cost and development time, increase possibility to access space and sustain frequent launches. Standard one unit CubeSat is a 10 cm cube with mass up to 1.33 kg. 2U and 3U Cubesats are also available and have been successfully launched. CubeSats can be integrated into commercial launchers with the Poly Picosallite Orbital Deployer (P-POD). Despite their small size, numerous scientific instruments can be integrated into CubeSats, allowing for multitude of experiments to be carried out in addition to their educational uses. Most CubeSats are on a science or technological demonstration mission.[32][41][81]

From space weather perspective the most useful application for a CubeSat would be to have a magnetometer on board. Accurate measurements would require a deployable boom to separate the magnetometer from the spacecraft hull. There are already designs available for those aboard CubeSats. Of the available boom designs, telescoping booms seem like the best candidate with current technology. Fixed booms are not acceptable due to the way CubeSats are launched. Deployment of the boom has to be also taken into account and there are several solutions available. CubeSat platform still has major obstacles to tackle before usage can become more widespread. For example, widespread use of commercial off-the-shelf (COTS) level components and very light structures mean that radiation and particle damage is significant thus reducing satellite lifetime.

Quakesat was a 3 U CubeSat designed to measure extremely low frequency magnetic field signal (see Figure 28). The objective was to study earthquakes at the San Francisco Bay Area, but the technology can be applied to space weather research as well. The satellite featured a deployable search coil magnetometer as the primary payload. The large power requirements of the magnetometer necessitated additional solar panels. 3U CubeSat was able to accommodate all the necessary systems and the technical demonstration mission was successful. [61][32]

In addition to magnetometers, CubeSats could be utilized for a large selection of other space weather measurements. These include ultraviolet and extreme ultraviolet spectrometers for coronal studies, energetic particle detectors, multi satellite missions for solar wind structures in the same way as the aforementioned Cluster and electric field detectors.[125]

One mission demonstrating CubeSat usage in the field of space weather research is the Norwegian CubeSTAR. It is a 2U CubeSat scheduled to be launched in 2013. The payload is four Langmuir probes, the multi-Needle Langmuir Probe (m-NLP) experiment. The probes are 0.51 mm diameter and 25 mm length, mounted on spring-loaded booms. These allow absolute electron density measurement of ionospheric plasma density structures in sub-meter scale. Since there are four probes, 3d measurements are enabled. Presence of multiple probes allows the determination of

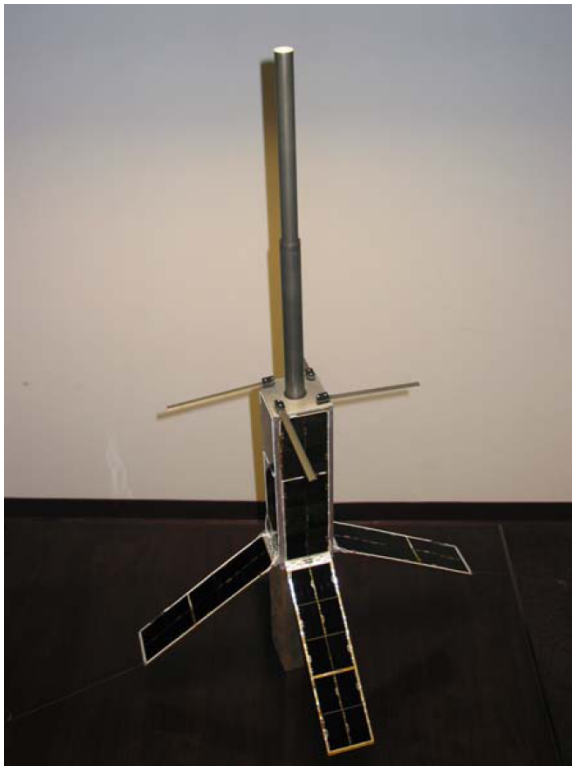

Figure 28: Quakesat on display, with boom and solar panels deployed.[61]

absolute electron density without knowing the electron temperature and spacecraft potential, only an estimate of spacecraft potential is required. Investigation of Cusp Irregularities (ICI-2) sounding rocket mission has flown the m-NLP instrument in 2008.[42][18]

Another planned mission displaying the possibilities of the CubeSat platform for space weather research is the The CubeSat Heliospheric Imaging Experiment (CHIME). It is a 3U Cubesat designed for wide-field sky camera imaging of Interplanetary Coronal Mass Ejections (ICME). Heliospheric imagers are rather rare, so mounting such a system to a CubeSat would be very useful. CHIME would initially consists of one CubeSat, but there are plans for a formation of 3-5 such satellites. Each one would have an expected lifetime of one year. The camera itself is a Commercial-Off-The-Shelf (COTS) scientific CCD camera. To reduce stray light, the camera will be mounted inside an elaborate baffle inside the CubeSat frame. Active thermal control, quite rare for a CubeSat, is implemented to allow the camera to stay within the 0-10 °C operating temperature. All components are COTS, except the baffle and S-band radio. It is estimated that CHIME could deliver ICME forecasts one day before they hit the Earth, with +/- 2 hours accuracy. The mission is currently in planning stages.[47]

5.2 Underwater instruments

Space weather observations require global measurements to be fully realized. Ground-based observations have one crucial problem: large portions of the Earth are covered by oceans. Possibility to place observatories to cover oceans would allow significantly better coverage of space weather events. There are however some observatory networks for underwater measurements where space weather observations could be conducted. One of these is the Canadian Northeast Pacific Undersea Networked Experiments (NEPTUNE) network in the North-East Pacific, covering much of the Juan de Fuca tectonic plate.

NEPTUNE is the largest and most advanced underwater observatory network in the world. First 800 km of cable and five observatories were completed in 2009. It currently hosts over a hundred instruments for numerous scientific applications. Main fields of research include tectonic processes, earthquake dynamics, climate change, ocean climate dynamics, recognition of natural hazards and renewable and non-renewable energy sources. The observatory chain is designed for 25 years of life, which would be long enough for space weather measurement time series. Instruments are fixed to platforms in the seabed, so a vector magnetometer could be kept in a fixed position to allow precise measurements. NEPTUNE features powerful data transfer capabilities, allowing real-time handling of measurements. This is essential for space weather forecasting services. The observatory is also modular, allowing magnetometers to be placed in their own compartment to mitigate measurement errors from other electronics. Figure 29 shows the NEPTUNE instrument platform. Similar observatory networks are planned in Japan, Taiwan and European Union.[15][129]

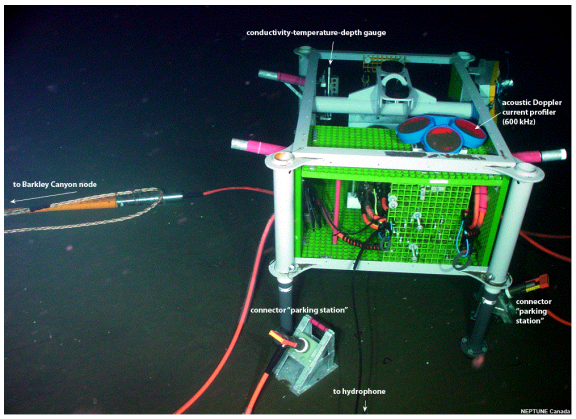

Figure 29: NEPTUNE Canada underwater instrument platform.[129]

Magnetometers would have to survive pressure of the sea floor, be watertight and stay in fixed position in order for the measurements to be useful. Magnetometers themselves are quite rugged and they have already been successfully integrated into space platforms, so underwater magnetometers are quite feasible.

Large body of water would affect the measurements. Fortunately there are already calculations available on the correlation between underwater magnetic fields

and space weather phenomena on the ground level.[21] Space weather effects have also been observed in the sea floor, in underwater cables. One example of these was during March 13th 1989 when 700 V fluctuations were observed in the TAT-8 fiber-optic trans-Atlantic cable.[21]

One important aspect of underwater networks would be to 'fill the gap' in IMAGE network at around auroral oval between Northern Norway and Svalbard. There are currently few observatories at this crucial area of auroral activity, but underwater magnetometers could be utilized here to help with measurements. European counterpart to the aforementioned NEPTUNE, European Seas Observatory NETwork (ESONET), Norwegian Cabled Observatories for MOnitoring of the Ocean System (COSMOS)[134] or other local iniatives could provide this opportunity.[142] As these kind of networks become more common, space weather instruments could be distributed far more widely than currently possible. Integration of the equipment into existing measurement platforms should not be too difficult.

5.3 E-sail

One interesting new development in the field of spacecraft propulsion affecting space weather is the electric sail. Current designs for electric sail consists of a set of rotating, charged tethers. Each tether forms an electric influence region around itself. Solar wind protons are deflected, and the tether experiences a push from the solar wind which depends on the tether's potential. Figure 30 illustrates e-sail operations. Electron guns would keep these tethers in a state of high positive potential. To reduce damage from micrometeoroid impacts, the tethers are made of multifilament Hoytether-type structure. These filaments are $\approx 20\mu$m thick, and feature multiple wires to make the overall structure more robust.

In a full-scale mission the number of these tethers could be as high as 50-100, with length of 20 km each. With this setup the electric sail gives $\approx$ 0.1-0.2 N thrust at 1 Astronomical Unit (AU) distance from the Sun. This creates a very low power, but extremely fuel-efficient propulsion system. Rocket equation is effectively bypassed as no fuel is carried with the spacecraft. Despite the massive size of the structure the tethers are very thin and light. They can be packaged in very small space, to be deployed once the spacecraft reaches orbit. Direction and potential of all tethers would have to be monitored during flight, to prevent tethers from colliding or mixing up.

The most interesting application for e-sail technology in relation to space weather is off-Lagrange point solar wind monitoring. Current solar wind monitors are located at L1 point between the Earth and the Sun. A better location for solar wind monitoring would be closer to the Sun. Current propulsion methods make this kind of mission highly impractical. E-sail powered spacecraft could however easily "hover" at this distance to allow continuous measurements with no need to use fuel. Such mission are conceivable in a time frame of roughly ten years.[174][90]

ESTCUBE CubeSat mission will fly a 10 m tether to test the theory behind e-sail in 2013. Aalto-1 CubeSat is expected to test a 100 m tether in 2014. Both of these tethers are meant to deorbit the satellite by use of the forces described above.

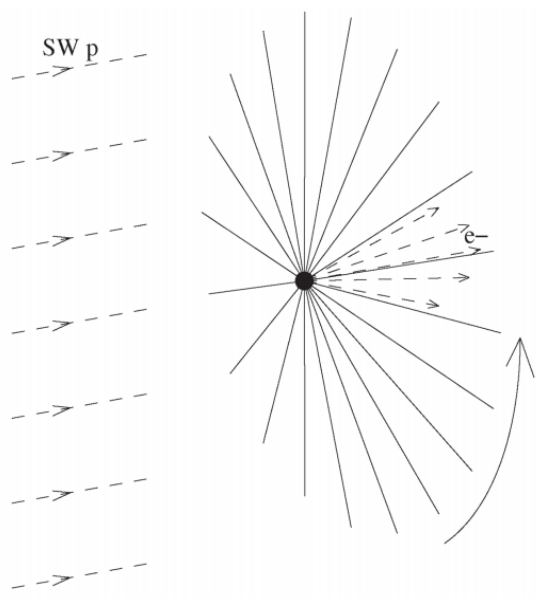

Figure 30: Illustration showing the rotating, charged tethers interacting with the solar wind.[90]

They are not meant to provide any kind of propulsion.[58][100]

6 Capability assessment and SWOT analysis

Based on the information gathered for this thesis we now present capability assessment and analysis of our current space weather infrastructure, covering measurements from the Sun, solar wind, magnetosphere and ionosphere. We have performed a SWOT analysis where strengths (S), weaknesses (W), opportunities (O) and threats (T) for the space weather measurements are analyzed.

6.1 Magnetometer measurements

Ground-based magnetometer coverage is fairly wide. Magnetic observatories are plentiful, and the systems are rather redundant and easy to replace. However, some geographical areas, such as the auroral ovals where the main activity occurs, are not well covered. The addition of underwater magnetometers would allow measurements from between Svalbard and mainland Norway. Auroral oval measurements would provide, for example, airlines with vital information on space weather affecting their operations. Figures 31, 32 and 33 illustrate magnetometer SWOT results and numerous magnetometers from this thesis. Smaller resolution allows better performance. We conclude ground-based magnetometer assets to be currently adequate.

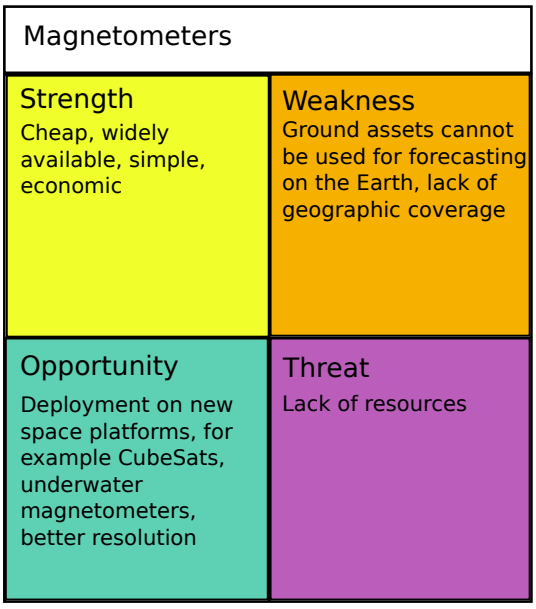

Figure 31: SWOT of magnetometer measurements.

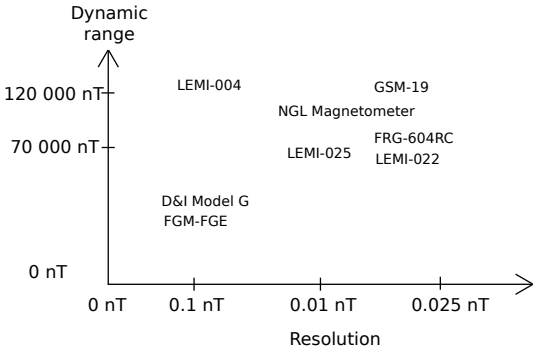

Figure 32: Ground-based magnetometers from this thesis.

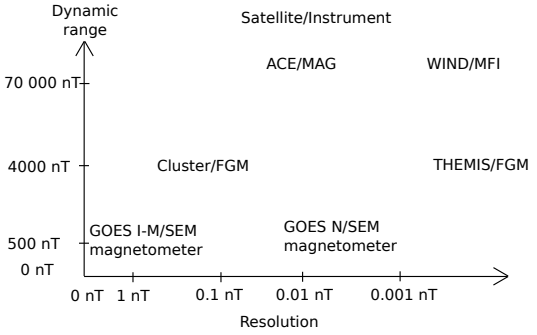

Figure 33: Space based magnetometers discussed in this thesis. Spacecraft/Instrument name.

Space based magnetometers are provided by several satellites in the near-Earth

area, however systems closer to the Sun are rather uncommon. Forward deployed magnetometers are present only at Lagrangian point L1. These L1 based assets are very valuable for forecasting purposes. CubeSats could be utilized as magnetometer platforms in near-Earth space in the very near future. The QuakeSat CubeSat mission has already demonstrated that such measurements are possible from nanosatellite platforms. Off-Lagrangian point measurement platforms would greatly enhance magnetometer measurements and provide better forecasting capabilities. These are, however, somewhat farther in the future. We classify space based magnetometer assets currently acceptable, but limited in coverage.

6.2 Ionospheric measurements

Ionospheric measurement capabilities from the ground are rather sparce. Incoherent scatter radars are a powerful and versatile tool for ionospheric measurements. Newer methods described here such as beacon receivers, GPS measurements and AARDDVARK provide more measurement options. Use of existing GPS infrastructure and very simple ground-based assets allows very economic and straightforward measurements. The coverage of measurement systems is, however, rather limited and time series from newer methods are very short. Ionospheric SWOT is presented in Figure 34. Ionospheric space climate measurement assets are classified as lacking, but promising.

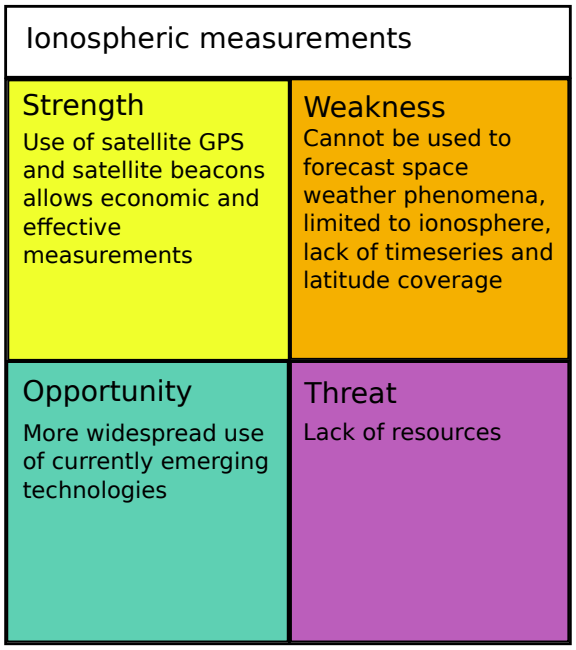

Figure 34: SWOT of ionospheric measurements.

6.3 Solar observations

Solar observations for space weather forecasting purposes are almost completely dependent on large, conventional satellite observatories. The sunspot number can be calculated easily by the numerous Earth-based observatories, but only space based telescopes allow accurate measurements of solar phenomena. SOHO is aging and has been partially superseded by the newer SDO. Solar Orbiter will compliment solar observation in the future. There does not seem to be any technologies in sight that could completely supersede orbital observatories. X-ray detectors are also employed for solar observations but they operate further from the Sun than conventional satellite observatories and do not provide data of comparable quality.

There is a danger that current capability to provide coronagraphs from orbital observatories simply will not be available in the future in case of failure on several satellite missions. Solar observation spacecraft themselves are at risk from numerous space weather phenomena. The issue is further compounded by the large build time of such missions: in case of complete system failure a replacement satellite could take years to launch. This would severely compromise our ability to forecast solar phenomena. However, the problem has been noted and Solar Orbiter is currently under construction while other satellites remain operational. Since solar observations cannot be entirely detached from conventional large missions, their availability in the future should be made certain. More compact instruments to replace current large telescopes would allow new fields of research to emerge. Solar observation SWOT and solar instruments are pictured in Figures 35 and 36 respectively. Space based solar observation capabilities are currently classified as sufficient.

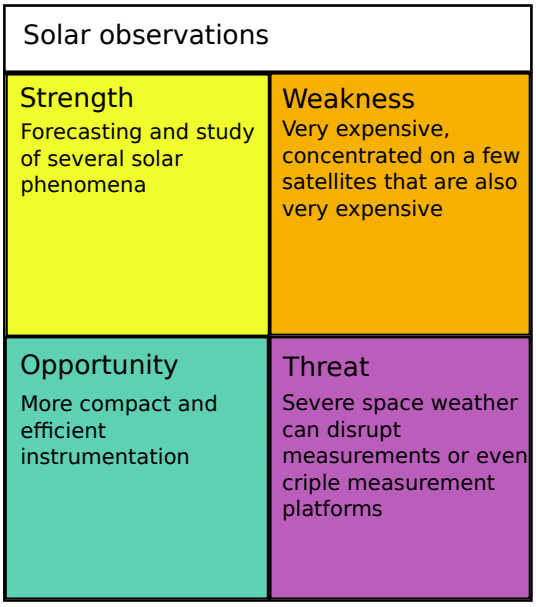

Figure 35: SWOT of solar observations.

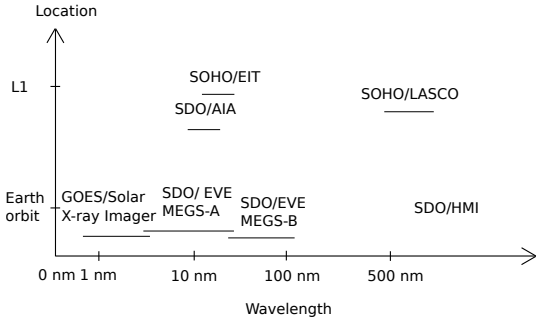

Figure 36: Solar observation instruments discussed in this thesis.

6.4 Solar wind measurements

Particle distribution measurements are conducted over a wide range of energies. For space weather forecasting purposes the research is done in L1 to detect oncoming particle flux by satellites such as ACE, SOHO and WIND. Satellites studying the magnetosphere, such as THEMIS and Cluster, that are deployed on a highly elliptical orbit are also utilized. The measurement site remains a major challenge, since the instruments have to observe oncoming particles far away from the Earth. The Deep Space Climate Observatory (DSCOVR) (previously known as Triana) is an upcoming mission that could be utilized in solar wind measurements. It would essentially replace the aging ACE satellite.[24]

It is worth noting that space based solar observations and *in situ* solar wind monitoring are currently one of the few ways to get reasonable advance warnings of incoming space weather phenomena. Furthermore, solar wind measuring equipment itself is very exposed to space weather events. This means that instrumentation design has to emphasize ruggedness and reliability. The Halloween storm of 2003 damaged several space weather related instruments on numerous satellites, for example on ACE and SOHO.[179]

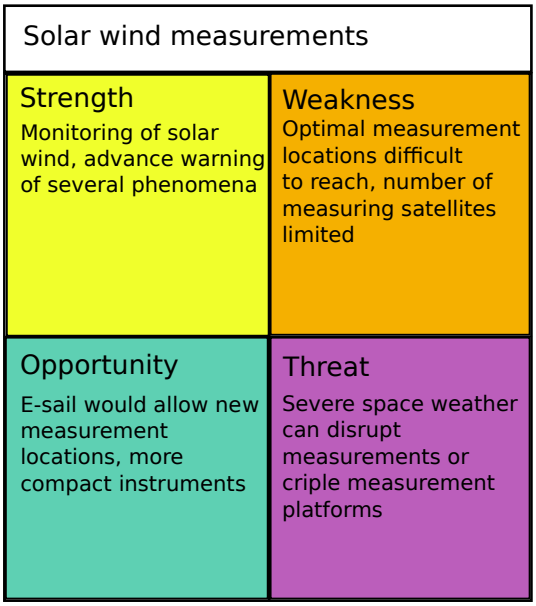

Figure 37: SWOT of solar wind measurements.

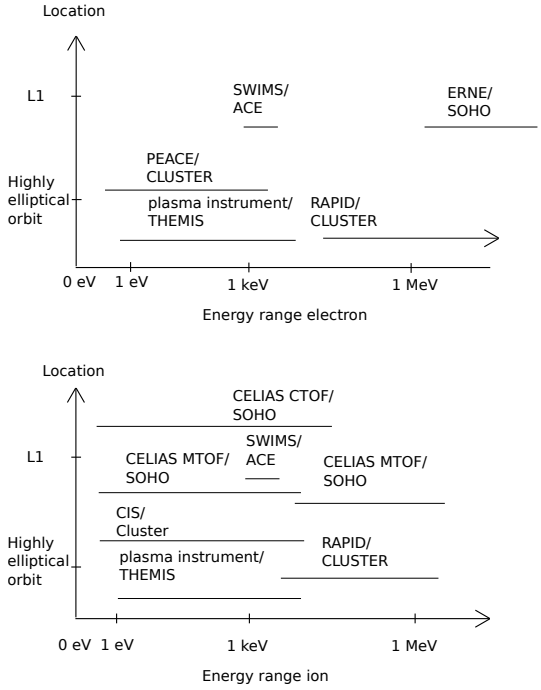

Figure 38: Solar wind composition and particle instruments in this thesis. Spacecraft/Instrument name.

The e-sail would provide a very good platform for solar wind monitoring. The unique propulsion method would allow spacecraft to be stationed off-Lagrangian point, a position rather hard to maintain with current propulsion methods. Furthermore, the very high fuel efficiency would allow a long duration of measurements.

Though e-sail testing is planned on CubeSat missions ESTCUBE and Aalto-1, actual e-sail powered spacecraft are years away from practical usage. Solar wind measurement capabilities are classified as alarming since they have more strict requirements for location than solar observations. Solar wind SWOT and an illustration of instrument energy ranges are given in Figures 37 and 38.

Solar wind measurements have the worst situation of our current space weather infrastructure due to the difficulty of reaching and maintaining required measurement locations at L1. Availability and continuity of measurements should be made certain at all times, otherwise forecasting of space weather events will be severely impaired.

Based on the SWOT and gap analysis we propose the following:

- We suggest that CubeSat based magnetometers be tried on technical demonstration missions. This would open up new types of CubeSat missions to satellite teams and open up further opportunities for space weather research. QuakeSat has demonstrated that boom mounted fluxgate magnetometers are feasible, thus allowing the use of the vital boom-mounted magnetometer. Other space weather related instruments are also conceivable on CubeSats, such as Langmuir probes.

- Underwater magnetometers should be deployed to widen the geographic coverage of measurements. The technology to conduct such measurements exists and they would fill gaps in coverage, especially over the auroral ovals.

- The new types of ionospheric measurement techniques described in this thesis should be widely adopted. Both beacon receivers and GPS measurements allow economic and effective measuring of the ionosphere. Currently time series and geographic coverage are looking rather grim, but these methods could easily improve the situation.

- The ability to conduct space based monitoring of solar wind and solar measurements should be maintained at all times. This unfortunately requires expensive, conventional satellite missions. Current technology does not allow any easy workarounds for this. However, new technological developments could miniaturize instrumentation to fit inside smaller types of spacecraft. Solar wind monitoring would still require positioning at L1 or other hard to reach locations. Our ability to forecast and thus prepare for major space weather phenomena is highly dependent upon these space based assets. Thus, despite their high cost such services should be always available.

7 Discussion and conclusions

Space weather research is needed as mankind extends its reach further into space. One of the difficulties facing future manned missions to the Moon and Mars is space weather. The crew would be exposed to numerous phenomena during their long voyage. Space weather research will help realize such missions. Despite several decades of operating numerous systems in space, many of the phenomena are still quite new to us. As lately as 2003 the Halloween storm caused quite a lot of damage and many of its effects took us by surprise. Also, many events happen in such time scales that we simply have not measured long enough to fully gasp them. The Sun has a 11 year activity cycle, but it also has far longer cycles that we are not entirely familiar with.

Only a few major space weather events have occurred during the space age, the most prominent of them the 2003 Halloween storm. If the largest known space weather event, the Carrington Event, would happen today, it would cause even more widespread damage to satellite systems while power grids would undergo massive strain on the ground. Millions of people could be left without power for months, causing widespread chaos.[12] Another event of comparable magnitude hitting the Earth is only a matter of time.

While we certainly can't prevent the Sun from erupting in such a way in the future, the understanding of the phenomena and the underlying causes will help us greatly mitigate the potential problems. Forecasting systems with better accuracy and longer early warning would allow satellite and power grid operators to take necessary precautions to soften the blow.

The scale of measurements is also quite significant in space weather. Our solar wind estimates come from a few satellites at strategic points between the Sun and the Earth. This means that their coverage area is quite insignificant when compared to the whole heliosphere. Likewise on Earth our sensors hardly cover the oceans at all, leaving notable gaps. The auroral ovals also have insufficient coverage. Some space-based sensors, such as solar wind monitors, are rather rare and in case of system failure some of our space weather forecasting services could be lost for years since large observatories are not easy to replace. Terrestrial weather observations with this kind of situation would be considered totally unacceptable.

A recent survey of space weather risks to Finnish infrastructure concluded that Finland is rather safe from space weather phenomena. However, power grid disturbances from neighboring countries could affect Finland. Furthermore problems with GNSS would cause global communication problems.[96]

New platforms for space based systems are rapidly becoming available and opening new opportunities. For example, the SOHO mission discussed in this thesis has an estimated total cost of a thousand million euros[162]. This is of course a very rough estimate of a single mission. Meanwhile, a single unit CubeSat's costs have been estimated to be around 50 000 US dollars.[83] While this is again a very rough estimate, it means that CubeSat mission costs are orders of magnitude smaller than conventional satellite missions.

Current technology allows the deployment of underwater magnetometers, which

would improve geographic coverage on the Earth. Several advanced underwater measurement networks exist where such instruments could be tried in a technical demonstration mission.

CubeSats and similar small satellites and especially constellations of those could be effectively utilized in space weather research. Several new types of instruments are also coming available for CubeSat and similar small satellite platforms.[125] Especially useful would be a "swarm" configuration (not to be confused with the Swarm mission described earlier), where dozens of small satellites make up a measurement network. This would enable numerous measurements, but each individual satellite would be redundant, economic and easily replaceable. The fact that several of the current space weather platforms are almost one-of-a-kind and very expensive highlights the benefits of such an arrangement. These formations do not exist yet, but many are planned.[40][69] The e-sail holds much promise since it would enable solar wind measurements at stable places beyond and between the currently used Lagrangian points.[90]

References

[1] AARDDVARK homepage, http://www.physics.otago.ac.nz/space/AARDDVARK_homepage.htm, 12 May 2013.

[2] Advanced Composition Explorer homepage, http://www.srl.caltech.edu/ACE/, 10 January 2013.

[3] ACE MAG instrument data from December 28. 2012, http://www.srl.caltech.edu/ACE/ASC/DATA/level3/mag/magsummary/magsummary_2012-363.pdf, 18 April 2013.

[4] Acuna, M.H., Space-based magnetometers, *Review of Scientific Instruments*, Volume 73, Number 11, 3717-3736, 2002.

[5] Aittola, J., Avaruuskäyttöiset magnetometrit ja magnetometri METNET-luotaimessa, Otaniemi TKK, Sähkö- ja tietoliikennetekniikan osasto, 2007.

[6] Alfvén, H., Existence of Electromagnetic-Hydrodynamic Waves, *Nature*, Volume 150, Number 3805, 405-406, 1942.

[7] Altschuler, M.D., Trotter, D.E., Coronal holes, *Solar Physics*, Volume 26, Number 2, 354-365, 1972.

[8] Amerl, P.V., Yau, A.W., Towards the Miniaturization of a Space-Borne Electrostatic Energy Analyzer: the Miniature Enhanced Geometry Electrostatic Analyzer (MEGEA), *Proceedings of the 2005 International Conference on MEMS, NANO and Smart Systems (ICMENS'05)*, 139-142, ISBN 0-7695-2398-6, 24-27 July 2005.

[9] Anderson, P.C., Characteristics of spacecraft charging in low Earth orbit, *Journal of Geophysical Research*, Volume 117, Issue A7, 2156-2202, doi:10.1029/2011JA016875, 2012.

[10] Angelopoulos, V., The THEMIS Mission, *Space Science Reviews*, Volume 141, Issue 1-4, 5-34, doi 10.1007/s11214-008-9336-1, 2008.

[11] Auroras Now!, http://aurora.fmi.fi/public_service/, 15 May 2013.

[12] Baker, D.N. et al., Severe Space Weather Events - Understanding societal and economic impacts, The National Academies Press, Washington D.C., ISBS 978-0-309-12769-1. 2008.

[13] Balch, C.C., Updated verification of the Space Weather Prediction Center's solar energetic particle prediction model, *Space Weather*, Volume 6., Issue 1, doi:10.1029/2007SW000337, 2008.

[14] Balogh, A., et al., The Cluster Magnetic Field Investigation: overview of in-flight performance and initial results, *Annales Geophysicae*, Volume 19, Number 10/12, 1207-1217, 2001.

[15] Barnes, C.R., Best, M.M.R., Johnson, F.R., Pautet, L., Pirenne, B., Challenges, benefits and opportunities in operating cabled ocean observatories: perspectives from NEPTUNE Canada, *Underwater Technology, 2011 IEEE Symposium on and 2011 Workshop on Scientific Use of Submarine Cables and Related Technologies*, doi: 10.1109/UT.2011.5774134, 5-8 April 2011.

[16] Basu, S., Groves, K.M., Specifications and Forecasting of Outages on Satellite Communication and Navigation Systems, Space Weather, Geophysical Monograph 125, 423-430, edited by Song, P., Singer, H.J., Siscoe, G.L., American Geophysical Union, ISBN 0065-8448, 2001.

[17] Baumann, G., High-Speed Stream Structures and Interaction with the Magnetosphere, Institute of Theoretical Physics of the University of Zürich, 2007.

[18] Bekkeng, T.A., Jacobsen, K.S., Bekkeng, J.K., Pedersen, A., Lindem, T., Lebreton, J-P., Moen, J.I., Design of a multi-needle Langmuir probe system, *Measurements Science and Technology*, Volume 21, Number 8, doi:10.1088/0957-0233/21/8/085903, 2010.

[19] Beynon, W.J.G, Williams, P.J.S., Incoherent scatter of radio waves from the ionosphere, *Reports on Progress in Physics*, Volume 41, Number 6, 909-955, 1978.

[20] British Geological Survey aa-index explanation, http://www.geomag.bgs.ac.uk/documents/aa-index_details.pdf, 20 May 2013.

[21] Boteler, D.H., Pirjola, R.J., Magnetic and Electric Fields Produced in the Sea During Geomagnetic Disturbances, *Pure and Applied Geophysics*, Volume 160, Issue 9, 1695-1716, 2003.

[22] Boteler, D.H., Space Weather Effects on Power Systems, Space Weather, Geophysical Monograph 125, 347-352, edited by Song, P., Singer, H.J., Siscoe, G.L., American Geophysical Union, ISBN 0065-8448, 2001.

[23] Browne, S., Hargreaves, J.K., Honary, B., An imaging riometer for ionospheric studies, *Electronics & Communication Engineering Journal*, Volume 7, Issue 5, 209-217, 1995.

[24] Burt, J., Smith, B., Deep Space Climate Observatory: The DSCOVR mission, *Aerospace Conference, 2012 IEEE*, doi:10.1109/AERO.2012.6187025, 3-10 March 2012.

[25] Campbell, A., McDonald, P., Ray, K., Single Event Upset rates in space, *IEEE Transactions on Nuclear Science*, Volume 39, Number 6, 1828-1835, 1992.

[26] CANMOS website, http://geomag.nrcan.gc.ca/obs/canmos-eng.php, 21 February 2013.

[27] CARISMA website, http://www.carisma.ca/, 20 February 2013.

[28] CELIAS/MTOF data, http://umtof.umd.edu/pm/, 8 May 2013.

[29] CELIAS instrument website, http://www.space.unibe.ch/soho/instrument.html, 14 March 2013.

[30] Cerruti, A.P., Kintner, P.M., Gary, D.E., Lanzerotti, L.J., de Paula, E.R., Vo, H.B., Observed solar radio burst effects on GPS/Wide Area Augmentation System carrier-to-noise ratio, *Space Weather*, Volume 4, Issue 10, S10006, doi:10.1029/2006SW000254, 2006.

[31] Chiu, M.C., Von-Mehlem, U.I., Willey, C.E., Betenbaugh, T.M., Maynard, J.J., Krein, J.A., Conde, R.F., Gray, W.T., Hunt,Jr. J.W., Mosher, L.E., McCullough, M.G., Panneton, P.E., Staiger, J.P., Rodberg, E.H. ACE SPACECRAFT, *Space Science Reviews*, Volume 86 Issue 1-4, 257-284, 1998.

[32] Christian, J., Jayaram, S., Swartwout, M., Feasibility of a Deployable Boom aboard picosatellites for instrumentation and control purposes, *Aerospace Conference, 2012 IEEE*, doi: 10.1109/AERO.2012.6187251, 3-10 March 2012.

[33] Clem, J.M., Dorman, L.I., Neutron monitor response functions, *Space Science Reviews*, Volume, 93, Issue 1-2, 335-359, doi:10.1023/A:1026508915269, 2000.

[34] Clilverd, M.A, et al., Remote sensing space weather events: Antarctic-Arctic Radiation-belt (Dynamic) Deposition-VLF Atmospheric Research Konsortium network, *Space Weather*, Volume 7, Issue 4, doi:10.1029/2008SW000412, 2009.

[35] Cliver, E.W., Svalgaard, L., The 1859 solar-terrestrial disturbance and the current limits of extreme space weather activity, *Solar Physics*, Volume 224, Issue 1-2, 407-422, 2004.

[36] Cliver, E.W., A Super Storm: Current Limits of Extreme Space Weather, *TIEMS Oslo Conference on Space Weather & Challenges for Modern Society*, 22-24 October 2012.

[37] Cluster mission website, http://sci.esa.int/science-e/www/area/index.cfm?fareaid=8, 10 January 2013.

[38] Cluster Active Archive, http://caa.estec.esa.int/caa/home.xml, 18 April 2013.

[39] Cluster EFW instrument, http://cluster.irfu.se/, 18 April 2013.

[40] Cockrell, J., Alena, R., Mayer, D., Sanchez, H., Luzod, T., Yost, B., EDSN Edison Demonstration of SmallSat Networks, *presentation at 2012 Small Satellite Conference*, Utah State University, 13 August 2012.

[41] CubeSat Design Specification, http://www.cubesat.org/images/developers/cds_rev12.pdf, 21 February 2013.

[42] CUBESTAR website, http://www.cubestar.no/, 24 April 2013.

[43] de Hoffmann, E., Mass Spectrometry, Kirk-Othmer Encyclopedia of Chemical Technology, John Wiley & Sons, Inc., doi:10.1002/0471238961.1301191913151518.a01.pub2, 2000.

[44] D&I Magnetometer Model G, http://www.space.dtu.dk/English/Research/Instruments_Systems_Methods/DI_Magnetometer_Model_G.aspx, 22 March 2013.

[45] Davis, G., History of the NOAA satellite program, *Journal of Applied Remote Sensing*, Volume 1, 012504, 2007.

[46] Delaboudinieére, J.-P., et al., EIT: Extreme-Ultraviolet Imaging Telescope for the SOHO Mission, *Solar Physics*, Volume 162, Issue 1-2, 291-312, 1996.

[47] Dickinson,, J., DeForest, C., Howard, T., The CubeSat Heliospheric Imaging Experiment (CHIME), *Aerospace Conference, 2011 IEEE*, doi: 10.1109/AERO.2011.5747285, 5-12 March 2011.

[48] Domingo, V., Poland, A., Fleck, B., SOHO Science Operations Plan, Issue 2.1, March 1995 ESA S/95/088/972.

[49] DTU 3-axis Fluxgate Magnetometer Model FGM-FGE, http://www.space.dtu.dk/English/Research/Instruments_Systems_Methods/3-axis_Fluxgate_Magnetometer_Model_FGM-FGE.aspx, 22 March 2013.

[50] Duret, D., Bonzom, J., Brochier, M., Frances, M., Léger, J.M., Odru, R., Salvi, C., Thomas, T., Perret, A., Overhauser Magnetometer For The Danish Oersted Satellite, *IEEE Transactions on magnetics*, Volume 31, Issue 6, 3197-3199, 1995.

[51] Eastwood, J.P., The science of space weather, *Philosophical Transactions of the Royal Society A: Mathematical, Physical and Engineering Sciences*, Volume 366, Number 1884, 4489-4500, doi: 10.1098/rsta.2008.0161, 2008.

[52] Picture of the Earth's magnetosphere, image courtesy of Eija Tanskanen.

[53] What is EISCAT, http://www.eiscat.se/about/whatiseiscat_new, 18 February 2013.

[54] ERNE website, http://www.srl.utu.fi/projects/erne/index_english.html, 14 March 2013.

[55] ESA Swarm website, www.esa.int/Our_Activities/Observing_the_Earth/The_Living_Planet_Programme/Earth_Explorers/Swarm/Overview, 4 February 2013.

[56] Escoubet, C.P., Fehringer, M., Goldstein, M., The Cluster mission, *Annales Geophysicae*, Volume 19, Number 10/12, 1197-2000, 2001.

[57] Escoubet, C.P., Schmidt, R., Cluster - Science and Mission overview, *Space Science Reviews*, Volume 79, 11-32, 1997.

[58] Estcube website, http://www.estcube.eu/en/home, 19 April 2013.

[59] Ferguson, D.C., New Frontiers in Spacecraft Charging, *IEEE Transactions on Plasma Science*, Volume 40, Issue 2, 139-143, 2012.

[60] Fennell, J.F., The IMS Source Book - Guide to the International Magnetospheric Study Data Analysis, American Geophysical Union, ISBN 0-87590-228-6, 1982.

[61] Flagg, S., Bleier, T., Dunson, C., Doering, J., DeMartini, L., Clarke, P., Franklin, L., Seelbach, J., Flagg, J., Klenk, M., Safradin, V., Using Nanosats as a Proof of Concept for Space Science Missions: QuakeSat as an Operational Example, *Proceedings of 18th Annual AIAA/USU Conference on Small Satellites*, 9-12 August 2004.

[62] Fleck, B., Müller, D., Haugan, S., Duarte, L.S., Siili, T., Gurman, J.B., 10 Years of SOHO, ESA Bulletin Number 126, 24-32, 2006.

[63] Fortescue, P., Stark, J. Swinerd, G., Spacecraft Systems Engineering, Third edition, ISBN 0-471-61951-5, John Wiley & Sons, 2005.

[64] Friis-Christensen, E., Lühr, H., Knudsen, D., Haagmans, R., Swarm - An Earth Observation Mission investigation Geospace, *Advances in Space Research*, Volume 41, Issue 1, 210-216, 2008.

[65] Garret, H.B., Whittlesey, A.C., Spacecraft charging, an update, *IEEE Transactions on Plasma Science*, Volume 28, Issue 6, 2017-2028, December 2000.

[66] 3D ionospheric tomography using GEOTRIM GPS measurements, http://www.space.fmi.fi/MIRACLE/Geotrim/index.html, 26 March 2013.

[67] GIC damaged transformer, http://solarscience.msfc.nasa.gov/suntime/images/trans3.jpg, 11 March 2013.

[68] GIC Now! website, http://aurora.fmi.fi/gic_service/, 20 May 2013.

[69] Gill, E., Sundaramoorthy, P., Bouwmeester, J., Zandbergen, B., Reinhard, R., Formation flying within a constellation of nano-satellites: The QB50 mission, *Acta Astronautica*, Volume 82, Issue 1, 110-117, doi:10.1016/j.actaastro.2012.04.029, 2013.

[70] Gjerloev, J.W., A Global Ground-Based Magnetometer Iniative, *Eos, Transactions American Geophysical Union*, Volume 90, Issue 27, 230-231, doi: 10.1029/2009EO270002, 2009.

[71] GSM-19 v7.0 Instruction Manual,http://www.allied-associates.co.uk/pdfmanuals/GSM-19%20Series%20v7%20Manual%20March%202008.pdf, 17 June 2013.

[72] GOES N DataBook, http://goes.gsfc.nasa.gov/text/goes.databookn.html, 26 April 2013.

[73] GOES-P Mission Operations Booklet, http://www.ulalaunch.com/site/docs/missionbooklets/DIV/div_goesp_mob.pdf, 16 April 2013.

[74] Transit of Venus as pictured by GOES SXI instrument, http://satdat.ngdc.noaa.gov/sxi/archive/browse/goes15/2012/06/05/SXI_20120605_230800164_BA_15.PNG, 18 April 2013.

[75] Gordon, D.I., Brown, R.E., Recent Advances in Fluxgate Magnetometry, *IEEE Transactions on magnetics*, Volume 8, Issue 1, 76-82, 1972.

[76] Gosling, J.T., Pizzo, V.J., Formation and evolution of corotating interaction regions and their three dimensional structure, *Space Science Reviews*, Volume 89, Issue 1-2, 21-52, 1999.

[77] Grard, R., Knott, K., Pedersen, Spacecraft Charging Effects, *Space Science Reviews*, Volume 34, 289-304, 1983.

[78] Gussenhoven, M.S., Mullen, E.G., SCATHA Retrospective: Satellite Frame Charging and Discharging in the Near-Geosynchronous Environment, *Proceedings of the 6th Spacecraft Charging Technology Conference*, 237-242, 2-6 November 1998.

[79] Gustafsson, G., et al., First results of electric field and density observations by Cluster EFW based on initial months of operation, *Annales Geophysicae*, Volume 19, Issue 10/12, 1219-1240, 2001.

[80] Hanser, F.A., Sellers, F.B., Design and calibration of the GOES-8 solar x-ray sensor: the XRS, *SPIE's 1996 International Symposium on Optical Science, Engineering and Instrumentation, International Society for Optics and Photonics*, 344-352, doi:10.1117/12.254082, 18 October 1996.

[81] Heidt, H., Puig-Suari, J., Moore, A.S., Nakasuka, S., Twiggs, R.J., CubeSat: A new Generation of Picosatellite for Education and Industry Low-Cost Space Experimentation, *Proceedings of the 15th Annual AIAA/USU Conference on Small Satellites*, 1-19, 21-24 August 2001.

[82] Henderson, M.G., Skoug, R., Donovan, E., Thomsen, M.F., Reeves, G.D., Denton, M.H., Singer, H.J., McPherron, R.L., Mende, S.B., Immel, T.J., Sigwarth, J.B., Frank, L.A., Substorms during the 10-11 August 2000 sawtooth event, *Journal of Geophysical Research*, Volume, 111, Issue A6, doi:10.1029/2005JA011366, 2006.

[83] Heyman, J., FOCUS: CubeSats-A Costing+ Pricing Challenge, http://www.satmagazine.com/cgi-bin/display_article.cgi?number=602922274, 19 April 2013.

[84] Hollweg, J.V., Alfvén waves in a two-fluid model of the solar wind, *Astrophysical Journal*, Volume 181, 547-566, 1973.

[85] Hudson, H.S., Acton, L.W., Freeland, S.L., A long-duration solar flare with mass ejection and global consequences, *The Astrophysical Journal*, Volume 470, 629-635, 1996.

[86] Hughes, A.LI., Rojansky, V., On the Analysis of Electronic Velocities by Electrostatic Means, *The American Physical Society*, Volume 34, Issue 2, 284-290, doi:10.1103/PhysRev.34.284, 1929.

[87] IMAGE website, http://www.geo.fmi.fi/image/, 8 May 2013.

[88] Iucci, N., Levitin, A.E., Belov, A.V., Eroshenko, E.A., Ptitsyna, N.G., Villoresi, G., Chizhenkov, G.V., Dorman, L.I., Gromova, L.I., Parisi, M., Tyasto, M.I., Yanke, V.G., Space weather conditions and spacecraft anomalies in different orbits, *Space Weather*, Volume 3, Issue 1, doi:10.1029/2003SW000056, 2005.

[89] International Space Environment Service website, http://www.ises-spaceweather.org/, 20 May 2013.

[90] Janhunen, P, The electric sail-a new propulsion method which may enable fast missions to the outer solar system, *Journal of the British Interplanetary Society*, Volume, 61, 322-325, 2008.

[91] Janzhura, A., private communication, 2 June 2012.

[92] Jones, J.B.L, Bentley, R.D., Hunter, R., Iles, R.H.A., Taylor, G.C., Thomas, D.J., Space weather and commercial airlines, *Advances in Space Research*, Volume 36, Issue 12, 2258-2267, doi:10.1016/j.asr.2004.04.017, 2005.

[93] Kallenbach, R., et al., Fractionation of Si, Ne, and MG isotopes in the solar wind as measured by SOHO/CELIAS/MTOF, *Space Science Reviews*, Volume 85, Issue 1-2, 357-370, 1998.

[94] Kallio, E.I., Pulkkinen, T.I., Koskinen, H.E.J., Viljanen, A., Slavin, J.A., Ogilvie, K., Loading-Unloading processes in the nightside ionosphere, *Geophysical Research Letters*, Volume 27, Number 11, 1627-1630, 2000.

[95] Karttunen, H., Donner, K.J., Kröger, P., Oja, H., Poutanen, M., Tähtitieteen perusteet, Helsinki, Tähtitieteellinen yhdistys Ursa, 2010.

[96] Karttunen, V., et al., Äärevien sää- ja avaruussääilmiöiden vaikutus kriittisiin infrastruktuureihin, Huoltovarmuuskeskus raportit 2013.

[97] Kauristie, K., private communication, 15 April 2013.

[98] Kerridge, D., INTERMAGNET: Worldwide near-real-time geomagnetic observatory data, *Proceedings of the Workshop on Space Weather*, ESTEC, Volume 34, 2001.

[99] Kessler, D.J., Johnson, N.L., Liou, J.-C., Matney, M., The Kessler Syndrome: Implications to Future Space operations, *American Astronautical Society 33rd Annual AAS Guidance and Control Conference*, 6-10 February 2010.

[100] Kestilä, A., Tikka, T., Peitso, P., Rantanen, J., Näsilä, A., Nordling, K., Saari, H., Vainio, R., Janhunen, P., Praks, J., Hallikainen, M., Aalto-1 nanosatellite - technical description and mission objectives, *Geoscientific Instrumentation, Methods and Data Systems*, Volume 2, 121-130, doi: 10.5194/gi-2-121-2013, 2013.

[101] Kilpua, E.K.J., Pomoell, J., Vourlidas, A., Vainio, R., Luhmann, J., Li, Y., Schroeder, P., Galvin, A.B., Simunae, K., STEREO observations of interplanetary coronal mass ejections and prominence deflection during solar minimum period, *Annales geophysicae: atmospheres, hydrosphers and space sciences*, Volume 27, Issue 12, 4491-4503, 2009.

[102] Kivelson, M.G., Russel, C.T., Introduction to Space Physics, Cambridge University Press, 1995.

[103] Korepanov, V., Best, A., Bondaruk, B., Linthe, H-J., Marianiuk, J., Pajunpää, K., Rakhlin, L., Reda, J., EXPERIENCE OF OBSERVATORY PRACTICE WITH LEMI-004 MAGNETOMETERS, *Revista geofisica*, Volume 48, 31-40, 1998.

[104] Koskinen, H., Johdatus plasmafysiikkaan ja sen avaruussovelluksiin, Limes ry 2010.

[105] Koskinen, H., Tanskanen, E., Pirjola, R., Pulkkinen, A., Dyer, C., Rodgers, D., Cannon, P., Mandeville, J.-C., Boscher, D., Rationale for a European Space Weather Programme, ESWS-FMI-RP-0002, Issue 2.3., 30 March 2001.

[106] Koskinen, H., Tanskanen, E., Pirjola, R., Pulkkinen, A., Dyer, C., Rodgers, D., Cannon, P., Mandeville, J.-C., Boscher, D., Space Weather Effects Catalogue, ESWS-FMI-RP-0001, Issue 2.2., 2 January 2001.

[107] LASCO HANDBOOK FOR SCIENTIFIC INVESTIGATORS, http://lasco-www.nrl.navy.mil/index.php?p=content/handbook/hndbk, 7 May 2013.

[108] Lebreton, J.-P., Stverak, S., Travnicek, P., Maksimovic, M., Klinge, D. Merikallio, S., Lagoutte, D., Poirier, B., Blelly, P.-L., Kovacek, Z., Salaquarda, M., The ISL Langmuir probe experiment processing onboard DEMETER: Scientific objectives, description and first results, *Planetary and Space Science*, Volume 54, Issue 5, 472-486, doi:10.1016/j.pss.2005.10.017, 2006.

[109] Lemen, J.R., et al., The Solar X-ray Imager for GOES, *Telescopes and Instrumentation for Solar Astrophysics, Proceedings of SPIE*, Volume 5171, 65-76, doi: 10.117/12.507566, 4 February 2004.

[110] LEMI-30 magnetometer specifications, http://www.isr.lviv.ua/lemi30.htm, 26 March 2013.

[111] LEMI magnetometers, http://lemisensors.com/?q=products, 24 April 2013.

[112] Lepping, R.P., Acuna, M.H., Burlaga, L.F., Farrell, W.M., Slavin, J.A., Schatten, K.H., Mariani, F., Ness, N.F., Neubauer, F.M., Whang, Y.C., Byrnes, J.B., Kennon, R.S., Panetta, P.V., Scheifele, J., Worley, E.M., The WIND magnetic field investigation, *Space Science Reviews*, Volume 71, Issue 1-4, 207-229, 1995.

[113] Lemen, J.R., et al., The Atmospheric Imaging Assembly (AIA) on the Solar Dynamics Observatory (SDO), *Solar Physics*, Volume 275, Issue 1-2, 17-40, doi: 10.1007/s11207-011-9776-8, 2012.

[114] Lenz, J.E., A Review of Magnetic Sensors, *Proceedings of the IEEE*, Volume 78, Issue 6, 973-989, doi:10.1109/5.56910, 1990.

[115] Lin, R.P., Anderson, K.A., Ashford, S., Carlson, C., Curtis, D., Ergun, R., McCarthy, M., Parks, G.K., Reme, H., Bosqued, J.M., Coutelier, J., Cotin, F., D'uston, C., Wenzel,
K.-P., Sanderson, T.R., Henrion, J., Ronnet, J.C., Paschmann, G., A three-dimensional plasma and energetic particle investigation for the WIND spacecraft, *Space Science Reviews*, Volume 71, Issue 1-4, 125-153, 1995.

[116] Lindblad, B.A., Lundstedt, H., A catalogue of high-speed plasma streams in the solar wind, *Solar Physics*, Volume 74, Issue 1, 197-206, doi:10.1007/BF00151290, 1981.

[117] Little, C.G., Leinbach, H., The Riometer - A Device for the Continuous Measurement of Ionospheric Absorption, *Proceedings of the IRE*, Volume 47, Issue 2, 315-320, doi:10.1109/JRPROC.1959.287299, 1959.

[118] Love, J. J., Finn, C. A., The USGS Geomagnetism Program and Its Role in Space Weather Monitoring, *Space Weather*, Volume 9, Issue 7, doi:10.1029/2011SW000684, 2011.

[119] Maeda, G., private communication, 4 July 2012.

[120] Mann, I.R., Milling, D.K., Rae, I.J., Ozeke, L.G., Kale, A., Kale, Z.C., Murphy, K.R., Parent, A., Usanova, M., Pahud, D.M., Lee, E.-A., Amalraj, V., Wallis, D.D., Angelopoulos, V., Glassmeir, K.-H., Russell, C.T., Auster, H.-U., Singer, H.J., The Upgraded CARISMA Magnetometer Array in the THEMIS Era, *Space Science Reviews*, Volume 141, Issue 1-4, 413-451, doi 10.1007/s11214-008-9457-6, 2008.

[121] McFadden, J.P., Carlson, C.W., Larson, D., Ludlam, M., Abiad, R., Elliott, B., Turin, P., Marckwordt, M., Angelopoulos, V., The THEMIS ESA Plasma Instrument and In-flight Calibration, *Space Science Reviews*, Volume 141, Issue 1-4, 277-302, doi 10.1007/s11214-008-9440-2, 2008.

[122] McPherron, R.L., O'Brien, T.P., Thompson, S., Solar wind drivers for steady magnetospheric convection, *Multiscale Coupling of Sun-Earth Processes*, Volume 1, 113-124, 2005.

[123] MFI instrument website, http://wind.nasa.gov/mfi/instrumentation.html, 20 May 2013.

[124] MIRACLE website, http://www.geo.fmi.fi/MIRACLE/, 9 April 2013.

[125] Moretto, T., Robinson R.M., Small Satellites for Space Weather Research, *Space Weather*, Volume 6, Issue 5, doi:10.1029/2008SW000392, 2008.

[126] Morrill, J.S., et al., Calibration of the SOHO/LASCO C3 White Light Coronagraph, *Solar Physics*, Volume 233, Issue 2, 331-372, doi: 10.1007/s11207-006-2058-1, 2006.

[127] Müller, D., Marsden, R.G., St. Cyr, O.C., Gilber, H.R:, The Solar Orbiter Team, Solar Orbiter Exploring the Sun-Heliosphere Connection, arXiv:1207.4579, 2012.

[128] NASA Goddard Space Weather Research Center, http://swc.gsfc.nasa.gov/main/, 11 April 2013.

[129] NEPTUNE Canada, http://www.neptunecanada.ca/, 3 April 2013.

[130] Nevanlinna, H., Revontulihavainnot Suomessa, 1748-2009, *Ilmatieteen Laitoksen raportteja 2009:3*, ISBN 978-951-697-697-9.

[131] NOAA online glossary, http://www.swpc.noaa.gov/info/glossary.html, 18 October 2012.

[132] NOAA Space Weather Prediction Center, http://www.swpc.noaa.gov/, 10 January 2013.

[133] NOAA Space Weather scales, http://www.swpc.noaa.gov/NOAAscales/NOAAscales.pdf, 18 April 2013.

[134] Norwegian Ocean Observatory Network Cabled Observatories for Monitoring of the Ocean System (COSMOS), http://www.oceanobservatory.com/, 23 May 2013.

[135] Norberg, J., private communication, 16 April 2013.

[136] Nygrén, T., Aikio, A., Kauristie, K., EISCAT 3D sirontatutka maailman huipulle, https://wiki.oulu.fi/download/attachments/23890364/EISCAT3D_Suomi_08.pdf?version=1&modificationDate=1316181980000, 18 February 2013.

[137] Ogilvie, K.W., Chornay, D.J., Fritzenreiter, R.J., Hunsaker, F., Keller, J., Lobell, J., Miller, G., Scudder, J.D., Sittler, E.C. Jr., Torbert, R.B., Bodet, D., Needell, G., Lazarus, A.J., Steinberg, J.T., Tappan, J.H., Mavretic, A., Gergin, E., SWE, a comprehensive plasma instrument for the WIND spacecraft, *Space Science Reviews*, Volume, 71, Issue 1-4, 55-77, 1995.

[138] Onsager, T.G., Grubb, R., Kunches, J., Matheson, L., Speich, D., Zwickl, R., Sauer, H., Operational uses of the GOES energetic particle detectors, *Proceedings of SPIE 2812, GOES-8 and Beyond*, Volume 281, doi:10.1117/12.254075, 18 October 1996.

[139] NOAA Office of Satellite Operations, http://www.oso.noaa.gov/index.htm, 24 January 2013.

[140] Parker, E.N., Space weather and The Changing Sun, Space Weather, Geophysical Monograph 125, 91-99, edited by Song, P., Singer, H.J., Siscoe, G.L., American Geophysical Union, ISBN 0065-8448, 2001.

[141] Pajunpää, K., private communication, 19 October 2011.

[142] Person, R., The European Deep Sea Observatories Network of Excellence ESONET, *OCEANS 2007-Europe*, 1-6, doi: 10.1109/OCEANSE.2007.4302235, 18-21 June 2007.

[143] Pérez-Suárez, D., Higgins, P.A., Bloomfield, D.S., McAteer, J.R.T., Krista, K.D., Byrne, J.P., Gallagher, P.T., Automated Solar Feature Detection for Space Weather Applications, *Applied Signal and Image Processing: Multidisciplinary Advancements*, IGI Global, Hershey, Pennsylvania, 207-225, doi:10.4018/978-1-60960-477-6.ch013, 2011.

[144] Pesnell, W.D., Thompson, B.J., Chamberlin, P.C., The Solar Dynamics Observatory (SDO), *Solar Physics*, Volume 275, Issue 1-2, 3-15, doi: 10.1007/s11207-011-9841-3, 2012.

[145] Primdahl, F., The fluxgate magnetometer, *Journal of Physics E: Scientific Instruments*, Volume 12, Number 4, 241-253. doi:10.1088/0022-3735/12/4/001, 1979.

[146] Prystai, A., Flux-gate Magnetometer LEMI-022 User Manual, National Academy of Sciences - National Space Agency of Ukraine, 2007.

[147] Pulkkinen, A., private communication, 18 March 2013.

[148] Purvis, C.K., Garret, H.B., Whittlesey, A.C., Stevens, N.J., Design Guidelines for Assessing and Controlling Spacecraft Charging Effects, National Aeronautics and Space Administration, Scientific and Technical Information Branch, Volume 2361, 1984.

[149] Raita, T., private communication, 29 April 2013.

[150] Reames, D.V., SEPs: Space Weather Hazard in Interplanetary Space, Space Weather, Geophysical Monograph 125, 101-107, edited by Song, P., Singer, H.J., Siscoe, G.L., American Geophysical Union, ISBN 0065-8448, 2001.

[151] Rosetta spacecraft Langmuir probe, http://upload.wikimedia.org/wikipedia /commons/9/9e/Rosetta_Langmuir_Probe.jpg, 18 April 2013.

[152] Russian Federal Service for hydrometeorology and environmental monitoring, Arctic and antarctic research institute, Department of Geophysics, http://geophys.aari.ru/index.html, 21 February 2013.

[153] Scherrer, P.H., Bogart, R.S., Bush, R.I., Hoeksema, J.T., Kosovichev, A.G., Schou, J., Rosenberg, W., Springer, L., Tarbell, T.D., Title, A., Wolfson, C.J, Zayer, I., The MDI Engineering Team, The Solar Oscillations Investigation - Michelson Doppler Imager, *Solar Physics*, Volume 162, Issue 1-2, 129-188, doi:10.1007/BF00733429, 1995.

[154] Schou, J., et al., Design and Ground Calibration of the Helioseismic and Magnetic Imager (HMI) Instrument on the Solar Dynamics Observatory (SDO), *Solar Physics*, Volume 275, 229-259, doi 10.1007/s11207-011-9842-2, 2012.

[155] Schwenn, R., Space Weather: The Solar Perspective, *Living Reviews in Solar Physics*, Volume 3, 2. URL (cited on 17.4.2013) http://www.livingreviews.org/lrsp-2006-2, 2006.

[156] SDO satellite, http://sdo.gsfc.nasa.gov/gallery/itl.php?v=item&id=37, 18 April 2013.

[157] Sodankylä Geophysical Observatory, www.sgo.fi/index.php, 1 November 2012.

[158] SIDC website, http://sidc.oma.be/, 8 May 2013.

[159] SIS: The Solar Isotope Spectrometer, http://www.srl.caltech.edu/ACE/CRIS_SIS/sis.html, 11 May 2013.

[160] Smith, C.W., L'Heureux, J., Ness, N.F., Acuna, M.H., Burlaga, L.F., Scheifele, J., The ACE Magnetic Fields Experiment, *The Advanced Composition Explorer Mission*, Springer Netherlands, 613-632, doi:10.1007/978-94-011-4762-0_21, 1998.

[161] Singer, H.J., Matheson, L., Grubb, R., Newman, A., Bouwer, S.D., Monitoring space weather with the GOES magnetometers, *Proceedings of SPIE*, Volume 2812, GOES-8 and Beyond, 299-308, doi:10.117/12.254077, 18 October 1996.

[162] SOHO fact sheet, http://sohowww.nascom.nasa.gov/about/docs/SOHO_Fact_Sheet.pdf, 19 April 2013.

[163] The Michelson Doppler Imager, http://soi.stanford.edu/, 17 January 2013.

[164] Soho EIT image composition, http://sohowww.nascom.nasa.gov/gallery/images/tricomp.html, 18 April 2013.

[165] Stoffregen, W., All-Sky Camera Auroral Research during the Third Geophysical Year 1967-58, *Tellus*, Volume 7, Issue 4, 509-517, doi: 10.1111/j.2153-3940.1955.tb01188.x, 1955.

[166] Stolle, C., private communication, 9 July 2012.

[167] Stone, E.C., Frandsen, A.M., Mewaldt, R.A., Christian, E.R., Margolies, D., Ormes, J.F., Snow, F., The Advanced Composition Explorer, *Space Science Reviews*, Volume 86, Issue 1-4, 1-22, 1998.

[168] Substorm Zoo, http://substormzoo.org/, 21 March 2013.

[169] Magnetometer Line Plots, http://supermag.jhuapl.edu/mag/, 19 February 2013.

[170] Szabo, A., Collier, M.R., WIND 2010 Senior Review Proposal, http://wind.nasa.gov/docs/Wind_2010_Senior_Review_Proposal.pdf, 13 February 2013.

[171] Tanskanen, E.I., Slavin, J.A., Tanskanen, A.J., Viljanen, A., Pulkkinen, T.I., Koskinen, H.E.J., Pulkkinen, A., Eastwood, J., Magnetospheric substorms are strongly modulated by interplanetary high-speed streams, *Geophysical Research Letters*, Volume 32, Issue 16, doi:10.1029/2005GL023318, 2005.

[172] Tanskanen, E.I., Slavin, J.A., Fairfield, D.H., Sibeck, D.G., Gjerloev, J., Mukai, T., Ieda, A., Nagai, T., Magnetotail response to proleonged southward IMF B_z intervals: Loading, unloading, and continous magnetospheric dissipation, *Journal of Geophysical Research: Space Physics*, Volume 110, Issue A3, doi:10.1029/2004JA010561, 2005.

[173] Thompson, B.J., Plunkett, Gurman, J.B., Newmark, J.S., St. Cyr, O.C., Michels, D.J., SOHO/EIT observations of an Earth-directed coronal mass ejection on May 12, 1997, *Geophysical Research Letters*, Volume 25, Issue 14, 2465-2468, doi:10.1029/98GL50429, 2012.

[174] Toivanen, P., private communication, 30 April 2013.

[175] Torsti, J., Valtonen, E., Anttila, A., Vainio, R., Mäkelä, P., Riihonen, E., Teittinen, M., Anomalous Cosmic-Ray Helium, Nitrogen and Oxygen in 1996 Measurements of the ERNE Instrument on-board SOHO, *Solar Physics*, Volume 170, Issue 1, 193-205, doi:10.1023/A:1004911017315, 1997.

[176] Tumanski, S., Induction coil sensors–a review, *Measurements Science and Technology*, Volume 18, Number 3, doi:10.1088/0957-0233/18/3/R01, 2007.

[177] Vanlommel, P., Cugnon, P., Van der Linden, R.A.M., Berghmans, D., Clette, F., The SIDC: World Data Center for the Sunspot Index, *Solar Physics*, Volume 224, Issue 1-2, 113-120, doi:10.1007/s11207-005-6504-2, 2004.

[178] Data Analysis Center for Geomagnetism and Space Magnetism, Graduate School of Science, Kyoto University, http://wdc.kugi.kyoto-u.ac.jp/wdc/pdf/pamphlet/wdc_pamp_e.pdf, 26 March 2013.

[179] Weaver, M, et al., Halloween Space Weather Storms of 2003, NOAA Tech. Memo OAR SEC-88, 2004.

[180] White, T., private communication, 17 October 2012.

[181] Wik, M., The Sun, Space Weather and Effects, Swedish Institute of Space Phycis, Department of Physics, Lund University, Thesis for the degree of Doctor of Philosophy in Physics, 2008.

[182] Wik, M., Pirjola, R., Lundstedt, H., Viljanen, A., Wintoft, P., Pulkkinen, A., Space weather events in July 1982 and October 2003 and the effects of geomagnetically induced currents on Swedish technical systems, *Annales Geophysicae*, Volume 27, 1775-1787, 2009.

[183] WIND mission, http://cse.ssl.berkeley.edu/stereo_solarwind/mission_WIND.html, 12 February 2013.

[184] WIND MFI instrument data from March 29. 2013, http://wind.gsfc.nasa.gov/mfi_swe_display_results.php, 18 April 2013.

[185] Woods, T.N., et al., Extreme Ultraviolet Variability Experiment (EVE) on the Solar Dynamics Observatory (SDO), *The Solar Dynamics Observatory*, 115-143, doi: 10.1007/s11207-009-9487-6, 2012.

[186] Yumoto, K. and the MAGDAS group, Space weather activities at SERC for IHY: MAGDAS, *Bulletin of the Astronomical Society of India*, Volume 35, 511-522, 2007.

[187] Zurbuchen, T.H., Fisk, L.A., Lepri, S.T., von Steiger, R., The Composition of Interplanetary Coronal Mass Ejections, *AIP Conference Proceedings 679(1)*, 604-607, doi:10.1063/1.1618667, 2003.